ABSTRACT

Title of thesis: EFFECTS OF CONTRAST AND SPATIAL FREQUENCY ON IDEALIZED COMPENSATORY TASKS

Daniel Richard Brown, Master of Science, 2014

Dissertation directed by: Professor Roberto Celi
Department of Aerospace Engineering

The present analysis describes a series of experiments to quantify the effects of loss of contrast on highly-idealized, compensatory piloting tasks. The effects of spatial frequency are simultaneously studied via the Modulation Transfer Function (MTF). The MTF can quantify the contrast and spatial frequency (relative size) of the objects that provide visual cues necessary for closing pilot control loops. A brief analysis is also performed on different input devices and their effects on task performance. The results show compensatory task performance can be modeled with multiple MTFs, each representing a unique numeric characterization of the pilot response in a single task. The results also quantify the intuitively known fact that physiological limits of human vision directly correlate to piloting task performance. Therefore, the MTF may represent a key building block of quantitative, objective rotorcraft Handling Qualities metrics for Degraded Visual Environments (DVE).

EFFECTS OF CONTRAST AND SPATIAL FREQUENCY ON IDEALIZED COMPENSATORY TASKS

by

Daniel Richard Brown

Thesis submitted to the Faculty of the Graduate School of the
University of Maryland, College Park in partial fulfillment
of the requirements for the degree of
Master of Science
2014

Advisory Committee:
Professor Roberto Celi, Chair/Advisor
Professor Inderjit Chopra
Associate Professor James Baeder

© Copyright by
Daniel Richard Brown
2014

Acknowledgments

I owe my gratitude to all the people who have made my Master's experience one that I will certainly never forget. I learned much more than I ever anticipated, and I enjoyed spending time with a group of great people.

First and foremost, I would like to thank my advisor, Professor Roberto Celi. I am very grateful that he offered me the opportunity to work on the Brownout & Degraded Visual Environment research tasks. As an aviator who has experienced both dangerous flight conditions, it has been both personally and professionally rewarding to work under his guidance. His decades of experience on numerous Rotorcraft areas of research have been an invaluable resource in developing the work presenting in the following pages. I hope that this work reflects well on all his help, and I hope I have been able to contribute something (no matter how small) to such a crucial research topic.

Thank you to Dr. Chopra and Dr. Baeder for serving on my thesis committee. These excellent professors taught a majority of the graduate classes I took here at UMD. Their thorough instruction in class and their passion for aerospace learning was a source of strong personal motivation for me. While this thesis concludes my graduate studies at the moment, I hope I have the opportunity to interact with them again down the road.

I would like to thank my fellow graduate students in our research group, affectionately known as the "Celi-copter" group. They have supported me through my graduate studies, specifically helping me get back into the academic mindset after

a six-year break from classes. I will miss the discussions on the way to class, ideas offered during group meetings, and even the jokes about my (relative) age.

I am indebted to all of the individuals who volunteered for participating as subjects in the research. This includes faculty members from the United States Naval Academy, faculty and students from the United States Naval Test Pilot School, and fellow members of the University of Maryland Department of Aerospace Engineering.

I would also like to thank two fellow UMD Aero alumni - Prof. Joseph Milluzzo from the United States Naval Academy, and Dr. John Tritschler from NAVAIR Flight Dynamics Branch. Both have been mentors for me during the pursuit of my degree, and I will always appreciate them sharing their expertise and advice.

My graduate studies would not have been possible if it were not for the United States Military Academy's Department of Civil & Mechanical Engineering. Thank you for giving me the opportunity to complete my degree and allowing me the time to pursue my research interests.

My friends and family helped me through this experience from the moment I applied to graduate school. Their constant support has kept me motivated and focused during the most strenuous of times. I hope I can return even a small fraction of this support.

Lastly, I would like to thank my fiancée Nancy. She has gone through this entire experience with me (even though she has her own demanding job) and has made some large sacrifices to do so. Her support has been 100% selfless, and will never be forgotten. Thanks for helping me complete my degree Nancy; I look forward to our next adventure together!

Table of Contents

List of Tables

List of Figures

List of Symbols

Greek Symbols

α	Angular diameter
δ	Physical displacement
ϵ	Liminal contrast
θ	Degrees subtended in FOV
Ω	Spatial frequency [cycles/deg]
ϕ	Angle from horizon used in spatial frequency calculation
τ	Operator input delay [seconds]

Symbols

B	RGB value of target
B'	RGB value of background
C	Confidence metric
D	Eye Distance from screen [inches]
E	Error [pixels]
J	Percentage of Joystick Deflection
K	Software Gain on control inputs
L	Location on the screen [pixels]
$\mathbf{M}$	Modulation (or "Contrast")
M	Mouse position
P	Screen size [pixels]
T	Time [seconds]
V	Velocity of the shape
v	Intrinsic noise value
W	Width of image (pixels or degrees)

Subscripts

$(\ )_a$	Actual
$(\ )_C$	Unique modulation and spatial frequency combination
$(\ )_d$	Desired
$(\ )_f$	Final value
$(\ )_G$	Group value
$(\ )_h$	Horizontal direction or component
$(\ )_i$	Initial value
$(\ )_J$	Joystick
$(\ )_O$	Operator shape
$(\ )_{OS}$	Operating System software value
$(\ )_r$	reaction
$(\ )_T$	Target shape
$(\ )_v$	Vertical direction or component

Abbreviations

CSF	Contrast Sensitivity Function
CSV	Comma Separated Value
DVE	Degraded Visual Environment(s)
FOV	Field of View
GVE	Good Visual Environment(s)
HQ	Handling Qualities
IMC	Instrument Meteorological Conditions
MTE	Mission Task Element
MTF	Modulation Transfer Function
NATO	North Atlantic Treaty Organization
OS	Operating System
PC	Proportional Control
RC	Rate Control
UCE	Usable Cue Environment
VCR	Visual Cue Rating

Chapter 1: Introduction

1.1 Degraded Visual Environments

Figure 1.1: OH-58D Kiowa Warrior flying in a GVE (with plenty of visual cues).

A Degraded Visual Environment (DVE) is a characterization of the visual cues available in a physical flight environment. These "degraded" conditions reduce quality and the quantity of visual cues available to the pilots. These reduced cues are, by definition, in direct contrast with a Good Visual Environment (GVE) where

the pilots have all the necessary visual cues to precisely control their aircraft.

DVE can encompass both man-made conditions (e.g. a rotorcraft hovering in a dusty environment) and natural phenomena (e.g. rainy, foggy, or hazy weather conditions). DVE can also result from the time of day, as night flight has degraded visuals compared to the same location during daylight hours [1]. Note the differences in the visual environments shown in Fig. 1.1 and Fig. 1.2, which portray a clear day and a dusty day, respectively. The clarity of the flight environment (and thus the visual cues available to the pilots) is obvious in Fig. 1.1, while there is significant qualitative degradation on the visual cues available in Fig. 1.2.

Figure 1.2: Pair of UH-60L Blackhawks parked in a DVE caused by a dust storm.

Estimates have shown that simple control of an un-augmented helicopter in DVE conditions can consume at least 70% of the pilot's available workload capacity. This leaves only 30% to perform all other functions of flying [2] such as performing

radio calls, maintaining proper clearance from obstacles, and reacting to changes in gusts of wind. As such, DVE (whether man-made or natural) continues to impact safe and precise rotorcraft flight operations.

Flight in DVE is particularly common in military flight operations, as doctrine has shifted towards operations at night and in bad weather [1]. The impact of DVE on NATO military operations alone has been the source of many studies with the specific goal of improving mission performance and reducing mishaps [1, 3].

1.2 Literature Review

Due to the many causes of DVE and its complex nature, research from many fields is relevant to the topic. The present work focuses the multi-disciplinary phenomenon of DVE down into the three specific topics of (i) Rotorcraft Handling Qualities (HQ), (ii) the Physical Environmental Characteristics, and (iii) Human Control Systems.

1.2.1 Rotorcraft Handling Qualities

As the main source of piloting feedback is from visual cues [4], DVE negatively affects pilot visual feedback loops. These loops, shown in Fig. 1.3, provide the necessary information for short, mid, and long-term aircraft control. When degraded, these visual feedback loops may be intermittently opened, or in severe DVE cases, may be completely opened. As visual feedback is lost as an input to the pilot transfer function, then the overall pilot-vehicle transfer function changes. The

extent to the change depends on the pilots responses, as well as the flying qualities and dynamics of the rotorcraft itself [1]. The coupled pilot-vehicle system will then exhibit a specific flight response in a particular set of DVE conditions.

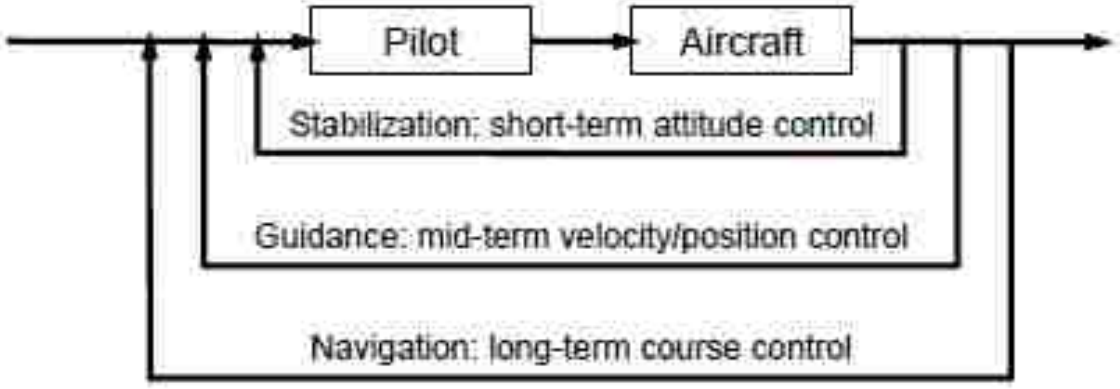

Figure 1.3: Three piloting functions, from Ref. [5].

One method of analyzing the aircraft's flight response is through the evaluation of its Handling Qualities (HQ). Cooper and Harper define Handling Qualities in [6] as " ... those characteristics which govern the ease and precision with which a pilot is able to perform those flight tasks in support of an aircraft role." Good handling qualities have always been, and will continue to be, important to safe and precise flight of an aircraft [7]. Cooper and Harper also defined a rating scale, seen in Fig. 1.4, which facilitate a subjective numerical rating of an aircraft's HQ. This HQ rating takes into account both the characteristics of the aircraft and the demands they place on the pilot while performing a specified task [6].

The myriad factors that influence handling qualities are summarized in Fig. 1.5 from [1]. Two specific influences, the "Mission Task Element" (MTE) and the

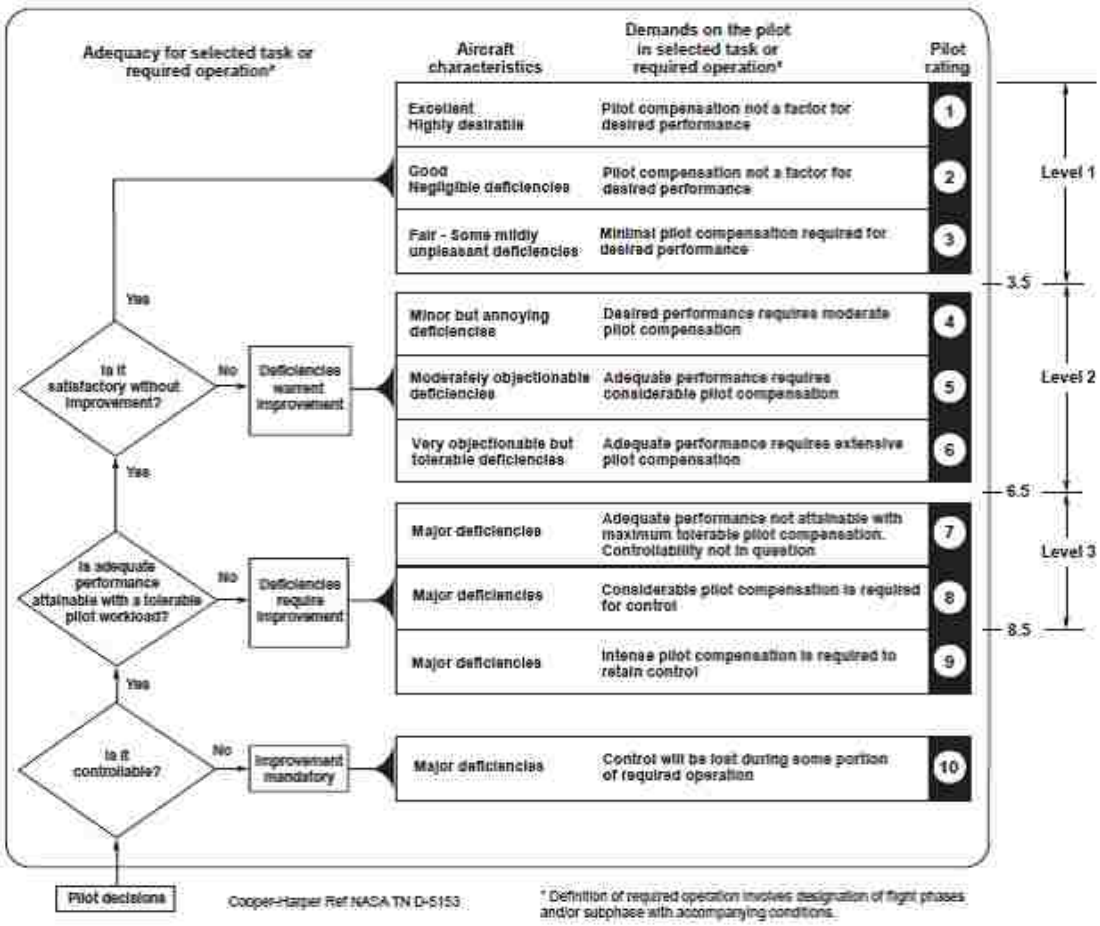

Figure 1.4: Cooper-Harper HQ rating scale, from Ref. [6].

"Usable Cue Environment" (UCE), are of significant importance to the present analysis.

The MTE is a particular flight maneuver that is fundamental to an aircraft performing its intended mission. The current specification for military rotorcraft, "Aeronautical Design Standard Performance Specification Handling Qualities Requirements for Military Rotorcraft" (ADS-33E), specifies MTE by rotorcraft mission category. These mission categories dictate many overall requirements, such as what maneuvers need to be demonstrated, what level of agility the aircraft must have,

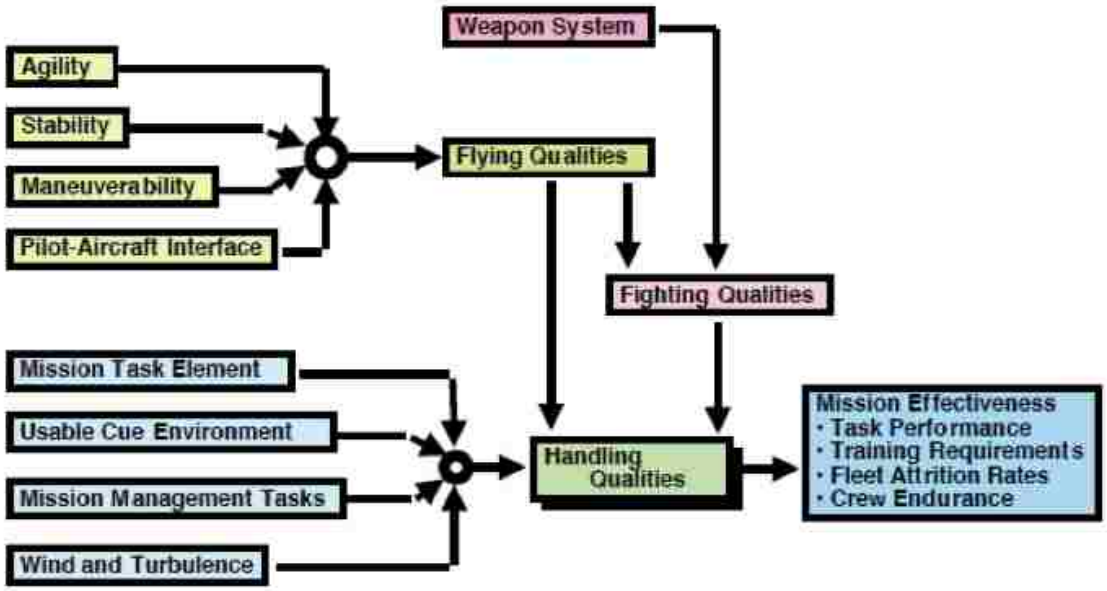

Figure 1.5: Influences on the mission effectiveness of an aircraft, from Ref. [1].

and whether or not a MTE has to demonstrated with a slung load [8]. An except of these requirements is shown in Fig. 1.6.

MTE	REQUIRED AGILITY	ROTORCRAFT CATEGORY				EXTERNALLY SLUNG LOAD
		ATTACK	SCOUT	UTILITY	CARGO	
Tasks in DVE						
Hover	L	✓	✓	✓	✓	✓
Landing	L	✓	✓	✓	✓	
Hovering Turn	L	✓	✓	✓	✓	
Pirouette	L	✓	✓	✓	✓	
Vertical Maneuver	L	✓	✓	✓	✓	✓
Depart/Abort	L			✓	✓	✓
Lateral Reposition	L			✓	✓	✓

Figure 1.6: ADS-33E MTE requirements in DVE based on aircraft mission category. Adapted from Ref. [8].

The UCE is of particular importance to the current specification of tasks performed in DVE. It was recognized from previous versions of ADS-33 that there

was a need for criteria relating to flight in DVE. From this, the Army included specific methodologies to relate flight qualities required for a helicopter based on degradation to visual cues [9]. UCE was developed as "a subjective rating scale intended to quantify the usability of the visual cue environment for stabilization and control during low-speed and hover operations near the ground" [9]. The inclusion of UCE into ADS-33 was an important step into bringing DVE into the overall context of handling qualities.

The UCE for ADS-33E is currently obtained from values of "Visual Cue Ratings"(VCRs) given from test pilots performing a particular MTE. Each pilot must give five separate VCRs; three for attitudes (pitch, roll, and yaw) and two for translational rate (horizontal and vertical). The VCR value is determined through the scale and description show in Fig. 1.7 from [8].

These ratings a fundamentally subjective, based on the pilots opinion on the ability to be "aggressive" and "precise" while performing a given MTE. The five VCRs assigned by the pilot for a particular MTE are then narrowed down to two; the "worst" (highest numerically) of the three attitude VCRs, and the "worst" of the two translational rates. These remaining two VCRs are then plotted on the appropriate axis from Fig. 1.7, and an overall value for UCE is obtained. While the boundaries on the UCE chart come from regression analysis performed in [10], the boundaries are still fundamentally based on subjective Cooper-Harper ratings provided by pilots from flight-testing.

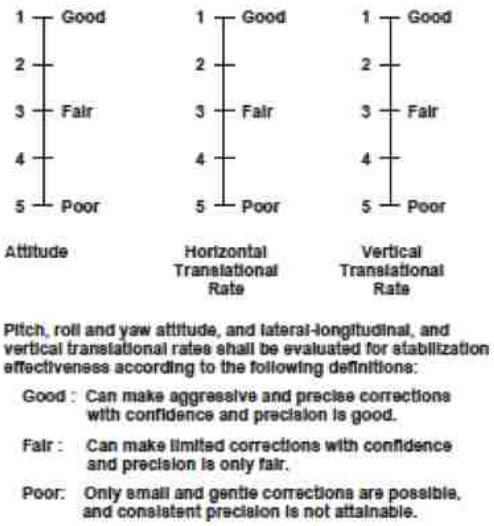

(a) VCR Criteria

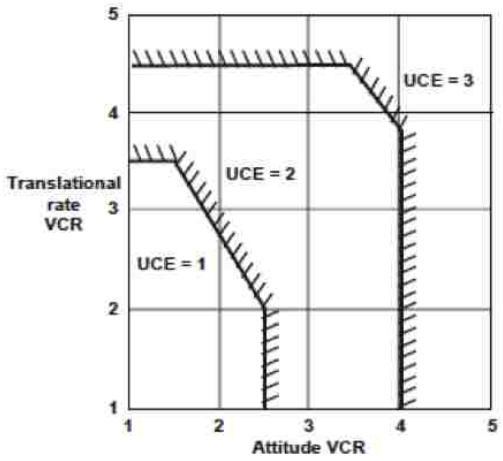

(b) UCE Criteria

Figure 1.7: VCR scale used to determine UCE, from Ref. [8].

1.2.2 Physical Environment Effects

At the heart of the DVE matter is the physical environmental effects themselves. Research on these effects has taken many forms. Rotor system design characteristics [11–13] and Flight-Path Optimization [5, 14] are just a few of the areas

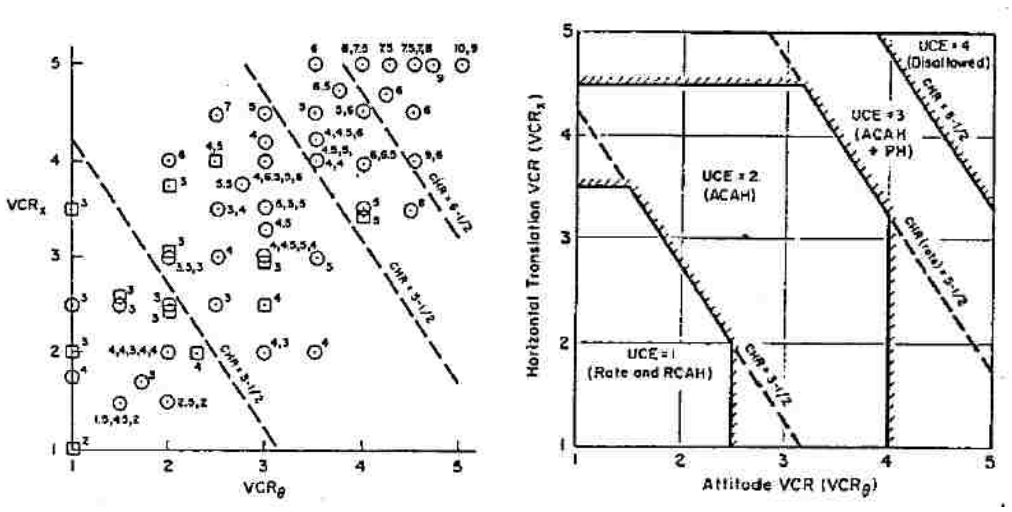

(a) Subjective CH Ratings w.r.t. UCE (b) Development of UCE Regions

Figure 1.8: Subjective data used to develop UCE currently used in ADS-33, from Ref. [10].

of research performed with the goal of mitigating man-made DVE (caused by rotorcraft operation near dusty or snowy environments). Developing the capability for pilots to "see-through" DVE has been developed and tested through the use of technologies like milli-meter wave (MMW) radar [15, 16] and LASER RADAR, or "LIDAR" [17, 18]. The visuals available to the pilots in the cockpit can be seen in Fig. 1.9.

Research has also been performed in an effort to quantify numerous characteristics of the physical environment by itself [5, 19, 20]. This is essential step in order to move from a subjective and qualitative analysis of the UCE to a more objective metric. Tritschler and Celi developed a method of measuring visual properties of "brownout" clouds developed by helicopters landing in a desert environment. One component of this work included adapting the Modulation Transfer Function

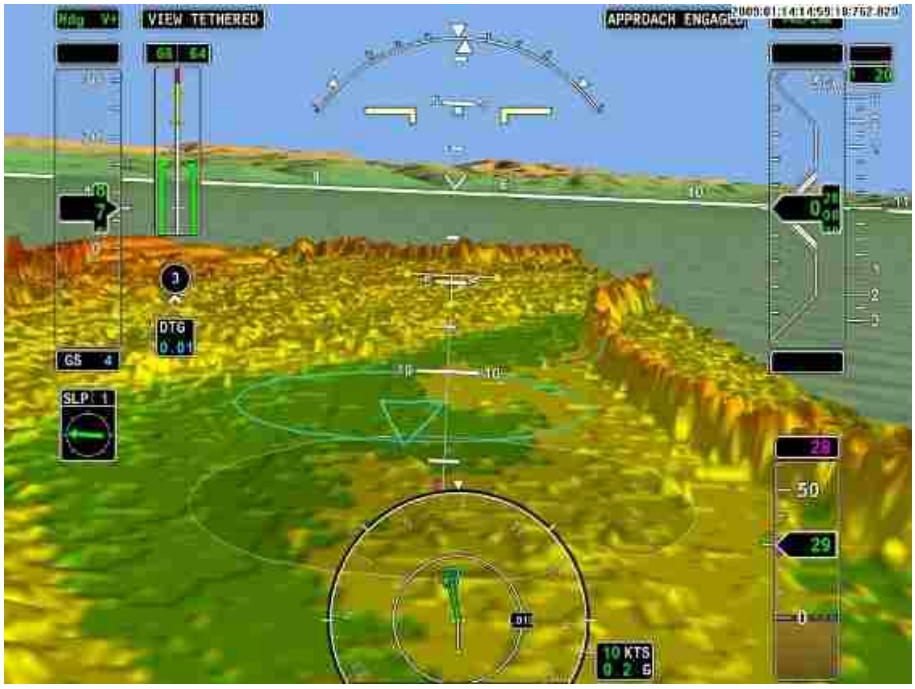

Figure 1.9: DARPA/Honeywell "Sandblaster" synthetic vision technology [16].

(MTF), originally developed to assess the quality of optical instruments [21], for use in quantifying the visual degradation caused by the brownout clouds [20].

This MTF analysis was performed using consumer-level video equipment, and with some simple post-processing, quantified the attenuation of both contrast and resolution of the brownout visual scene as seen in Fig. 1.10. In particular, it helped quantify the effects of the physical brownout phenomenon on both the fine-grained details (characterized by high spatial frequencies) and the large objects (characterized by low spatial frequencies) [20].

While this work was focused on rotorcraft brownout, the methodology could be used for DVE caused by other phenomena as well. Sadot and Kopeika have used the MTF to classify the effects of electromagnetic radiation absorption by aerosols

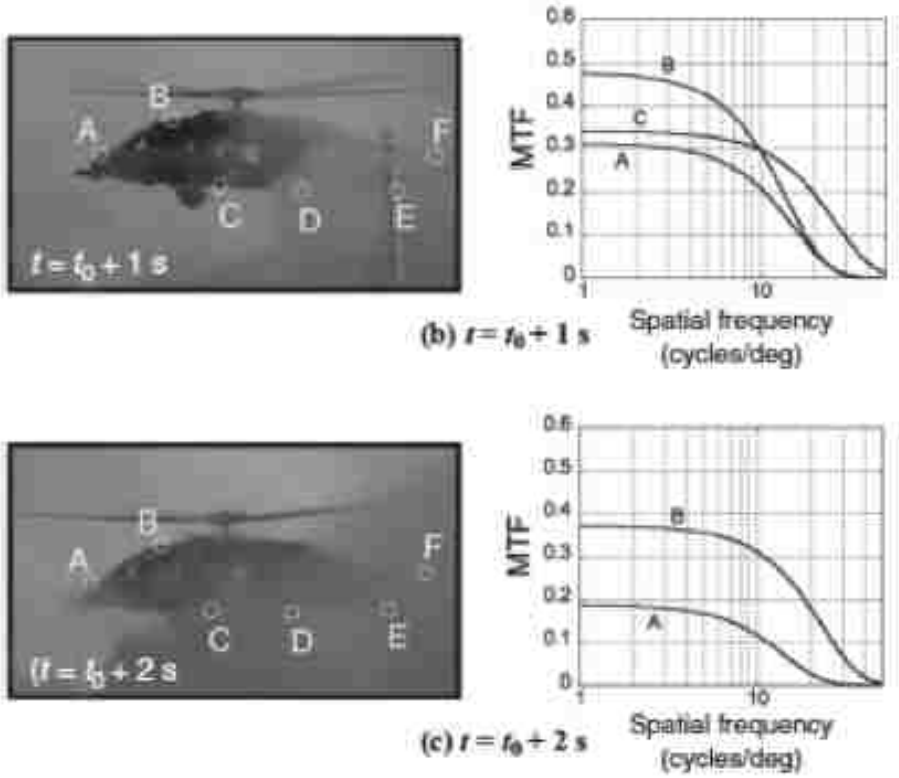

Figure 1.10: Use of the MTF to quantify the effect of brownout clouds. Excerpt of Figure 18 from Ref. [20].

and molecular particulates [22], which could characterize physical DVE phenomena such as fog, haze, and even sea-spray.

Hoh used the MTF to describe the approximate human transfer function of the human visual system and how this vision is impaired under simulated DVE conditions. Additionally, Hoh proposed a MTF that described the visual information required by a pilot for perform hovering tasks with a reasonable workload [23]. This region, titled "Need Visual Information in This Region," can be seen in Fig. 1.11

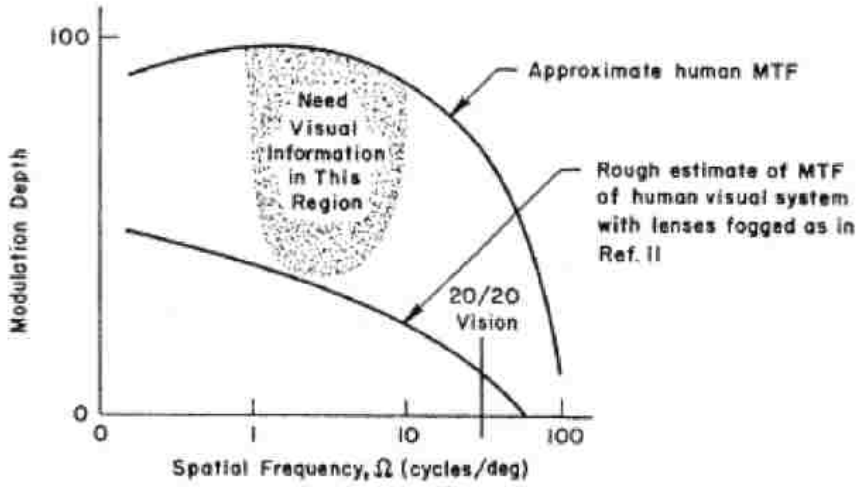

Figure 1.11: Estimation of the visual cues needed for hovering flight, from Ref. [23].

1.2.3 Human Control System Studies

The third topic in the present analysis of DVE is that of human control system studies. A few notable rotorcraft-specific human control experiments will be highlighted to characterize the human pilot as a control system. The effects of a few vision-related variables (such as contrast and image size) will be briefly covered in order to provide a summary of the previous work in the field.

1.2.3.1 Rotorcraft Control Experiments and Modeling

In an attempt to model a human pilot performing hovering flight tasks, Dillow developed the "Paper Pilot" [24], which has seen many updates over the years for different tasks and feedback models [25]. McRuer and Krendel proposed the "Crossover Model" in which the frequency domain characteristics of the pilot transfer function adapt to maintain a -20 dB/decade slope on the Bode Plot of the

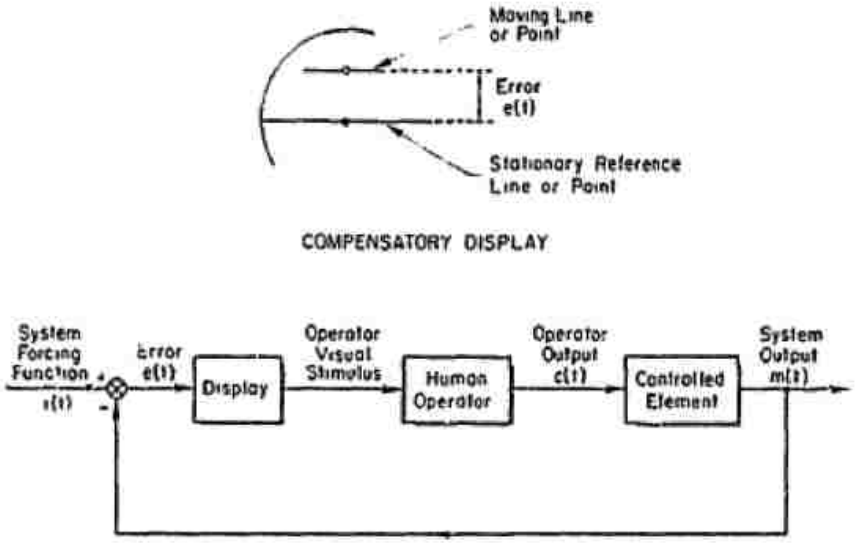

Figure 1.12: Compensatory task design and block diagram from Ref. [26].

pilot-vehicle system dynamics [26].

One of the most notable contributions from experimental research also came from McRuer and Krendel. One component of their work involved an instructor pilot performing a simple compensatory task. In this case, the pilot had a joystick that would control a single, horizontal line on a screen. There was a second line on the screen, which would move vertically with pseudo-random movement.

The pilot's task, illustrated in Fig. 1.12, was to keep his line direct overlapped with the randomly moving line via the joystick in an effort to reduce the value of Error, "e(t)" [26]. The value of the error at any instant was the visual input to the pilot transfer function, which gave insight into pilot control law preference and time delays of the coupled pilot-vehicle system.

The visuals used in the experiment did not vary, however. Therefore the

effects of the visual properties available to the pilot during the testing were not part of the work's resulting mathematical models. As mentioned in Sec. 1.2.1, visual information is the main source of piloting feedback. In order to better characterize the pilot's performance as a human control system, visual variables need to be analyzed.

1.2.3.2 Effect of Contrast on Vision

For the purposes of the present analysis, the ability to "see" will be defined as the ability to perform a given task based on visual detection of the necessary inputs.

One classification of visual detection refers to the "liminal contrast" value (ϵ). This is the value of contrast where the human has a 50% probably of detection of the desired object [27]. The value for liminal contrast is influenced by many factors such as object size, background luminance, and object shape. In general, the liminal contrast required to see an object can be simplified by Ricco's Law, shown in Eqn. (1.1).

$$\epsilon\alpha^2 \;=\; constant \tag{1.1}$$

where α is the angular diameter of the stimulus. This law implies that the total energy received from the stimulus is the main factor defining the detection threshold. With Ricco's Law being equal to a constant value, both the liminal contrast *and* the size of the object have significant roles in visual detection [27] and must be examined simultaneously.

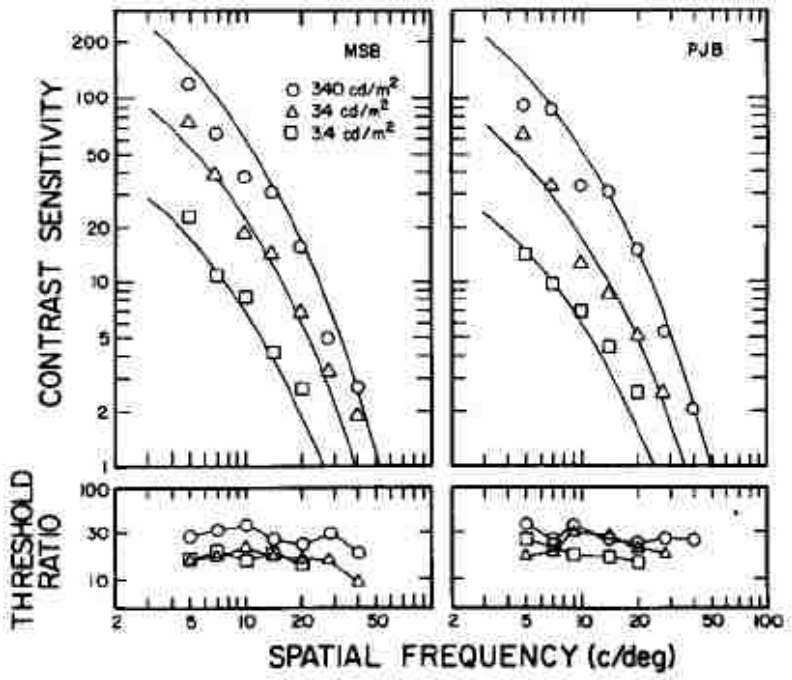

Figure 1.13: Contrast Sensitivity Function (CSF) based on different background luminance values. The human sensitivity to contrast is a function of object size (in this case expressed as spatial frequency). Image from Ref. [29].

The coupled relationship between contrast and image size has been examined by researchers focusing on the properties of the human visual system. Many studies used spatial frequency (which quantifies the light-to-dark or dark-to-light "cycles" an image has within a given FOV) as the metric for image size. Van Nes and Bouman measured the threshold modulation for a sine wave at different spatial frequencies [31]. Howell and Hess performed an experiment where they measured the sensitivity of the human visual system to sinusoidal gratings [28]. Banks *et al.* studied the experimental effects of changing background luminance [29]. These experiments all presented data in terms of spatial frequency. Representative results are shown via a "Contrast Transfer Function" in Fig. 1.13 from Ref. [29].

The relationship between contrast (also referred to as "modulation") and im-

age size can be expressed in a combined form as the Modulation Transfer Function (MTF). The MTF is commonly used in the optics community to describe the performance of a lens [21]. This classification is important as optical lenses typically replicate low spatial frequency (large) objects well, but then cause a degradation in image quality as spatial frequency increases [30].

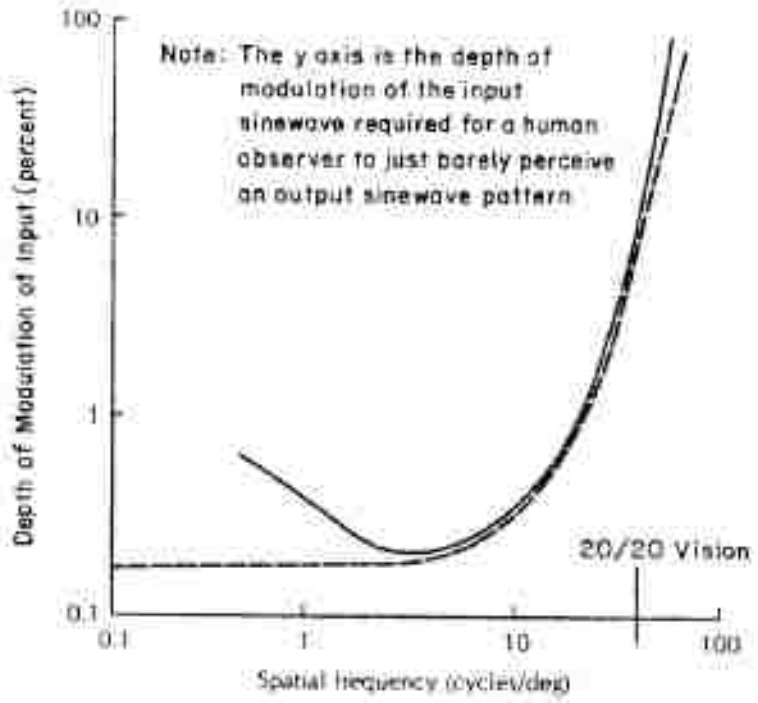

Figure 1.14: Modulation Transfer Function (MTF) of human visual system. Image from Ref. [23].

Numerous attempts have been made to measure the MTF of the human visual system [30], as the human visual system itself could reasonably be assumed to be a form of "lens,". Unlike an optical lens however, the human visual system attenuates both low *and* high spatial frequencies. These characteristics is seen in Fig. 1.14. The dashed line represents the expected performance of an optical lens [31] and the

solid line represents the human visual system [30].

1.2.3.3 Effect of Contrast on Control

The previous section covered just a few of the myriad metrics used to classify the human vision system based on visual input. The next step in the present human control system analysis is to determine what effects those visual inputs have on a human's performance of a control task.

Li *et al.* quantified the effects of contrast on a moving line by development of an experiment patterned after Ref. [26]. This variation faded the visuals of the line through the course of compensatory testing. The results of their work quantified the contrast dependencies of visual perception by analyzing both the closed-loop and the open-loop transfer functions of the subjects. Halving the contrast was found to decrease the operators' internal gain by 17% (while simultaneously adding 35-milliseconds of delay). This contrast study also included the effect of two control laws, velocity control and acceleration control. The position and the motion cues used to control the moving line for both control dynamics were found to be similarly sensitive to contrast [32].

A portion of the performance degradation resulting from reduced contrast may be the result of perceived speed. Stone and Thompson changed the contrast of moving gratings in a 1992 experiment which showed that lower contrast gratings appeared to move slower to the subjects compared to the same grating at a higher contrast. This trend occurred across a wide range of contrasts (2.5-50%) and did

not appear to saturate at higher value [33].

This contrast correlation has also been tested in the automotive research community. A 1998 series of experiments by Snowden *et al.* asked drivers to maintain a certain speed in a driving simulator. The speedometer was then covered up and the visuals were changed to misty then to foggy conditions. As the contrast was incrementally reduced to replicate deteriorating visual driving conditions, the test subjects actually increased their speed. The reduced contrast of the poor weather caused the perceived speed to slow down, resulting in the subject's accelerating [34]. Testing by Blakemore and Snowden in 1999 found that the slowest moving visual patterns were the most susceptible to decrease in perceived speed resulting from reducing contrast [35].

1.2.3.4 Additional Factors Effecting Control

Besides contrast and perceived speed studies, work had been done in regards to the effect of delay and the effect of object separation in human compensatory tasks.

Miall *et al.* introduced varying levels of delay into their tracking experiment. After approximately 150-milliseconds of delay, the subjects began to adopt a new tracking strategy to overcome these programmed delays. The subjects began to mimic the movements of the target shape rather than attempting to correct the current positional error of their own shape. The increase in delay caused the operators to switch from a feedback control method to an open-loop feed-forward method [36].

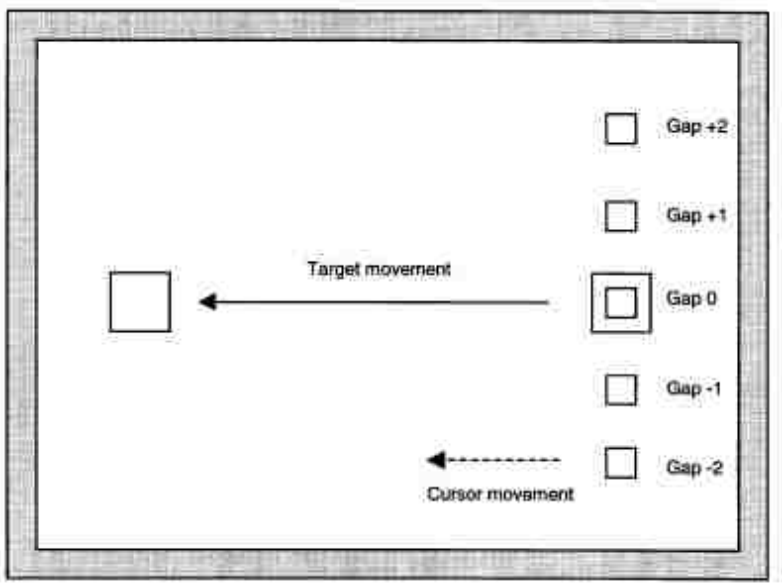

Figure 1.15: Effects of visual separation on human control systems. Image from Ref. [37].

The physical distance separating the objects in a tracking task also affects the human control system. Reed *et al.* found that large separation of objects in a tracking task made the tracking response smoother, but overall less accurate. Sample visuals from this experiment are shown in Fig. 1.15. This work determined that each cue (the target shape and the operator's shape) made an equal contribution to the visuomotor feedback control. That is, each shape acted as a reference to the other. This feedback control was dependent on the subjects' efficiency of positional comparison, and thus became less accurate as the shape's physical separation increased [37].

1.3 Research Objectives

The objectives of the present research were:

1. Understand combined effects of contrast and size of visual cues on the ability to perform a compensatory task.

2. Develop computer-based tests to highlight key parameters such a compensatory task error, input device preference, and control law preference based on varying contrast levels and size of visual cues.

3. Develop quantitative objective metrics, which could represent building blocks for future rotorcraft Handling Qualities specifications, specifically in regards to flight in Degraded Visual Environments.

1.4 Thesis Objectives

The thesis is divided into four chapters. The first chapter outlines the problem of flight in Degraded Visual Environments. It further describes the multidisciplinary nature of the DVE problem, highlighting a portion of previous work in each of three main fields that are the basis for the present analysis.

The second chapter describes the methodology used in the development of the computer-based experiments. The motivation behind the experiments is discussed and the specific details and nuances of each computer experiment are laid out in detail. Additionally, the evolution of the experiments over the span of the present analysis is also discussed.

The third chapter presents the results of the three categories of testing performed. Results from the simple update of the McRuer and Krendel line-based testing are presented, which was the evolutionary basis of the remaining two ex-

periments. It also presents the results from the compensatory task experiments involving vertically-moving circles. The idealized lateral repositioning experiment results are the final component of this chapter.

The fourth and final chapter gives a summary of the conclusions drawn from the battery of experiments, while also provided recommendations for future research.

Chapter 2: Methodology

2.1 Motivation

This chapter will cover the methodology behind the various experiments central to the present analysis. The concept for the computer-based testing, specifically as an update of previous work conducted in Refs. [26, 32] will be covered initially. The evolution and variants of each of the experiments will be covered through the remainder of the chapter. Representative visuals, measurements, and goals will be included for each of the three categories of testing performed.

2.2 Concept

The present analysis began with the development of a series of computer-based experiments designed to quantify human ability to perform a simple compensatory task. Each task was designed to be an idealized representation of a task that the human operator would have to perform as part of a pilot-vehicle system. Operator performance was evaluated over a range of different visual cues. These cues used in the experiments had varying levels of contrast ("modulation") and also varying image size ("spatial frequency"). These two properties of visual cues are combined

in the MTF, which becomes the basis for evaluating task performance.

When the results of the "pilot-vehicle" experimental interaction are presented in an MTF format, they allow for comparison to prior research on human physiology (Ref. [30]), in-flight piloting tasks (Ref. [23]), and DVE physical characterizations (Refs. [5, 20]) in an effort to bring a multi-disciplinary approach to studying DVE.

These experiments were intended to be a small evolutionary step from previous work performed in Ref. [26], in which the visual cues were constant during the experiment, and also to Ref. [32], where the effect of contrast was studied. Similar to those prior experiments, the present work will study the effect of vehicle control laws, specifically Proportional Control (PC) systems and Rate Control (RC) systems.

The testing contained three categories, each aimed at gaining specific insight into pilot performance of that idealized control task. The first category used rectangular shapes (or "lines") with a single vertical degree of freedom, which was design as a proof-of-concept for testing varying visual cues. The second category used simple circles with a single vertical Degree-of-Freedom (DOF) to test individual performance under varying control laws and input devices. The third category again used circles in a highly-idealized representation of the "Lateral Reposition" Mission Task Element from Ref. [8].

2.3 Line-Based Experiments

2.3.1 Goal

The goal of the first series of tests was to develop an experimental "Proof-of-Concept" that performance of simple compensatory tasks could be tested using a simple desktop computer apparatus. The compensatory task comprised of a pair of "lines" (which could also be seen as rectangles) similar the experimental methods used in Ref. [26]. The lines in this series of testing would have varying visual properties corresponding to discrete, desired points on the MTF.

2.3.2 Description of the Experiment

2.3.2.1 Visuals Presented to the Operator

The pseudo-random patterns were developed to be representative of control movements required for piloting a helicopter. Rather than using a mathematical sum-of-sines approach, actual control inputs of a rotorcraft pilot were recorded via the joystick and computer apparatus. The pilot moved the joystick with the goal of replicating the cyclic deflections required to perform stabilized hover-taxi flight.

Using actual pilot cyclic inputs rather than sum-of-sines was done for two reasons. First, in preliminary "beta" testing, the sum-of-sines proved difficult to implement successfully with the computer software used to display the experiment. This was attributed to the on-screen size of the some of the smaller spatial frequency objects. The large size of these objects required a very limited maximum

displacement on the screen. When the sum-of-sines was tuned to meet this criteria, the beta-testing operators did not feel the compensatory task was qualitatively "difficult" enough. The second reason for using actual pilot cyclic inputs was to introduce an additional level of realism to the compensatory task (and required joystick displacements).

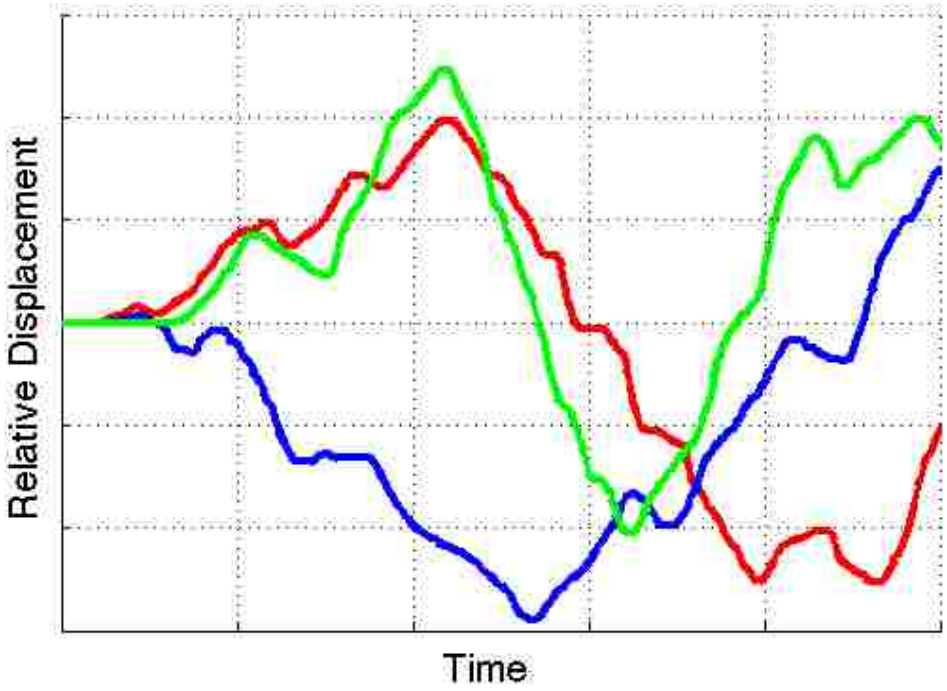

Figure 2.1: Three of the displacement time histories used to move the target.

The pilot's movements were recorded as ten "candidate" 12-second time histories of simple 1-DOF displacement. These candidate time histories were qualitatively evaluated on three specific metrics. First, any history with a maximum displacement of more than 300 pixels from the neutral joystick position were eliminated. Second, any time history that crossed the neutral joystick position value three times or more was eliminated. Lastly, any time history that had a velocity of over 600

pixels per second was eliminated.

These three evaluation criteria narrowed down the 120 seconds of raw time history into three unique, 10-second time histories that had the same qualitative "difficulty." These three control displacement histories, shown in Fig. 2.1, were put into the computer as six "pseudo-random" target time histories (the three unique histories plus their negative counterparts).

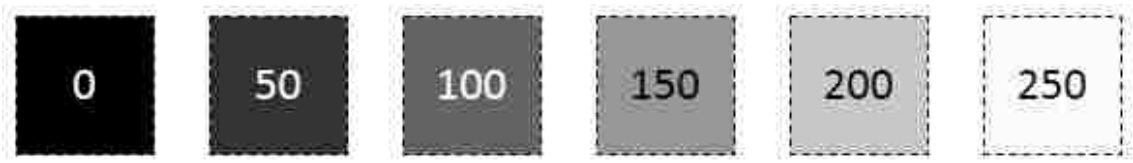

Figure 2.2: Examples of the six unique modulation levels used in testing (with corresponding 8-bit RGB greyscale value).

The visuals presented had six distinct modulation levels as shown in Fig. 2.2. These levels were controlled by adjusting the 8-bit RGB greyscale values of the shapes and/or the background, with the value of 255 corresponding to pure white, and 0 corresponding to pure black. Six unique values of modulation were chosen from 1.00 (perfect black-to-white) down to approximately 0.02 by linear spacing. The RGB values required to produce these desired levels of contrast were then calculated using Eq. (2.1) from [27], where B is the RGB value of the target, B' is the RGB value of the background, and $\mathbf{M}$ is the resulting modulation.

$$\mathbf{M} = \frac{(B - B')}{B'} = \frac{\Delta B}{B'} \tag{2.1}$$

The visuals presented also had six distinct spatial frequencies. Desired values

of spatial frequency Ω_d were chosen from approximately 1 to 100 cycles per degree with logarithmic spacing. For any given shape displayed on the screen, there were two contrasting cycles (a light-to-dark cycle and a dark-to-light cycle). The number of cycles was held consistent at two during the test, and a representative diagram is shown in Fig. 2.3. For simplicity of programming the computer graphics, the edges were kept at a sharp transition from light-to-dark. In the frequency domain, this would introduce infinite frequencies into the analysis. A Gaussian blur should have been used as in Ref. [32] in order to allow for more in-depth analysis of the experimental results.[1]

The denominator of the spatial frequency calculation Eq. (2.2) depended on the number of degrees that the shape would subtend in the individual's field-of-view (FOV). The degrees subtended θ_d by the desired spatial frequency Ω_d could then be found by Eq. (2.3). The desired spatial frequency was indirectly controlled by adjusting the number of pixels used to draw the shapes on the computer screen. The distance from the individual's eyes to the screen was held constant for the testing, and the screen's size (in inches) and resolution (in pixels) were known from manufacturer data. The Pixels-Per-Inch (PPI) was easily found to be approximately 108.79 PPI in both the vertical and horizontal direction.

The number of pixels required to achieve a shape that subtended the desired FOV (corresponding to the desired spatial frequency) could then be calculated from Eq. (2.4).

[1]This point was brought to the author's attention by Dr. Barbara T. Sweet, NASA Ames Research Center.

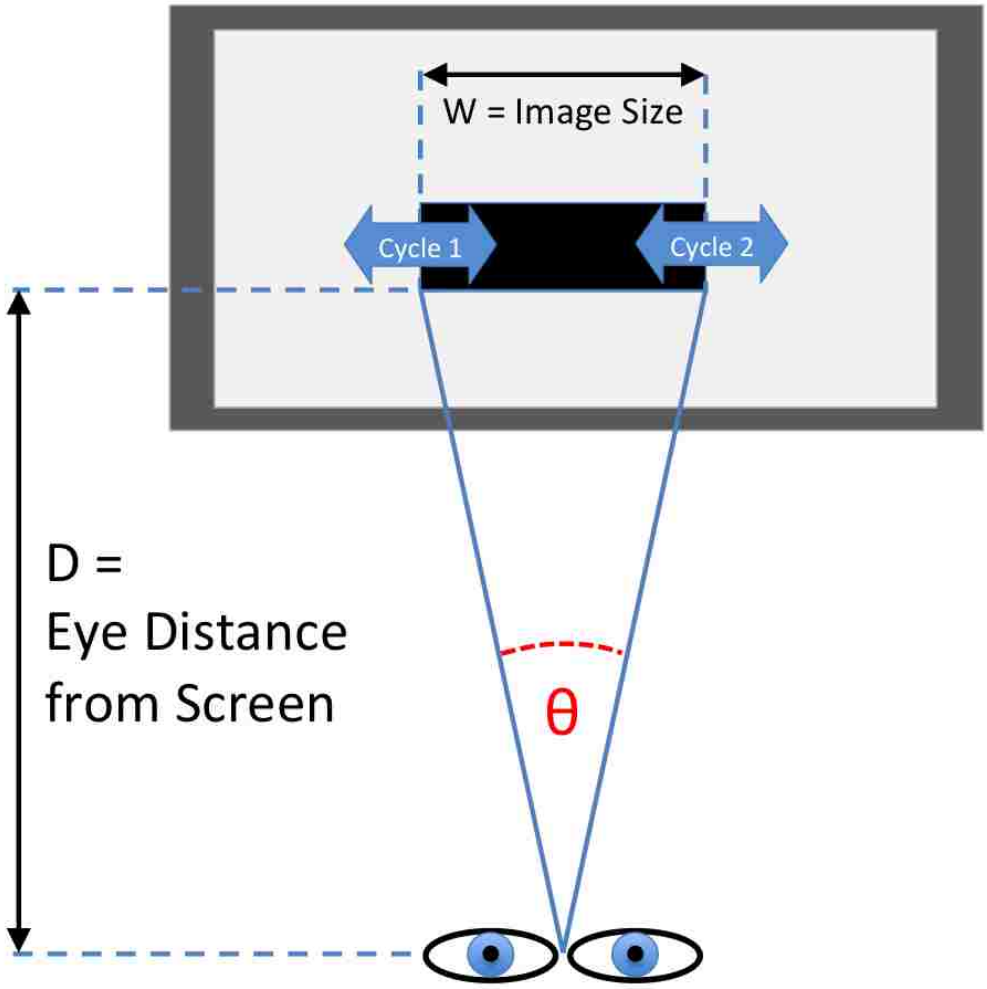

Figure 2.3: Spatial frequency for visuals with two cycles.

$$\Omega_d \left(\frac{\text{cycles}}{\text{deg}} \right) = \frac{2 \text{ cycles}}{\text{Degrees subtended in FOV}} = \frac{2}{\theta_d} \tag{2.2}$$

$$\theta_d \, (\text{deg}) = \frac{2 \text{ cycles}}{\Omega_d} \tag{2.3}$$

$$W \, (\text{pixels}) = \frac{\theta_d \times PPI}{\arctan\left(\frac{1}{D}\right)} \tag{2.4}$$

Like the RGB values used in modulation calculations, the number of pixels was also limited to integer values for purposes of displaying the images on the screen. The desired number of pixels was rounded to the nearest whole number. The calculations performed in Eq. (2.2)-(2.4) then were performed in reverse.

The integer pixel value for W_a was substituted into Eq. (2.5) to find the *actual* degrees subtended θ_a. The θ_a value was used in Eq. (2.6) to find the *actual* spatial frequency Ω_a that the computer was able to display at the 48-inch viewing distance. This resulted in spatial frequencies that were not perfect logarithmically spaced from 1 to 100 cycles per degree.

$$\theta_a\,(\text{deg}) = \frac{W_a \times \arctan(\frac{1}{D})}{\text{PPI}} \tag{2.5}$$

$$\Omega_a \left(\frac{\text{cycles}}{\text{deg}}\right) = \frac{2\ \text{cycles}}{\theta_a\,(\text{deg})} \tag{2.6}$$

For testing, small objects actually had a higher spatial frequency than large objects, as the same number of two contrasting cycles were presented on the screen subtending a smaller portion of the individual's FOV. Table 2.1 contains representative relationships between image size and spatial frequency. Note the pixel values are integers.

2.3.2.2 Changing the Visuals during the Experiment

Each experiment had 36 unique combinations of modulation and spatial frequency. Each combination had one of six levels of modulation between the geometric

Table 2.1: Relation of image size to spatial frequency at 48" viewing distance

Image Size W [pixels]	Image Size W [in]	FOV Subtended θ_a [degrees]	Spatial Frequency Ω_a [cycles/degree]
2	0.018	0.022	91.14
5	0.046	0.054	36.45
12	0.110	0.129	15.19
29	0.267	0.312	6.29
73	0.671	0.786	2.50
182	1.673	1.958	1.00

shapes and the program's background, and each state had one of six distinct spatial frequencies for the target shape. The 36 unique combinations of modulation and spatial frequency are shown in Fig. 2.4.

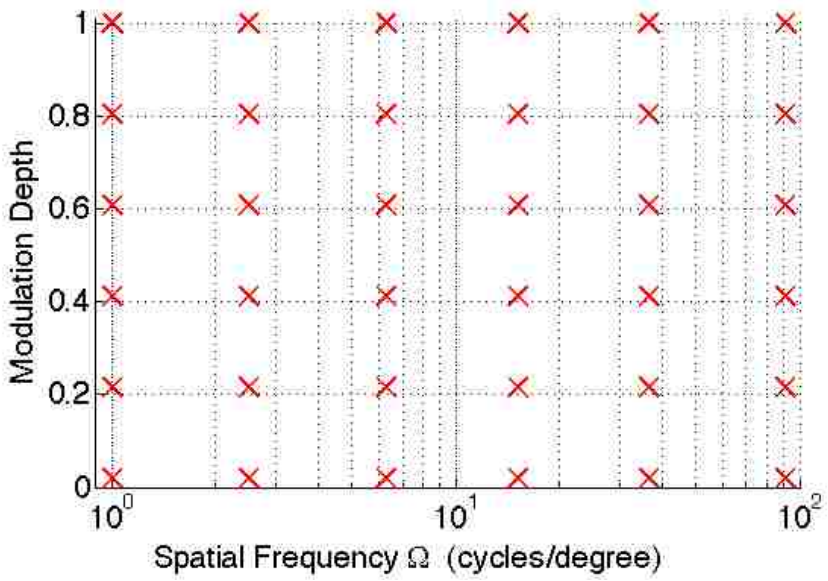

Figure 2.4: Example test parameters - 36 unique combinations of modulation and spatial frequency.

The experiment started with the combination that had the highest modulation

and the lowest spatial frequency. The next five states would be at this same modulation value, but with increasing spatial frequency (decreasing object size). After the smallest object was presented in the sixth combination, the seventh combination would be the next-highest value of modulation with the smallest spatial frequency. The spatial frequency would systematically increase for the next five combinations, until the modulation was changed for the 13th state. This progression would continue until all 36 unique combinations of modulation and spatial frequency were tested.

2.3.2.3 Operator Task

For the first category of testing, the operators were presented with a target line (represented by a thin rectangle) and a controllable line (also represented by a thin rectangle) similar to the method performed in Ref. [26]. The goal for the operator was to keep their shape superimposed directly over the target shape through all 36 combinations that made up an individual experiment. The operator's shape was proportionally larger than the target shape. Additionally, the operator's shape was bright red, which did not change color during a test. See Fig. 2.5 for a sample depiction of the visuals used.

During each combination, the individual would attempt to keep their controlled shape overlapped with the target shape as closely as possible for approximate six to eight seconds. At that point, the program would momentarily pause, the old shapes disappeared, and a "new" pair of shapes were displayed in the middle of the

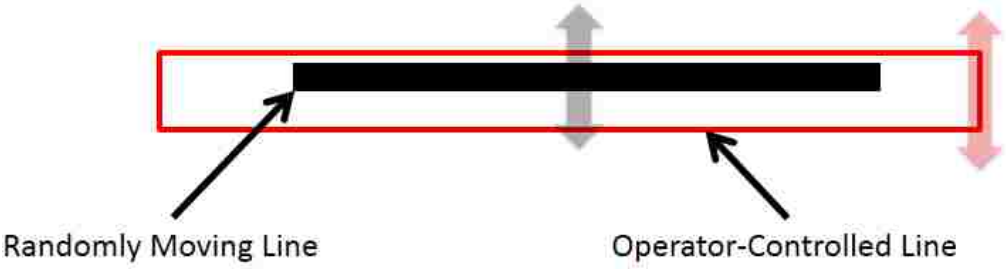

Figure 2.5: Sample visuals for experiment with lines.

computer screen. These new shapes had the contrast and size properties associated with another unique combination of modulation and spatial frequency, respectively. Pseudo-random motion of the target shape (as defined in Sec. 2.3.2.1) would restart, and the individual would attempt to overlap the shapes for the duration of this new combination.

This cycle of approximately eight seconds of testing per modulation and spatial frequency combination would continue until all 36 combinations had been tested.

2.3.2.4 Experiment Hardware and Software

The computer testing was performed using a desktop computer with built in display. The LED-backlit display had a diagonal screen measurement of 27 inches, and had 2560 horizontal by 1440 vertical pixel resolution in a 16:9 aspect ratio. The screen had relative "brightness" (luminosity) adjustments through the operating system software. This relative luminosity value was set at the middle preset (#8 out of 15 available) for the entire testing regime.

The input device was a USB gaming joystick. The joystick had the traditional

2-DOF (fore-aft & left-right) design, with the addition of a twist axis most easily described as yaw. Each axis had built-in springs to maintain static joystick position and provide tactile feedback of displacement. Each axis could output values for instantaneous displacement corresponding to a percentage of displacement possible for that axis. For example, in the lateral axis, full-left physical joystick deflection corresponded to an output value of 0, full-left physical deflection of 100, and the spring's static "neutral" position of 50.

$$L_O = (J - 50)K_{J,r} + \frac{P_v}{2} \tag{2.7}$$

The computer software took in the integer joystick displacement percentage values and computed a position on the computer screen. For this series of testing, the controlled shape had an output displacement that was a scaled version of the joystick input displacement (the system was "PC"). The scaling was performed by a joystick gain in the vertical axis $K_{J,v}$ which was multiplied by the joystick displacement from mid-point $J - 50$. This output displacement was added to the vertical midpoint of the screen ($\frac{P_v}{2}$). The final vertical location on the screen (in pixels) was then found from Eq. (2.7). For this testing, the gain $K_{J,v}$ was kept constant throughout at a value of 6 pixels. This value was chosen because it allowed the operator to displace the shape over the necessary screen area to complete all portions of the compensatory task, while not being qualitatively "overly-sensitive" per evaluations by the beta-testers.

The computer apparatus, shown in Fig. 2.6, was placed on an office desk, with

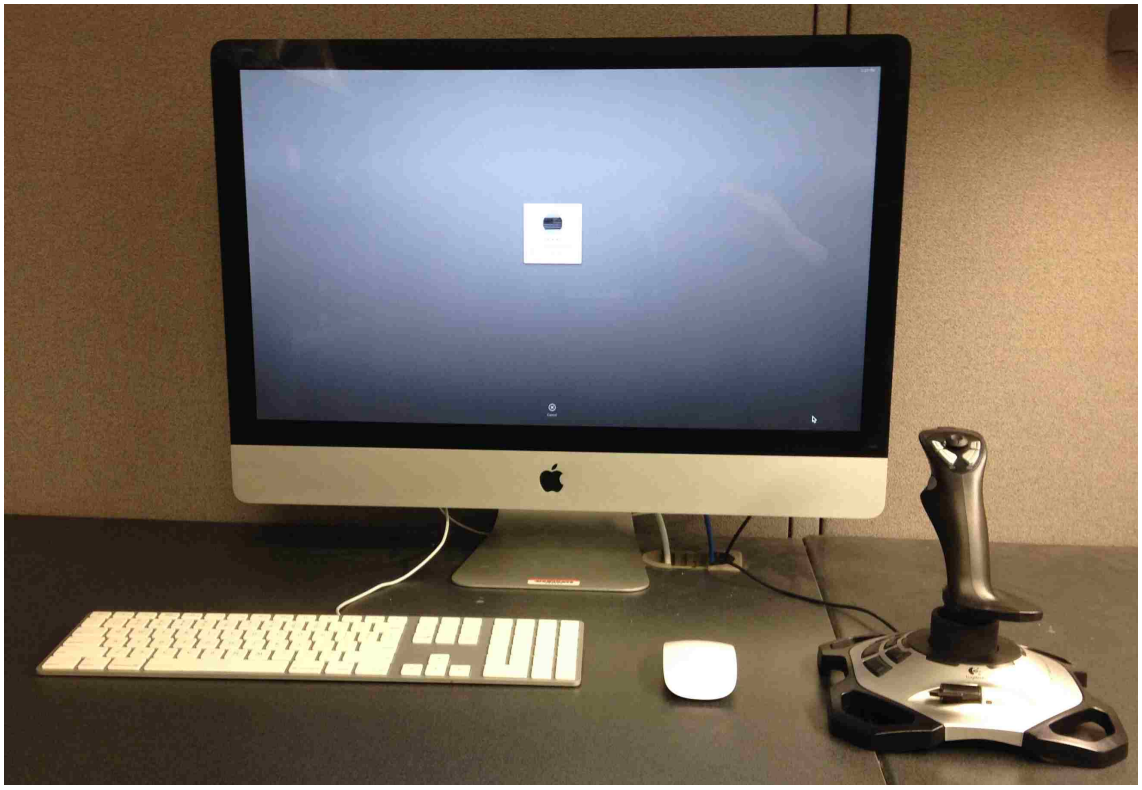

Figure 2.6: Computer appartus used in testing. Note: The keyboard was not used as an input device for this testing

space on the desk for the particular input device used by a given test (no test used simultaneous input from both the mouse and the joystick). Before each test, the user was seated such that the computer screen position and tilt was oriented directly towards their eyes, and that their eyes were 48 inches ($D = 48$) from the center of the screen.

2.3.3 Measurements and Representative Results

The computer program output up to 12 different parameters in a Comma-Separated-Value (CSV) file. These parameters were stored approximately every 16 milliseconds over the course of the test. A CSV file was generated for an operator

on each and every test they performed. An abridged example of the data recorded by this testing is shown in Table 2.2. An example time history showing how a few of the experimental parameters were determined is shown in Fig. 2.7.

The middle of the shape was used as the point to determine absolute location on the computer screen. The difference between the absolute location of the target L_T and the absolute location of the observer's shape L_O at any given time was determined to be the error E, as shown in Eq. (2.8). The operator's average error E_C was found for each of the 36 combinations of modulation and spatial frequency. This was the average amount of error in pixels that the center of the operator's shape L_O was off from the center of the target's shape L_T, as seen in Eq. (2.9).

$$E(t) = L_T(t) - L_O(t) \tag{2.8}$$

$$E_C = \frac{\sum_{t=t_i}^{t=t_f} |E(t)|}{(t_f - t_i)} \tag{2.9}$$

The average error for a modulation and spatial frequency combination was also found for the entire group. This value, $E_{C,G}$ was calculated using Eq. (2.10). This data was displayed in MTF format, with two representative examples of data shown below. A single operator's performance at each of the 36 combinations is shown in Fig. 2.8a and the group's average performance is shown in Fig. 2.8b.

$$E_{C,G} = \frac{\sum_{i=1}^{N} E_{iC}}{N} \tag{2.10}$$

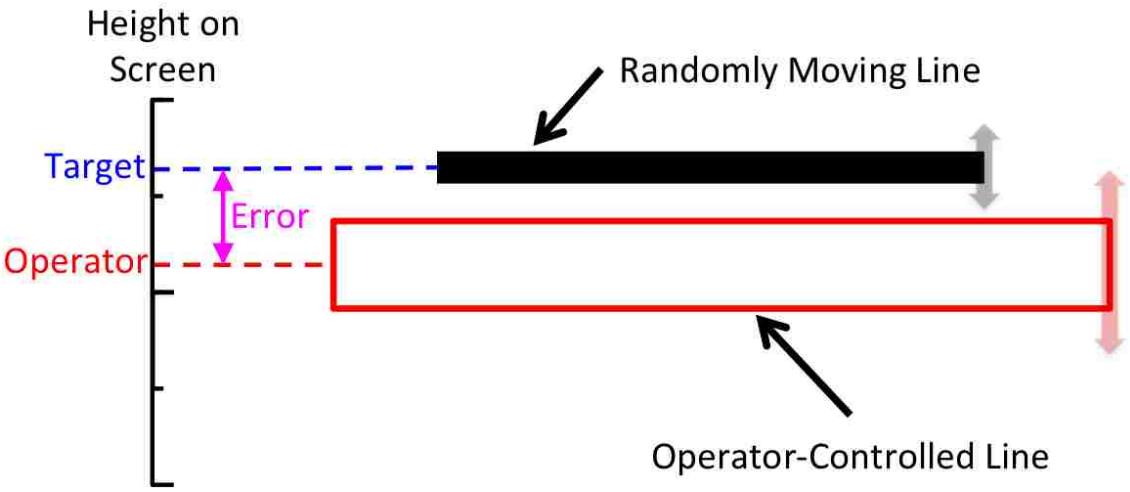

(a) Data extraction from test visuals

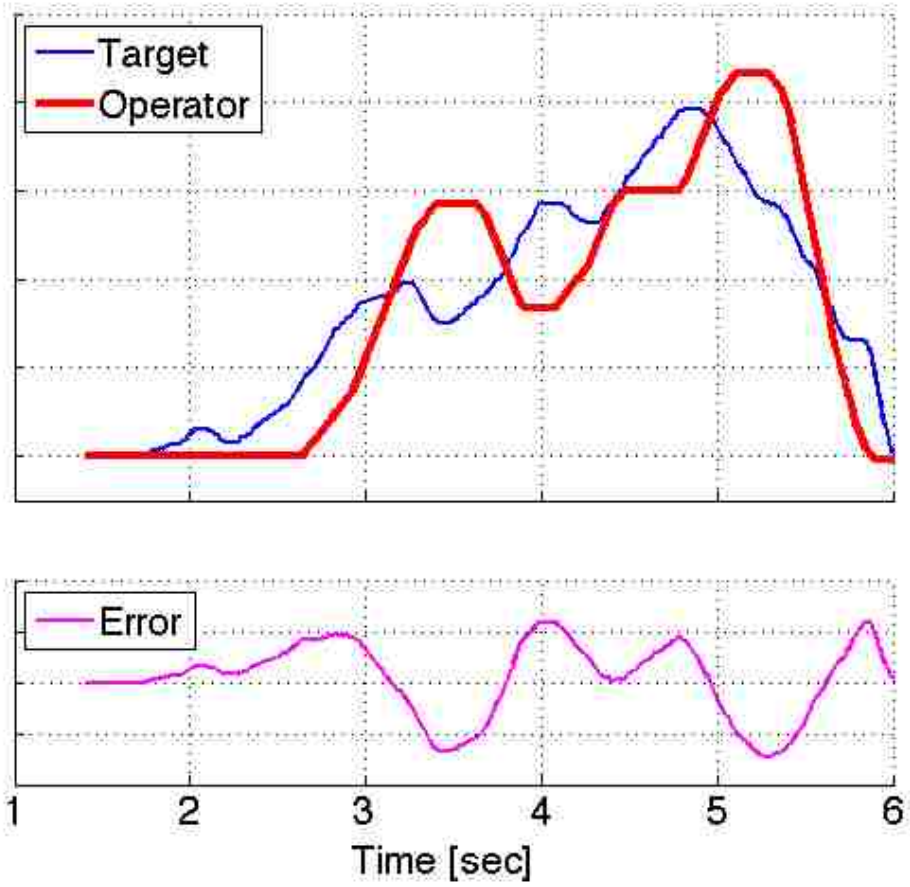

(b) Sample time histories

Figure 2.7: Sample measurements and time histories.

Table 2.2: Example measurements from line testing. These values were taken from the CSV files automatically generated by the computer program.

Reticle Pixels	Target RGB	Time [sec]	Target Location	Operator Location	Error [pixels]	Joystick %	Gain	Background RBG
182	0	1.713	400	400	0	50	6	255
182	0	1.729	401	400	1	50	6	255
182	0	1.745	402	400	2	50	6	255
182	0	1.761	403	400	3	50	6	255
182	0	1.777	403	400	3	50	6	255
182	0	1.793	404	400	4	50	6	255
182	0	1.809	404	406	-2	51	6	255
182	0	1.825	405	406	-1	51	6	255
182	0	1.841	405	406	-1	51	6	255
182	0	1.857	407	406	1	51	6	255
182	0	1.873	407	406	1	51	6	255

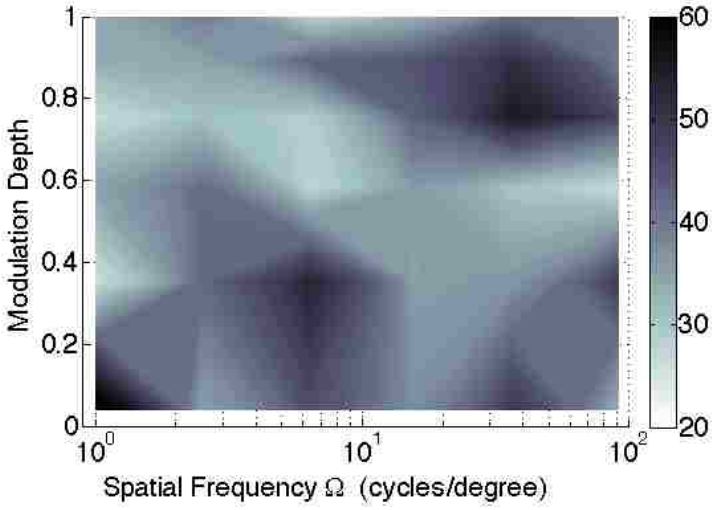

(a) Individual Error (pixels)

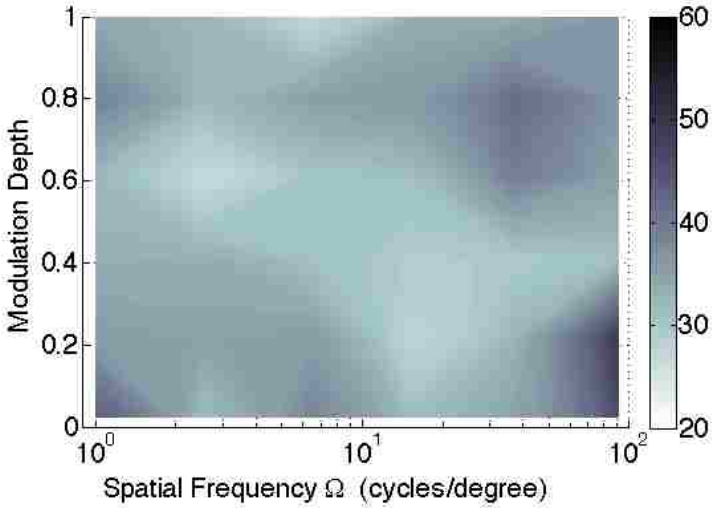

(b) Group Average Error (pixels)

Figure 2.8: Representative results for line experiments

2.3.4 Alternate Line Shapes

After the first few individuals were tested on this experiment, the group average errors showed a lot of variability across different values of modulation and spatial

frequency, with no noticeable trends. Some individuals tested made the comment that there was nothing "hard" about the test, even at the lowest values of contrast.

This was attributed to the specific visuals used in this testing. The smallest shape presented in this format was a "line" with a size of 600 pixels in the horizontal direction and a height of 2 pixels in the vertical direction. The spatial frequency of this shape was very high, around 91 cycles/degree in the vertical direction. However, the horizontal direction of the shape had a very low spatial frequency (approximately 0.3 cycles/deg), which corresponded to almost 4-inches on the computer screen. Even when the line was at its "thinnest" value of 91 cycles/deg in the vertical direction, the users were able to use the large horizontal size of the visual cue to complete the compensatory task.

Therefore, a variant to the line-based testing was developed using horizontally-shrinking lines. This test kept the vertical height of the lines constant at two pixels. The horizontal component of the line was then the variable, which ranged in size from 182 pixels down to the lowest value of two. The sample visuals for this variant are shown in Fig. 2.9.

2.3.5 Preliminary Results

Since the line-based tests were designed as a "Proof of Concept," only four individuals were tested. As mentioned above, the lack of trends in the group average error for the vertically-shrinking lines (Fig. 2.10a) resulted in the development of the second variant with horizontally-shrinking lines. Trends began to emerge with

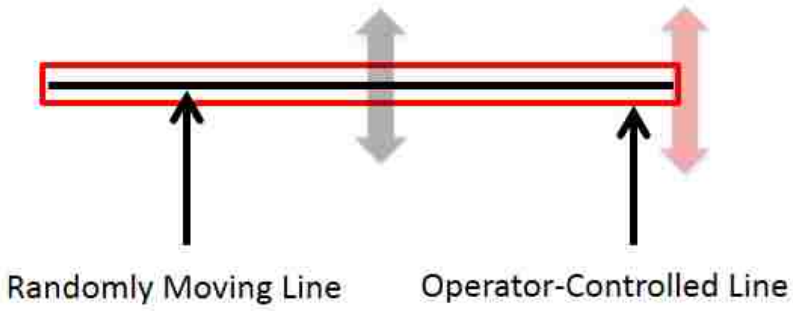

(a) Lower spatial frequency

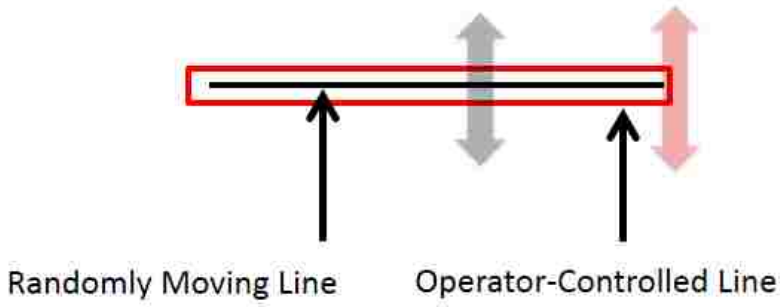

(b) Higher spatial frequency

Figure 2.9: Horizontally-shrinking lines example visuals. Note that the visuals in (a) have a lower spatial frequency than the visuals in (b) due the fact that target line is physicaly wider. The vertical size of both target lines were 2 pixels.

the horizontally-shrinking lines, as the group average error (Fig. 2.10b) showed a significant increase at the lowest values of modulation and at the largest spatial frequencies. The error well exceeded 60 pixels in Fig. 2.10b, however the same scales were used for both subfigures to emphasize the onset of error in the lower-right corner of the horizontally-shrinking case.

These preliminary results highlighted two key pieces of information for use with further testing.

First, the operator used the "major" dimension of the line in order to deter-

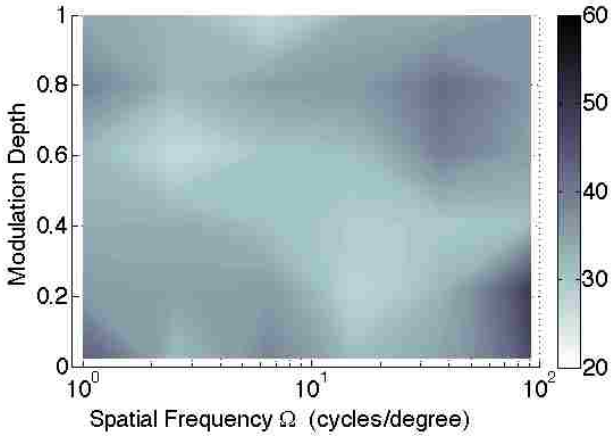

(a) Vertically-shrinking lines

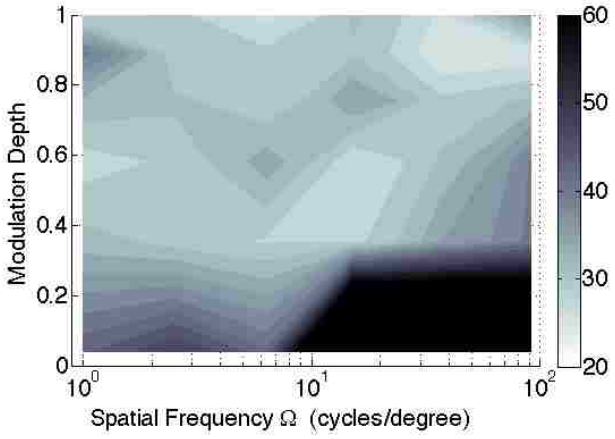

(b) Horizontally-shrinking lines

Figure 2.10: Group error for both line-based experiments.

mine its position. When the line was held sufficiently wide in the vertically-shrinking lines, there was almost no degradation in relative performance. In the second iteration, the only increase in relative error came at the lowest value of contrast, for the three smallest shapes. These three combinations were the points at which contrast was sufficiently low such that performance in tracking the smaller shapes began to deteriorate. The second key piece of information was that the dimensional compo-

nent of spatial frequency was highly important to further testing. As visual cues, the lines theoretically had an infinite number of spatial frequencies. The spatial frequency depended on the angle at which the two light-dark cycles were analyzed, as seen in Fig. 2.11.

2.4 Circle-based Experiments

2.4.1 Goal

Based on the preliminary results from the line-based tests, a second category of testing was developed using circles instead of lines for both the operator-controlled shape and the target shape. Circles were selected instead of lines because a circle has the same spatial frequency in both the vertical and the horizontal directions whereas a line (or rectangle) does not. This allowed for a more rigorous objective analysis of the effects of spatial frequency as a visual cue.

Additionally, this second series of tests included variants to examine the effects of control laws, input devices, and idealized spatial awareness. These variants will be discussed in their own individual sections.

2.4.2 Description of the Experiment

For the primary variant of the circle experiment, the compensatory task for the operator remained fundamentally the same from the line-based experiments. That is, the operator's task was to keep their shape (now the outer, larger, red circle) directly overlapped with the target shape (now the inner, fading circle) at all times.

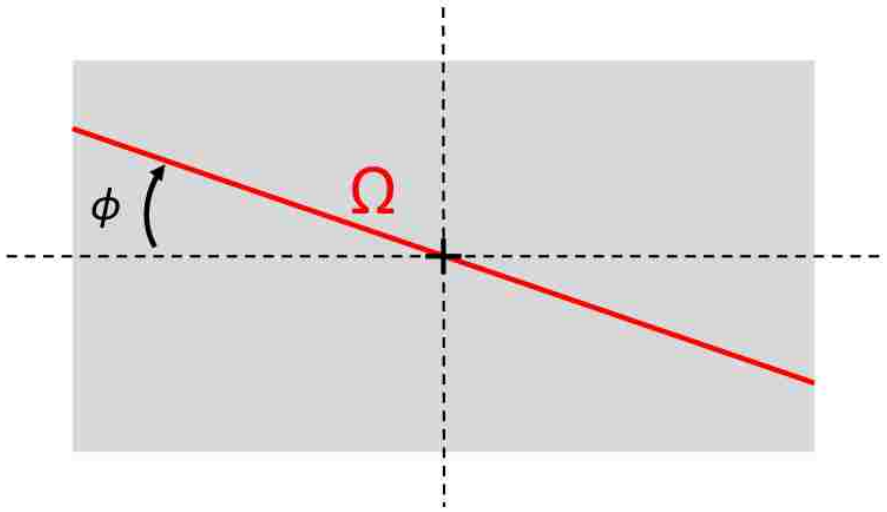

(a) Pictorial relationship

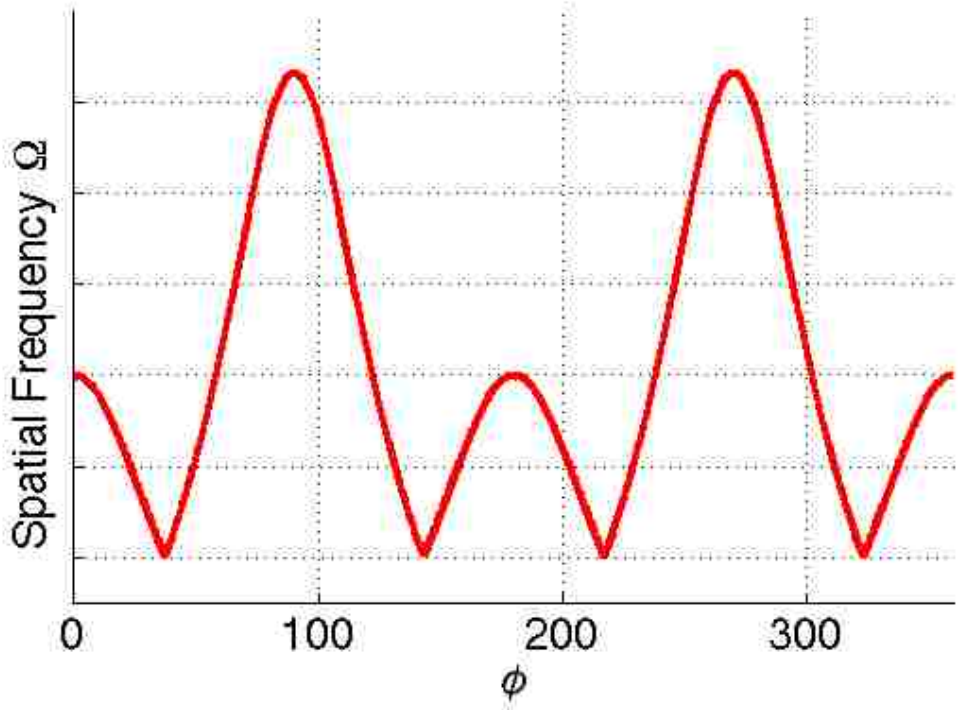

(b) Graphical relationship

Figure 2.11: Example of spatial frequency dimensionality. The rectangle in (a) is highlighted with a single spatial frequency Ω based on angle from the horizon ϕ used for analysis. As the angle ϕ [degrees] is increased, the resulting spatial frequency Ω varies as seen in (b).

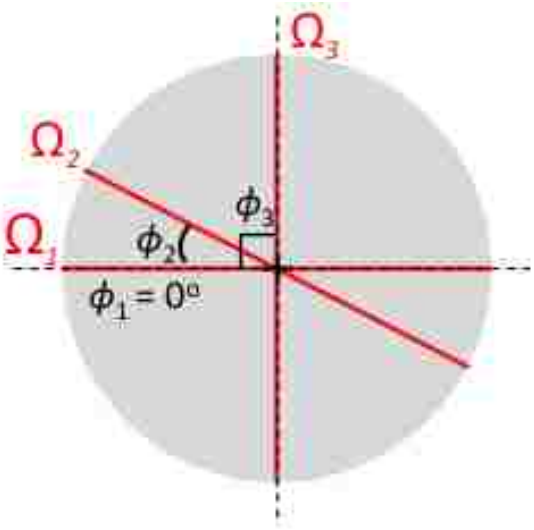

Figure 2.12: Spatial frequency representation with circles. Similiar to the method shown in Fig. 2.11, this circle has three different angles (ϕ_1, ϕ_2, ϕ_3) used for determining three spatial frequencies (Ω_1, Ω_2, Ω_3). However, since a circle has a constant diameter, the spatial frequencies are the same ($\Omega_1 = \Omega_2 = \Omega_3$) regardless of the angle used for analysis.

To be more precise, since circles were now being used, the goal was to actually keep the operator's circle *concentric* with the target circle. Sample visuals are shown in Fig. 2.13, with the operator too low in Fig. 2.13a and perfectly concentric (yielding no error) in Fig. 2.13b.

Besides using circles due to their non-dimensional spatial frequency, this entire series of testing also had an additional improvement. In the line-based experiments, the background was always kept at an RGB value of 255, associated with "pure" white. The prior method of changing the modulation was to simply fade the target line from an RGB value of "pure" black (0) to increasing RGB values that faded the line to varying shades of grey. At the lowest value of contrast (approximately 4% in the line experiment) the target was just slightly darker (slightly "less white" with RGB values around 245) than the pure white background. While this may be

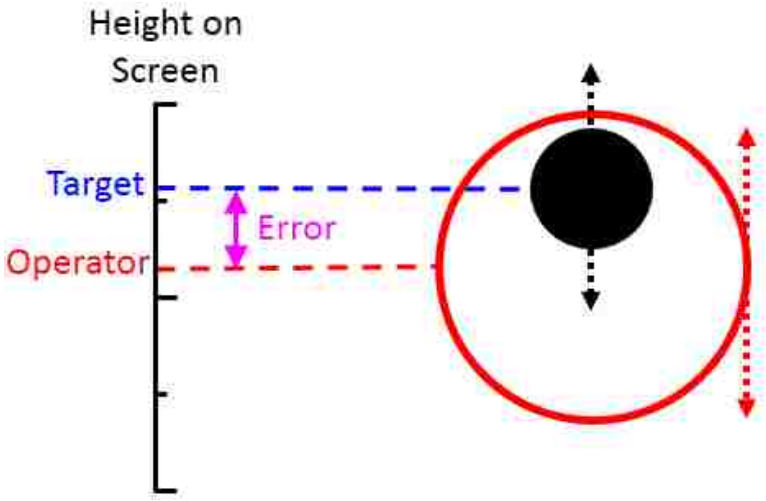

(a) Operator's shape too low

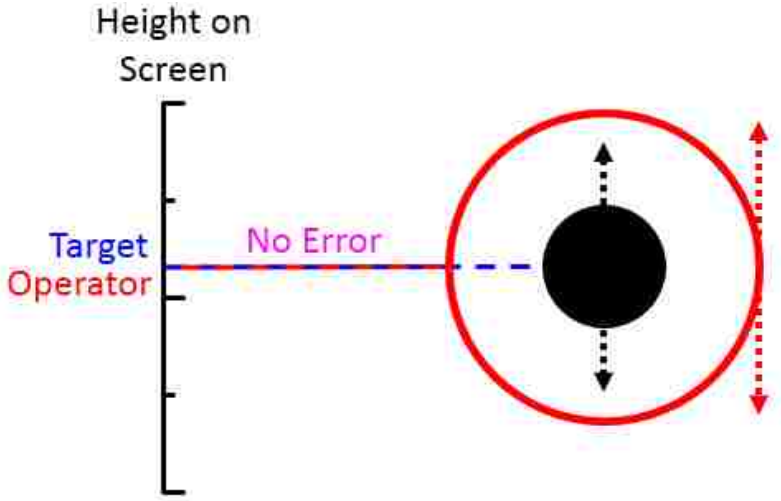

(b) Operator and Target concentric

Figure 2.13: Sample visuals used in circle-based experiments.

a fair idealized representation of the type of contrast seen in a snowy, "whiteout," type DVE, it does not idealize most other common causes of DVE.

For the circle experiments, both the target *and* the background would change RGB values to achieve a desired modulation. This was done to better idealize the (lack of) contrast available in a DVE scenario, whether from fog, brownout, rain,

etc. The background would initially start with a RGB value of 255 for pure white, and then over the course of the experiment, would change to varying levels of grey (never less then an RGB value of 128). Simultaneously the target RGB value would increase from the pure black of 0 to a grey value of no more than 127. Equation (2.1) can still be used to perform this calculation, but now the value of B' (background RGB value) will change concurrently with B (target RGB value).

An example of the visuals created by changing both the target and the background RGB values is shown in Fig. 2.14. The background has gone from white in Fig. 2.13 to a light grey. Additionally, the target circle also changed color from black in Fig. 2.13 to a dark grey in order to achieve the desired modulation.

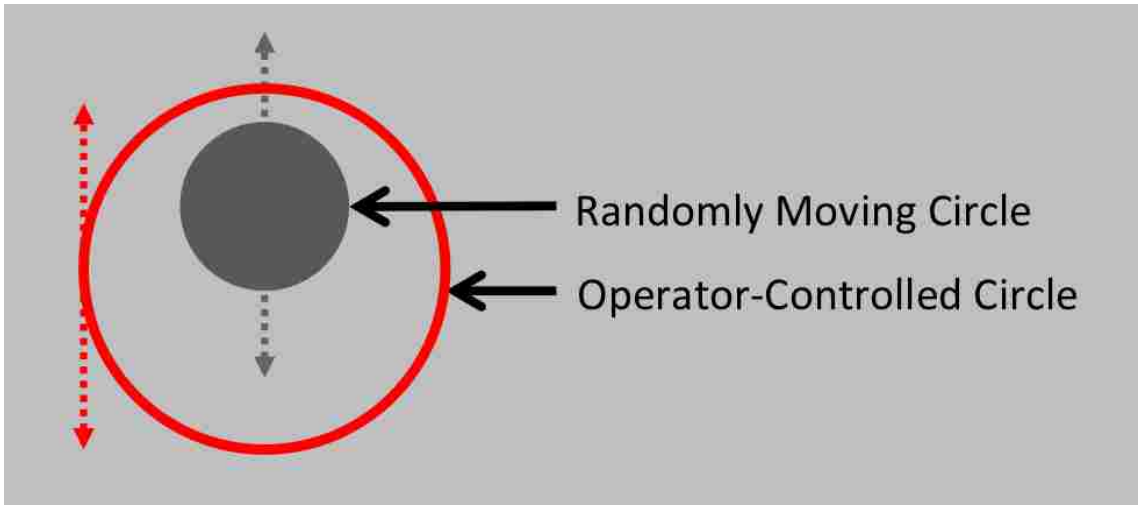

Figure 2.14: Sample sisual of fading target and background.

Other than the use of circles, and the dual-mode fading, the testing kept the same procedures from the line-based experiments.

2.4.3 Variants

The preliminary lessons-learned from the line-based testing allowed for the scope of the testing to expand using circles. First, in an effort to extend a portion of the work performed in Refs. [26, 32], different control laws were implemented for governing the dynamics of the controlled shape. Second, a small procedural variation was also included in an attempt to idealize operator spatial awareness in DVE conditions. This idealized spatial awareness included the use of different input devices. This allowed for a comparison on performance of the compensatory tasks using the joystick followed by the use of a traditional computer mouse.

In total, there were six unique circle experiments performed. They are listed below, and the details of the variations will be described in the following sections:

- Outer-Circle controlled by Joystick (Proportional Control)
- Outer-Circle controlled by Joystick (Rate Control)
- Inner-Circle controlled by Joystick (Proportional Control)
- Inner-Circle controlled by Joystick (Rate Control)
- Inner-Circle controlled by Mouse (Proportional Control)
- Inner-Circle controlled by Mouse (Rate Control)

2.4.3.1 PC and RC Dynamics

In order to gain better insight into the relation between MTF-based visuals and input control laws, the Rate Control (RC) variation of the experiment was developed. For the RC dynamics, a constant operator control displacement generated a constant *rate* of the controlled circle. The block diagram for the resulting RC system is shown in Fig. 2.15b.

In order to accomplish the the desired dynamics, the coding of the software had to be changed. For the PC system, the scaled joystick displacement directly determined the location on the screen per Eq. (2.7). For a RC system, the operator input would directly specify only a velocity of the shape (not the velocity *and* the position). The velocity V was determined from the joystick input as:

$$V = K_{RC} * (J - 50) \tag{2.11}$$

where K_{RC} is the unique gain for the Rate Control system. The value of K_{RC} was held at 0.2 for this testing, and the $J - 50$ term determined the joystick deflection from the static neutral point of 50%. The velocity V had a unit of pixels per code iteration.

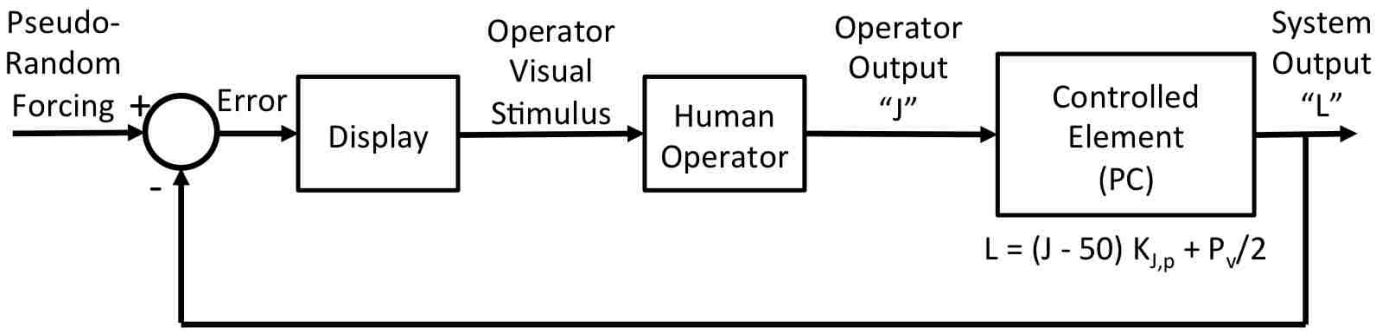

(a) Joystick with proportional control

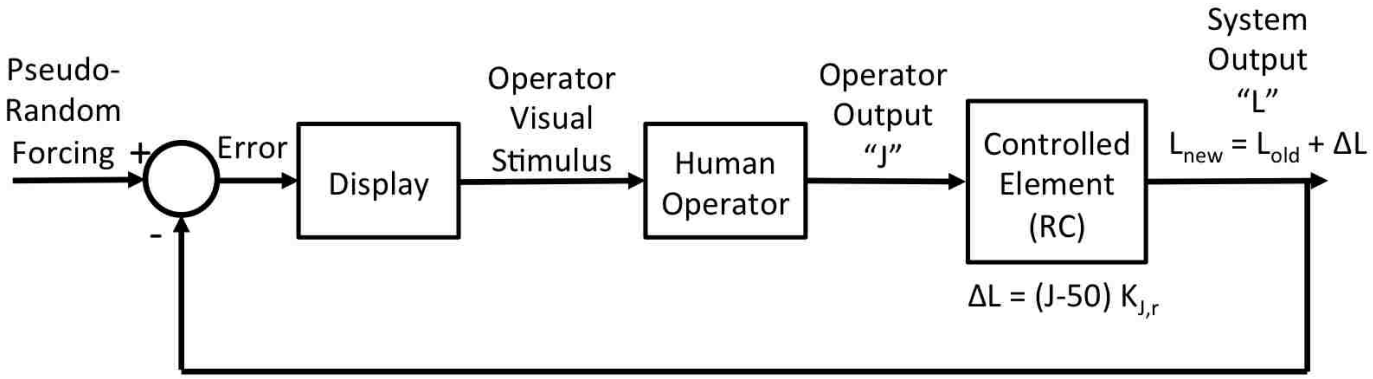

(b) Joystick with derivative control

Figure 2.15: Joystick experiment block diagram - adapted from Ref. [26].

The velocity of the shape found in Eq. (2.11) was converted into a change in location on the screen. The underlying computer source code would perform one iterative loop approximately every 16-milliseconds, which included all necessary calculations and display visual updates. Therefore the code loop time of 16-milliseconds was used for the Δt value in Eq. (2.12) to determine the change in location on the screen ΔL of the operator-controlled shape:

$$\Delta L = V\Delta t \approx V \times (0.016\text{-seconds}) \tag{2.12}$$

Once the approximation for the change in the shape's location for the present cycle of code ΔL was known, the position of the shape required a simple update. The change in location was added to the old location of the shape L_{old} providing a new location L_{new} per Eq. (2.13).

$$L_{new} = L_{old} + \Delta L \tag{2.13}$$

The new location was used by the code to draw the shape on the screen at the end of the 16-millisecond cycle. The raw location data was also stored by the program in the CSV file for analysis purposes.

2.4.3.2 Controlled Inner Circle - Joystick and Mouse

In the first variant, the operator controlled the outer, red circle, while the target circle would change contrast over the course of the experiment (as described in Sec. 2.3.2.3). This was a highly-idealized, 1-DOF representation of a pilot that

was meant to study the pilot's ability to execute a simple task when given visual cues of various characteristics.

In the second version, the individual instead controlled the smaller, inner circle. This circle was also the one that would change values of contrast over the course of the test. This meant the individual would have trouble seeing their own position at various times during the test, but could always see the desired position of the randomly-moving red circle. This was a highly-idealized, 1-DOF representation of a pilot losing spatial awareness. This version was intended to study the the pilot's spatial awareness when given visual cues of various characteristics.

These two variants were also modified to quantify the effect of type of input device on operator performance. Instead of using the joystick, a computer mouse was used.

The joystick had built-in springs that helped "reset" the joystick position to a neutral point when the operator relaxed pressure. Due to its inherent characteristics as an input device, the mouse lacked this "feature." Therefore, the testing software was modified such that the relative displacement of the mouse was reset to zero between a specific modulation and spatial frequency combination, acting as a software "neutral point." This kept the operator from having to physically reset the mouse to a particular location on the desk during the brief pause between combinations. Having to physically move the mouse would have introduced a great deal of random error, as it essentially would have been an *additional* compensatory task unrelated to the one under experimental investigation.

Since the mouse resulted in a different input value to the computer program,

the equations governing the shape motion also had to be adjusted. A constant displacement of the mouse from the software "neutral point" resulted in a constant value of displacement from the middle of the screen. The gain of the mouse was determined by the Operating System (OS) settings of the computer. Like the screen luminosity software setting mentioned in Sec. 2.3.2.4, this value was also relative. This "OS gain" K_{OS} his was kept constant at preset "8" out of 10 (where 10 was the fastest) in the "tracking speed" section of the computer "System Preferences."

This setting was qualitatively chosen (similar to the numeric gain values associated with the joystick) such that the operators could make their shape cover the full range of the screen with modest physical displacements of the mouse on the desk. It is important to note that the numeric value of the software gain K_{sw} is not directly known. This software gain is multiplied within the operating system by the physical displacement of the mouse on the desk δ_M. This determines the location on the screen L in accordance with Eq. (2.14).

$$L = (K_{OS}\ \delta_M) + \frac{P_v}{2} \tag{2.14}$$

$$L = M + \frac{P_v}{2} \tag{2.15}$$

where L was location on the screen in pixels, M was the reported mouse location from the computer OS, and $\frac{P_v}{2}$ was the vertical midpoint of the screen in pixels.

The first numeric value reported to the experimental software is that of the resulting mouse location M from the computer's operating system. Therefore,

Eq. (2.15) better represents the determination of the shape's vertical location on the screen L based off the operator's input. The time history of both the resulting mouse location and the shape's vertical location on the screen were recorded by the software and logged in the CSV file for each operator tested.

The mouse RC input required similar steps to the joystick RC case discussed earlier in this section. Equation (2.16) was used to find the shape velocity V:

$$V = K_{M,r}\ (M - \frac{P_v}{2}) \tag{2.16}$$

where $K_{M,r}$ was the gain of the mouse for this RC system, M was the reported mouse location from the computer OS, and $\frac{P_v}{2}$ was the vertical midpoint of the screen in pixels. The value of $K_{M,r}$ was set to 0.03 in order to keep the velocities at values that allowed a qualitatively sufficient operator response to the movement of the target shape, without being overly "sensitive."

The velocity V was used in Eqs. (2.17) to determine the updated location of the operator controlled shape on the screen L_{new} similar to the method used in Eqs. (2.12)-(2.13). At the beginning of each combination of modulation and spatial frequency M was re-assigned to be equal to $\frac{P_v}{2}$, and L_{old} was reset to 400 pixels (the middle of screen).

$$L_{new} = L_{old} + V \times (0.016\text{-seconds}) \tag{2.17}$$

The experimental block diagrams for the Mouse PC and the Mouse RC are shown in Fig. 2.16.

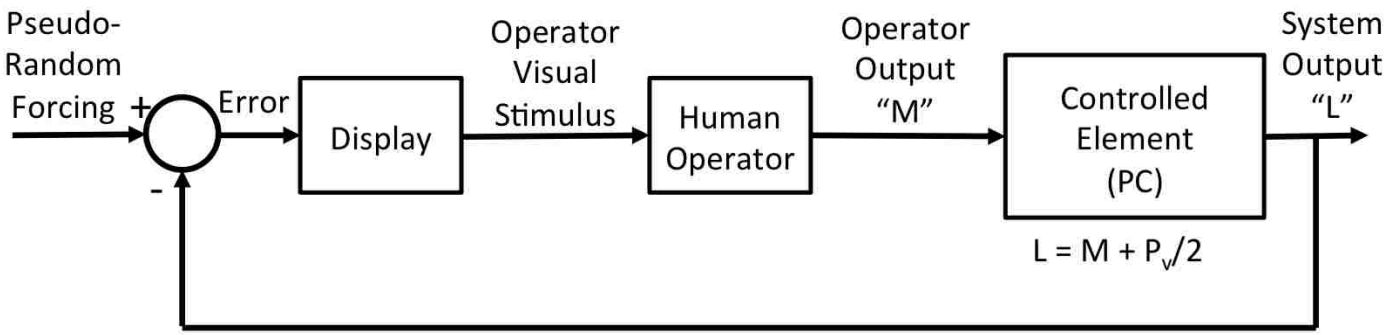

(a) Mouse PC Block Diagram

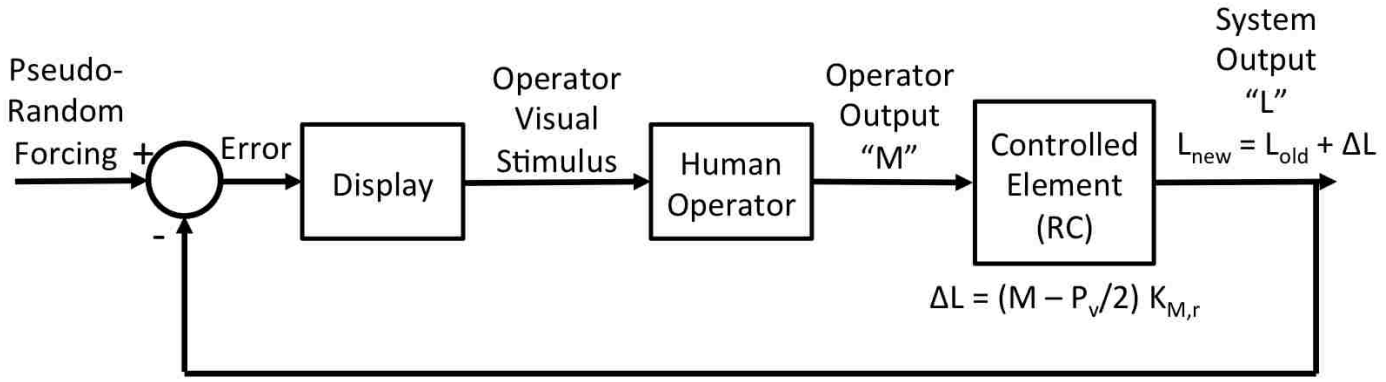

(b) Mouse RC Block Diagram

Figure 2.16: Mouse experiment block diagram - PC and RC. Note that the equations governing the PC dynamics shown in (a) are given in Eq.2.15. The RC dynamics were governed by Eqns. 2.16 and 2.13. This block diagram was adapted from Ref. [26].

2.4.3.3 Summary

In summary of the "Controlled Inner Circle" sub-section, there were four total experiments. These experiments, and their respective equations are:

1. Joystick PC - Equation (2.7).
2. Joystick RC - Equations (2.11) - (2.13).
3. Mouse PC - Equations (2.14) - (2.15).
4. Mouse RC - Equations (2.16) - (2.17).

2.5 Lateral Repositioning Experiments

2.5.1 Goal

The third type of tests used circles as a highly-idealized representation of the Lateral Repositioning MTE in DVE. The current ADS-33E criteria are based on the ability to make "aggressive and precise corrections with confidence and (good, fair, or poor) precision" (Ref. [8]) in DVE conditions. The goals of this testing were (i) to determine the basic effects of contrast and size on the ability of the pilot to complete the idealized maneuver; and (ii) to determine if various subjective characteristics of the operators' responses such as "confidence" and "precision" could be quantified in relation to the MTF of the visual cues presented.

2.5.2 Description of the Experiment

In all cases of the idealized lateral repositioning task, the target circles were the shape that changed in both contrast and spatial frequency. The user controlled the larger red circle. This compensatory task was the same as the previous circle experiment except the targets moved horizontally. The control law over the user's circle was solely Rate Control, which was calculated as before by Eq. (2.11). This category of testing also used 36 combinations of modulation and spatial frequency. The modulation values used were $\mathbf{M}$ = [1.00, 0.80, 0.61, 0.41, 0.22, 0.02] and the spatial frequencies were Ω = [1.00, 2.50, 6.29, 15.19, 36.45, 91.14] cycles/degree.

The target circle's pseudo-random movement was horizontal and was limited to approximately one half of the computer screen. To start off a combination, the user would track the pseudo-random horizontal movement of the target on the left half of the screen (Fig. 2.17a). After three to four seconds, the target circle would instantaneously shift to the right half of the screen and resume pseudo-random movement. At the same time, a stationary green circle would appear near the upper left of the screen (Fig. 2.17b).

The green circle (highlighted with the letter "A" in Fig. 2.17b) was used as a visual cue in aiding the operator during some of the combinations. For instance, if the operator was having trouble tracking the first target circle on the left side of the screen (due to low modulation and/or high spatial frequency) the operator may not know when it was time to look to the right side of the screen to acquire the second target. This green circle let the operator know to begin visually searching on the

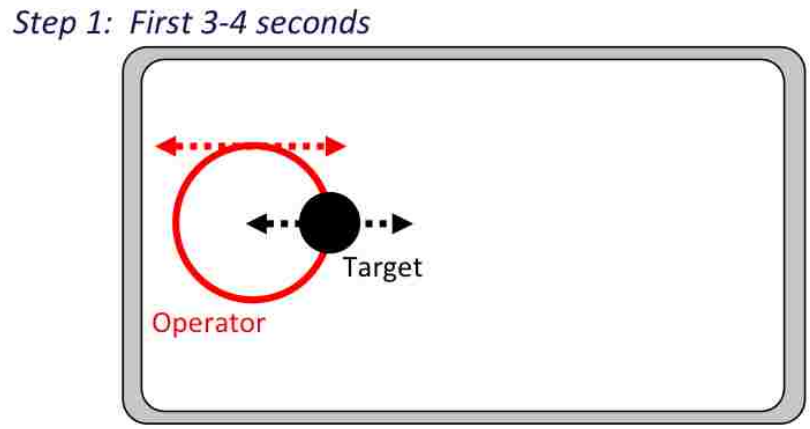

(a) First Compensatory Task

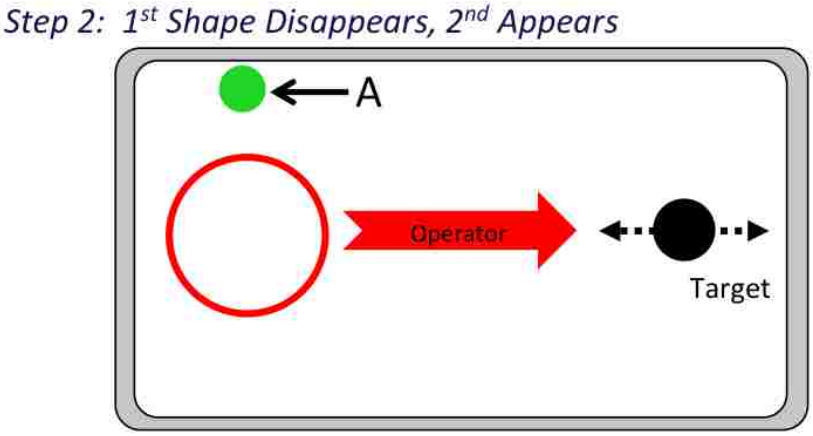

(b) Lateral Repositioning Task

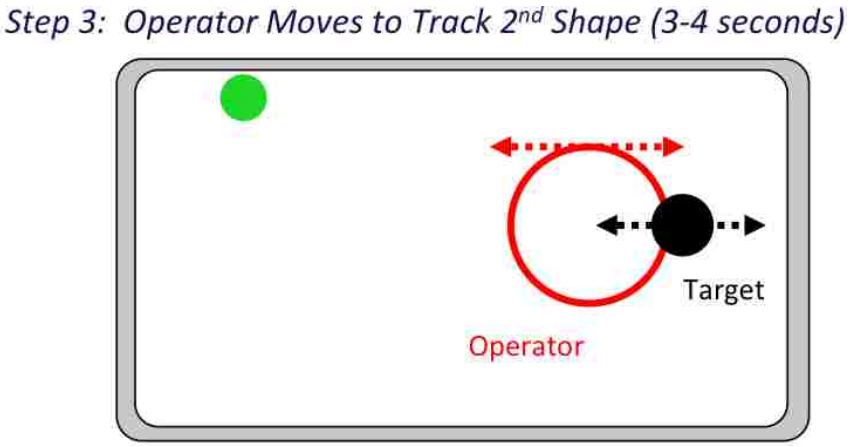

(c) Second Compensatory Task

Figure 2.17: Example visuals used in idealized lateral repositioning. The circle labeled with an "A" was used as a supplemental cue.

right side of the screen. The green circle does not represent any practical component of the Lateral Repositioning MTE; it is simply an aid to the experimental testing.

After the first target circle disappeared (and the green cue simultaneously appeared), the operator would visually acquire the "new" target position and laterally reposition their circle to the right side of the screen. The second compensatory task would begin, which required the operator to again track the pseudo-random movement of the second target circle (this time on the right side of the screen, as seen in Fig. 2.17c).

After an additional three to four seconds for the second compensatory task, the program would momentarily pause to change combinations. Similar to previous testing, the target shape would reset to the left side of the screen, and would change modulation and/or spatial frequency. A new combination would begin with tracking pseudo-random movement on the left side of the screen, and the process would iterate until all 36 unique combinations had been presented.

2.5.3 Variants

This experiment only had one variant. This variant added a delay of approximately 160-milliseconds on the operator's joystick displacement inputs to the compensatory system. This was done by storing the operator's joystick displacements in a ten-position vector such that the current inputs were not immediately used by the software to change the operator-controlled shape's position.

The "oldest" value of control displacement from this ten-position vector was

used to update the velocity (and thus the position) of the operator's shape. This value was then deleted from the end of the vector, and the remaining nine values were shifted one index to the right. The current value of the operator's control displacement was placed in the first index of the vector for storage.

The software code would then iterate, read the current joystick position, update the control-displacement vector, and refresh the position of the shapes on the screen. Since each iteration of the software took about 16-milliseconds, the ten-position vector of joystick displacements resulted in a delay of approximately 160-milliseconds before an input would be used by the software to move the operator-controlled shape on the screen.

The visuals and the testing procedure for this variant remained unchanged other than the control-input delay.

2.6 Test Population

The tested population includes a mix of both military personal and graduate students. In total, 25 personnel participated in one or more of the tests associated with the present work. From this population, 18 personnel had piloting experience, with 16 of those being current or former military aviators. Of the 18 people with flight experience, half of those had time flying rotorcraft. Fourteen of the 18 personnel with piloting experience reported their flight time, with the average reported experience being just over 2600 flight hours. Six of the military aviators had a flight test background.

Chapter 3: Results

This chapter chapter discusses the results of the present research. The experimental results will be presented in the order that each category was developed and tested. The MTF format (spatial frequency vs. modulation) was used to present most of the results with associated tabular data included where applicable.

3.1 Line-based Experiments

3.1.1 Vertically-Shrinking Lines

As mentioned in Section 2.3.5, the results of the vertically-shrinking lines showed a lot of variability with no noticeable trends. The MTF contour plot associated with this small portion of testing is shown in Fig. 3.1a.

The average error values for a given combination were fairly low, ranging from approximately 30 to 40 pixels across the sample population. The only portion of the MTF that shows a high amount of relative error is in bottom right corner of the contour plot, where the values increase to approximately 50 pixels of error. This corner corresponds to the lines with the two lowest modulation values (approximately 20% and 2% for this experiment). These lines also had the highest spatial frequency, at

approximately 91 cycles/degree, corresponding to a line height of just 2 pixels on the computer screen.

The increase in relative error for these two combinations show that the low modulation values start negatively affecting operator performance when coupled with visual cues of small size. However, the test population noted that this experimental testing was not very challenging, as the horizontal component of the line was still qualitatively sufficient for performing the compensatory task. Recall that the horizontal section of the target line was held constant at approximately 600 pixels wide, which corresponded to approximately 4 inches on the computer screen. Even when the combination called for a spatial frequency of 91 cycles/degree, it was still a 600-pixel wide by 2-pixel high visual cue.

In order to gain additional insight into the relative error increase that manifested in the bottom right corner of Fig. 3.1a, the next variant was developed and tested as mentioned in Section 2.3.4.

3.1.2 Horizontally-Shrinking Lines

For this variant of line testing, the vertical height of the lines was held constant at two pixels. The horizontal component of the line was then the variable, which ranged in size from 182 pixels (corresponding to a spatial frequency Ω of 1.00 cycles per degree) down to the lowest value of 2 pixels ($\Omega = 91.14$ cycles per degree).

The average group error for each of the 36 combinations is shown in Fig. 3.1b. This data showed better consistency across the tested population. A majority of the

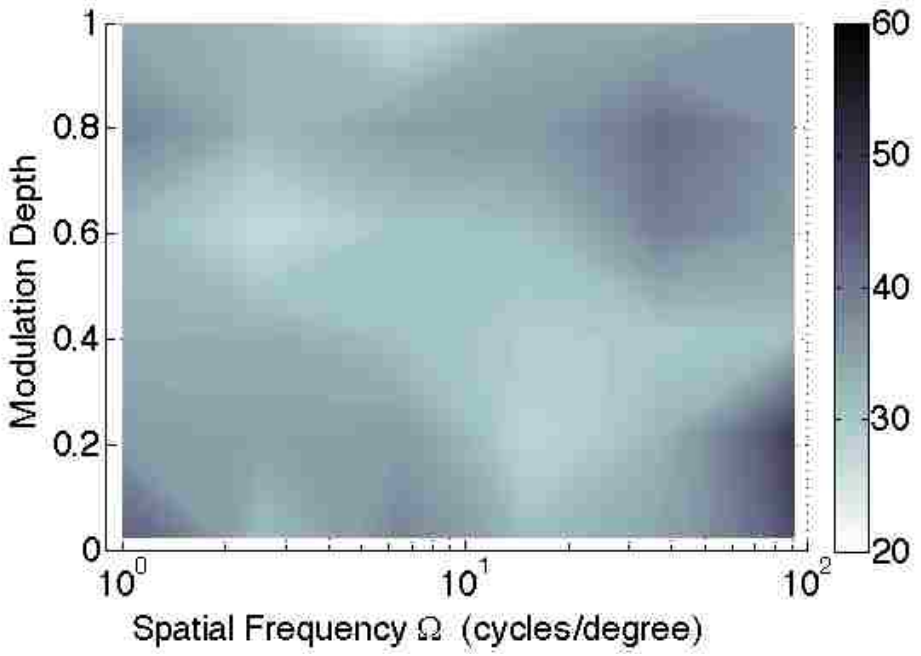

(a) Vertically-Shrinking Lines Group Error (pixels)

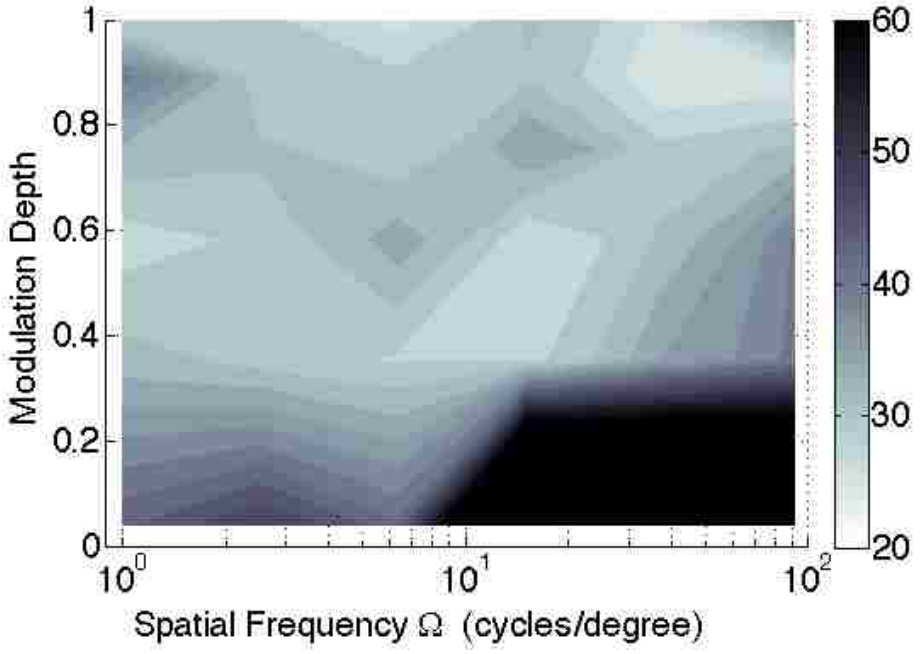

(b) Horizontally-Shrinking Lines Group Error (pixels)

Figure 3.1: Group average error (pixels) for line-based experiments

test points had error values consistently around 30 pixels, which is represented by the darkest regions. These lower values for error generally occurred at modulation values of approximately 40% and higher, with no variation in regards to spatial frequency.

The relative error began to increase once the modulation was reduced below 40%, as seen in the bottom portion of Fig. 3.1b. There was a slight increase for the largest objects at this low modulation, as seen in the lower-left portion of the contour plot.

A large increase in average error developed as the size of the cues was reduced, as shown in the lower-right portion of the contour plot. At the lowest modulation (approximately 4% for this experiment), the combinations with the three smallest target lines had average error values of approximately 110 pixels. When comparing visual cues of the same size, but at higher modulation values, this represents a relative increase in error of almost 300%.

The results from this variant showed that reducing modulation and reducing object size negatively affected compensatory task performance. Objective trends began to emerge with specific regards to spatial frequency. While smaller objects are intuitively harder to track, the MTF shows the ability to numerically describe degradation in task performance.

However, the stark difference in results between the vertically-shrinking variant (Fig. 3.1a) and the horizontally-shrinking variant (Fig. 3.1b) show that there was a dimensional component to the present work that needed further analysis.

3.1.3 Spatial Frequencies for non-circular shapes

The differences in results for the vertically-shrinking lines and the horizontally-shrinking lines show that the shape of the object has an important effect on its spatial frequency that needed to be addressed.

When the lines were shrunk vertically, the *minor* axis was the only axis to change spatial frequency between combinations, while the *major* axis stayed constant at a length of 600 pixels. The smallest shape for this case was 600 pixels wide and 2 pixels tall, which was a thin (but wide) line. The horizontal component of the target provide a visual cue 600 pixels wide, which corresponded to a spatial frequency of 0.30 cycles/degree in that axis.

Overall, the smallest target presented as a visual cue had a spatial frequency of 91 cycles/degree vertically and 0.30 cycles/degree horizontally. An example of an object having different spatial frequencies in different dimensions is shown in Fig. 2.11, which is repeated from Chap. 2.

This large difference between the spatial frequencies in the two dimensions helps account for both the "quantitative" ease (i.e., the low average error values) and the "qualitative" ease (reflected by the operators' comments) with which this test could be performed. The low spatial frequency of the horizontal axis appeared to provide a sufficient visual cue to perform the compensatory task, with only two of the 36 combinations having a combination of modulation and spatial frequency that resulted in increased error. These two combinations were both at the smallest object size for this variant, and at the two lowest modulation values as shown in

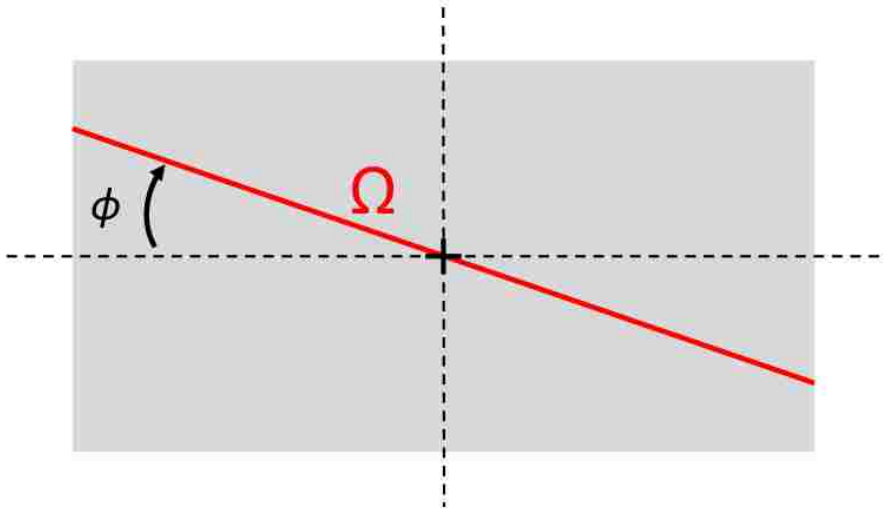

(a) Pictorial relationship

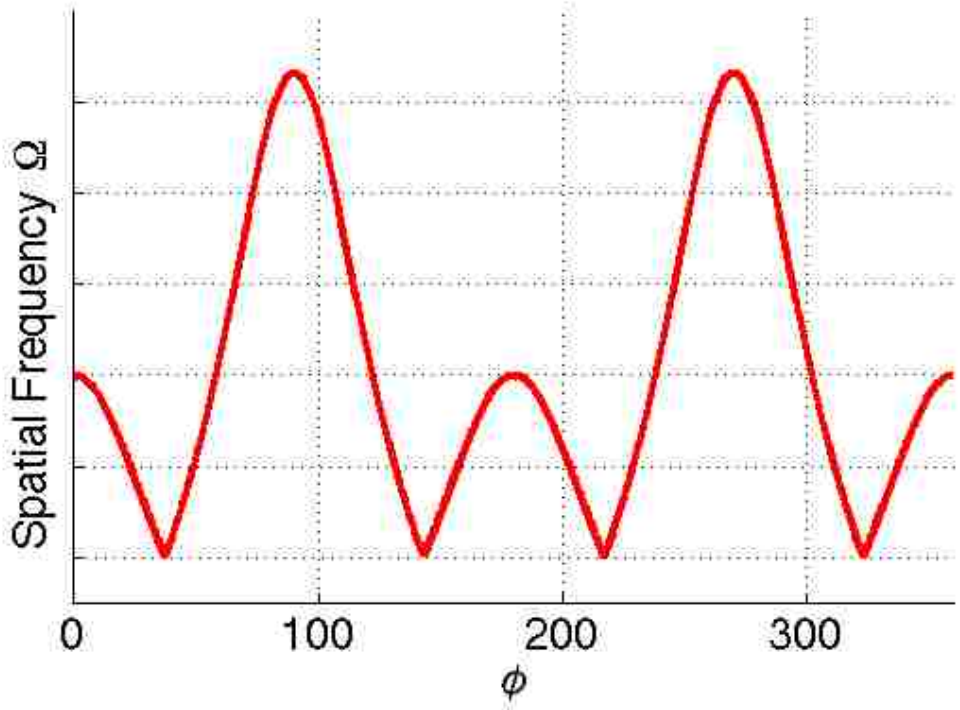

(b) Graphical relationship

Figure 2.11: Example of spatial frequency dimensionality. The rectangle in (a) is highlighted with a single spatial frequency Ω based on angle from the horizon ϕ used for analysis. As the angle ϕ [degrees] is increased, the resulting spatial frequency Ω varies as seen in (b). This figure repeated from Chapter 2.

Fig. 3.1b.

When the lines were shrunk horizontally in the second variant, only the *major* axis changed spatial frequency, and the vertical axis was held 2 pixels high. As the horizontal axis cue shrunk from 182 pixels wide down to 2 pixels wide, the spatial frequency in this axis began to come numerically closer to 91 cycles/degree. This is the same value of spatial frequency that was held constant in the vertical axis for this variant.

The smallest shape was therefore 2 pixels wide and 2 pixels tall, which was essentially a small square with a spatial frequency of 91 cycles/degree in both axes. However, a diagonal spatial frequency analysis (such as Ω_2 in Fig. 2.11) shows that there are still multiple spatial frequencies being presented to the operator when a square is used.

In order to provide a more rigorous analysis of the effect of spatial frequency on compensatory task performance, further testing would need to determine whether there is one ore more single spatial frequencies that the pilot prefers as a visual cue.

3.2 Circle-based Experiments

The results from the previous section showed that a generic shape contains several values of spatial frequency, which appears to affect the results of the test.

Therefore, a second series of tests used circles instead of lines, because circles only have one spatial frequency. Figure 2.12, repeated from Chap. 2, is again shown to highlight the constant spatial frequency ($\Omega_1 = \Omega_2 = \Omega_3$) associated with a circle.

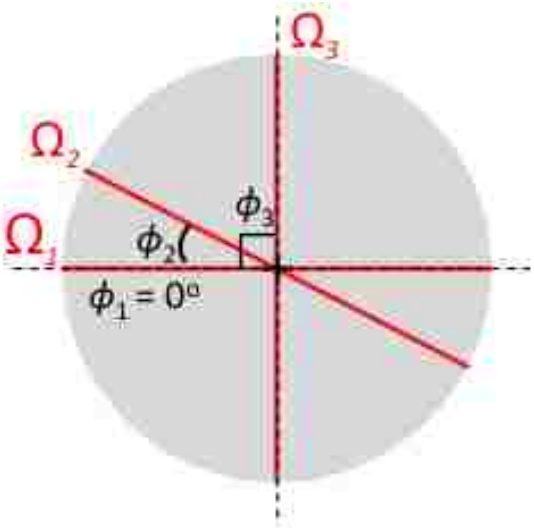

Figure 2.12: Spatial frequency representation with circles (repeated from Chp. 2).

3.2.1 Measurements and Example Time Histories

An example time history for a single operator performing this series of testing is shown in Fig. 3.2. The relative vertical position on the computer screen of both the target and the operator are shown in the top part of the plot. The corresponding error between the two (in pixels) is shown on the bottom part of the plot. This six second time history is for one specific combination of modulation and spatial frequency (in this case $\mathbf{M} = 1.00$, $\Omega = 1.00$).

The operator performed the task well in region A. This is evidenced by the relative proximity in the position of both shapes on the top portion of the figure and the corresponding low *average* value of the error in region A on the bottom portion of the figure. An aggressive overshoot is seen in region B, followed by the operator aggressively correcting in region C. This operator had an average error value for entire combination shown in the time history of 29.2 pixels.

A time history of three additional operators is overlaid on this same data in Fig. 3.3. This data is for the same single combination of modulation and spatial frequency. This figure highlights the variability between the individual operators performing the compensatory task. While the magnitude of the error values were different, the error curves in the bottom portion of the plot have a similar shape.

The average error for a single combination was found for each operator. These values are shown in Fig. 3.4 for all 36 combinations. Each operator had different levels of average error for a given combination. However, as the test moved towards lower contrast values, the group average error increase.

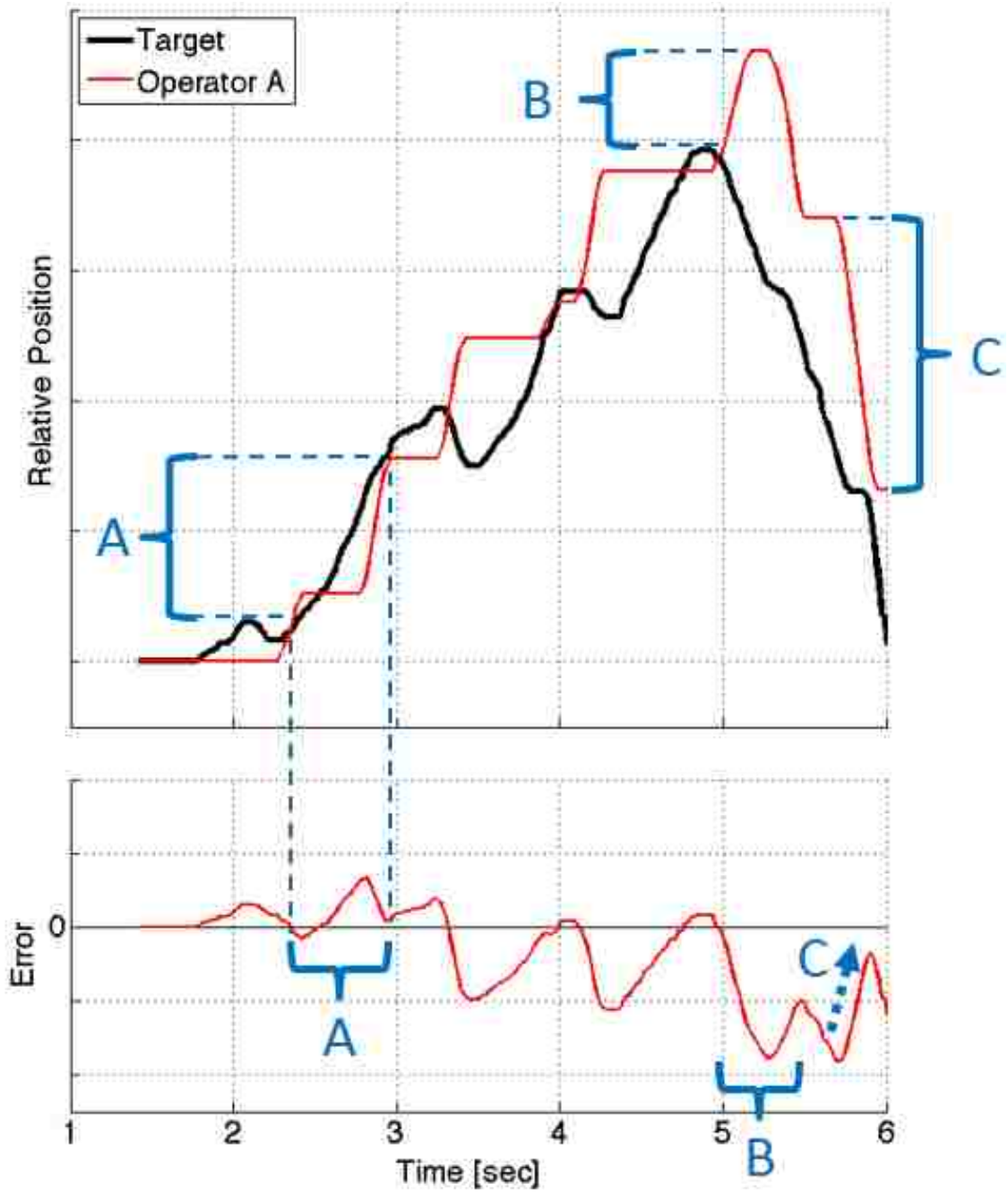

Figure 3.2: Sample annotated time history of one operator at a single modulation and spatial frequency combination.

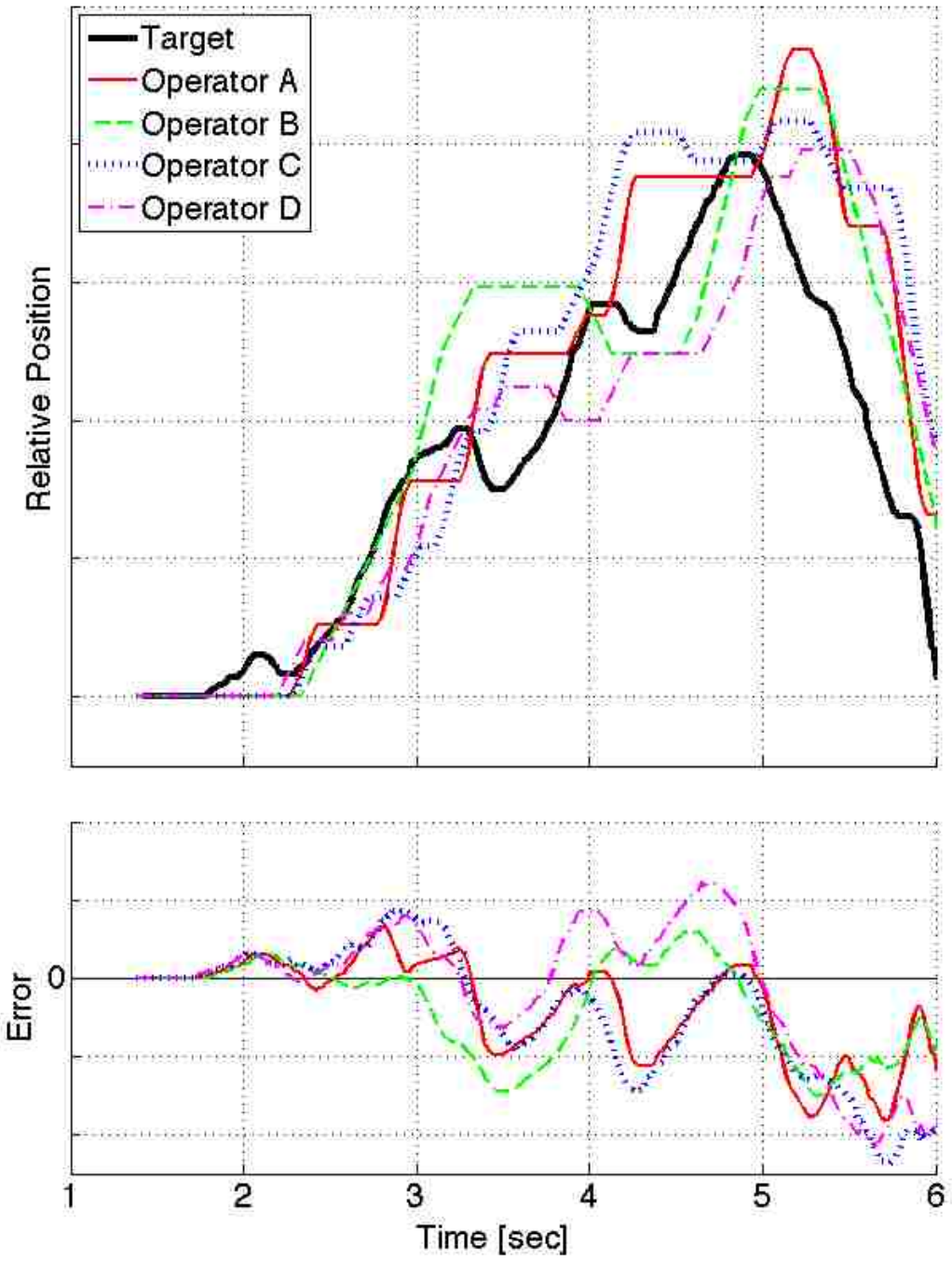

Figure 3.3: Sample time histories of multiple operators at a single modulation and spatial frequency combination. This is the same combination as shown in Fig. 3.2.

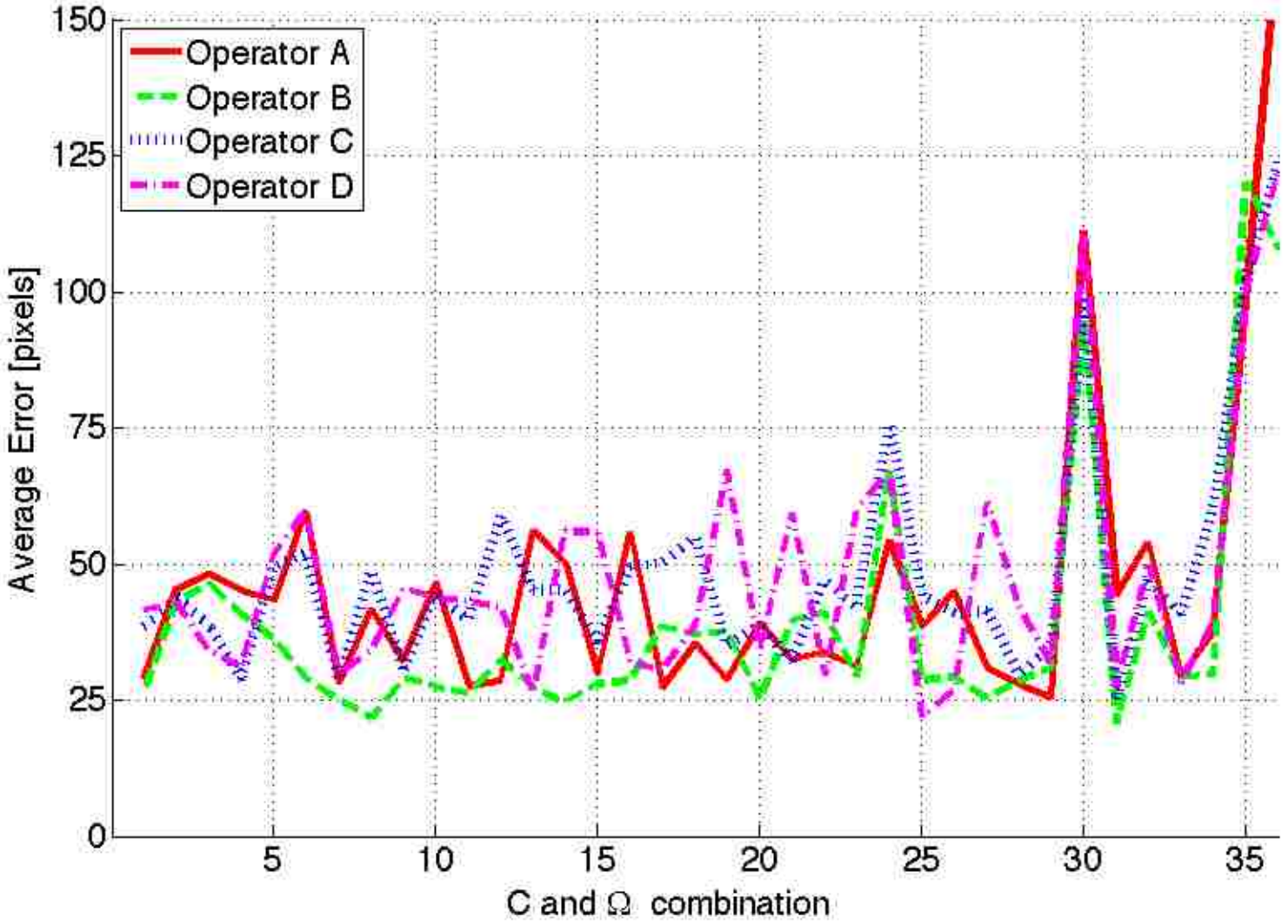

Figure 3.4: Operator variability for all test combinations of modulation and spatial frequency.

The individual average for each of the operators shown in Fig. 3.3 is plotted at "Combination 1" in Fig. 3.4. The group average error value across all operators tested was then found for each of 36 combinations. These values were presented in a similar method to the line-based experiments. Since there were a few variants of the circle testing, numeric comparisons could be made between input devices or control laws, as shown in Fig 3.5. The group average error value (28.3 pixels) from "Combination 1" in Fig. 3.4 is circled in region A of Fig. 3.5b, as the data shown was from a RC system.

3.2.2 Outer Circle Controlled

3.2.2.1 PC & RC Joystick Input

The MTF of the group's average error for the PC variation is shown in Fig. 3.6a, with the error listed in Table form in Table 3.1.

There are two distinct areas of interest in the PC contour plot. First is a large area of relatively low error (shown by the darker regions). Second, there is a region on the right side of the graph that shows a sharp increase error at the smallest object sizes.

The largest region of relatively low error is comprised of 29 of the 36 combinations. For spatial frequencies ranging from 1.00 to 36.45 cycles/degree, the error values ranged from approximately 27 pixels/degree up to approximately 40 pixels per degree. Out of these five spatial frequencies, the second-largest size ($\Omega = 2.50$) had the lowest error at every modulation level except $\mathbf{M} = 1.00$. This point was the

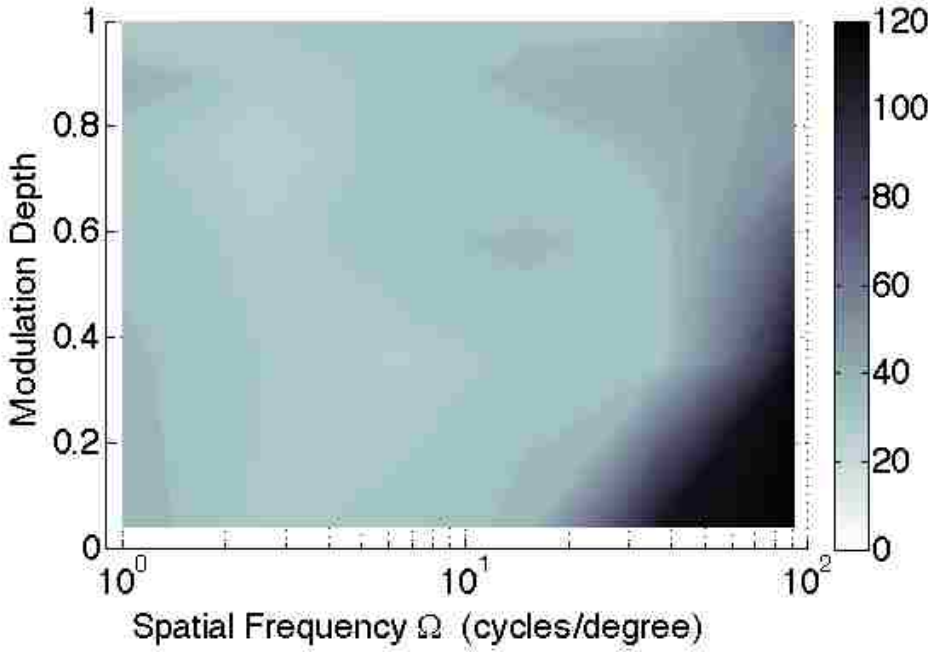

(a) Proportional control

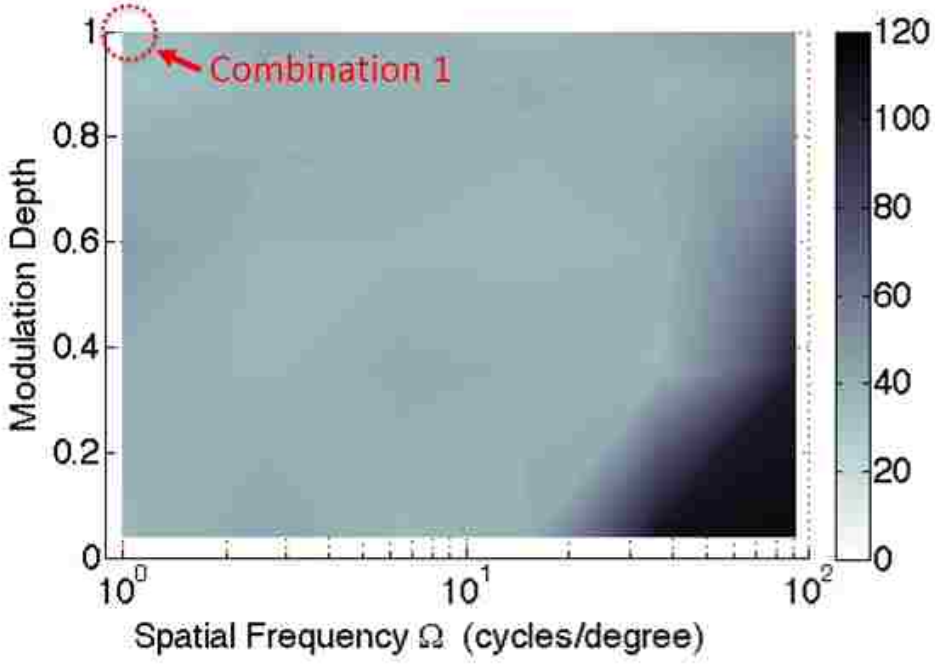

(b) Rate control

Figure 3.5: Effect of control law on group error, joystick input, proprotional control (a) and rate control (b).

lowest average error in this test at 28.0 pixels, which corresponded to the largest target ($\Omega = 1.00$) at the highest modulation ($\mathbf{M} = 1.00$).

This data suggests that the largest objects may not provide the best visual cues for performing the compensatory tasks. A few of the operators tested made comments indicating that the largest target did not appear to be moving very fast. The movement of the target shape itself was one of three pre-programmed patterns as mentioned in Chapter 2. Therefore, the movement (and associated velocities) was independent of spatial frequency. The operators comments appear to indicate not that the target motion itself was slow, but that *perceived* motion of the large shape was not very fast. Based on these comments, and the comparatively higher error across most modulations, it would appear that the spatial frequency of $\Omega = 2.50$ provides the visual cues (through perceived motion) necessary to minimize error of the compensatory task with PC dynamics.

The region of high error develops sharply near the higher spatial frequency values. The values of error for $\Omega = 91.14$ are higher at every modulation level than any other spatial frequency. For $\Omega = 36.45$ at the lowest contrast value ($\mathbf{M} = 0.04$), there is also a sharp increase in error.

The RC control law, seen in Fig. 3.6b and Table 3.2, showed similar trends. There was a defined region of relatively low error, and then a sharply-defined region of high error for the lowest spatial frequencies.

The large region of relatively low error had slightly more variability in the RC system then in the PC system. While a few of the error values for $\Omega = 2.50$ were lower than $\Omega = 1.00$ for the same modulation, there was not the same trend of lower

error for $\Omega = 2.50$ as there was in the PC system. The values of error for the PC system were generally lower for almost all combinations of modulation and spatial frequency.

The region of high error had similar development in the RC system. Again, the errors were the highest for every modulation level at the highest spatial frequency ($\Omega = 91.14$), and there was the same increase at ($\Omega = 36.45$ & $\mathbf{M} = 0.04$). The region of higher relative error will be discussed in more detail in the section that follows.

Table 3.1: Outer circle PC joystick group average error (pixels) as a function of Modulation ($\mathbf{M}$) and Spatial Frequency (Ω)

		Spatial Frequency – Ω (cycles/degree)					
		1.00	**2.50**	**6.29**	**15.19**	**36.45**	**91.14**
Modulation – M	**1.00**	28.0	31.4	33.8	33.9	34.5	58.9
	0.89	39.8	30.0	32.2	38.5	40.4	47.9
	0.76	32.1	26.8	34.4	31.4	38.3	52.7
	0.58	34.9	29.3	35.2	36.8	32.7	78.3
	0.36	36.7	31.5	28.6	33.2	31.6	115.4
	0.04	37.7	30.5	33.1	38.1	108.8	120.2

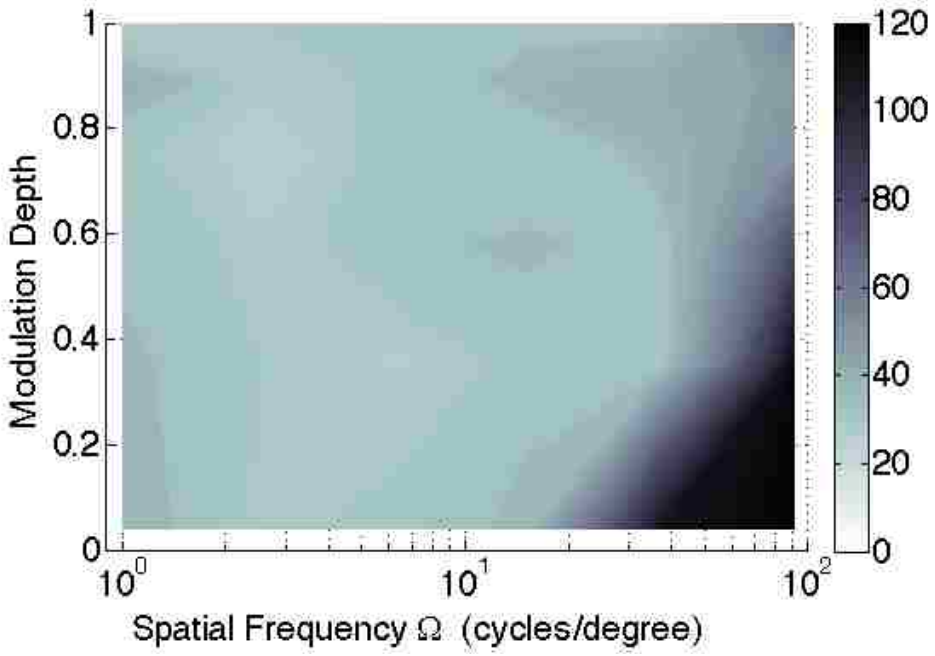

(a) Proportional Control

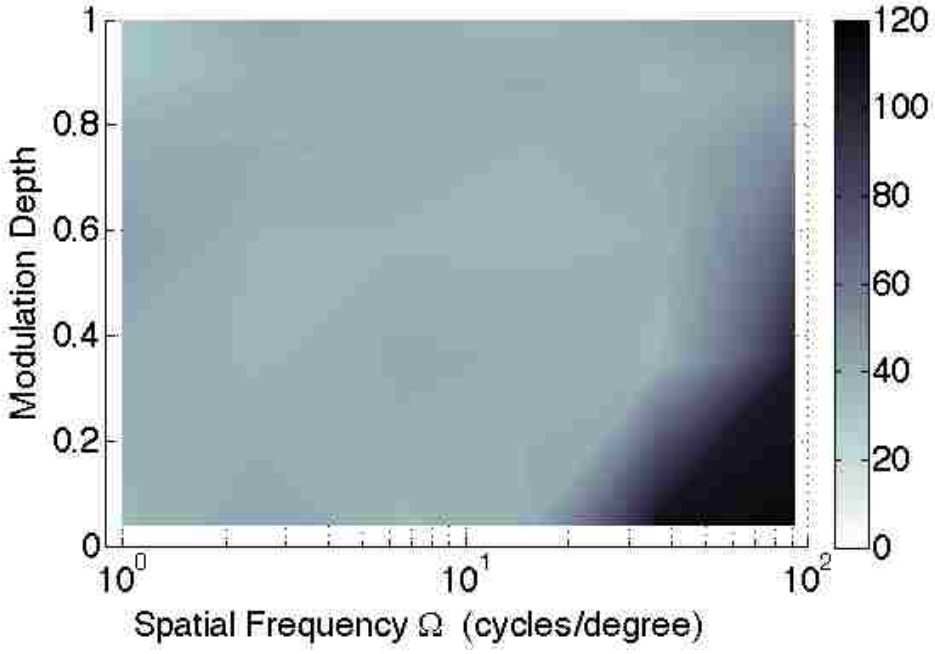

(b) Velocity Control

Figure 3.6: Outer circle - joystick input group average error [pixels]

Table 3.2: Outer circle RC joystick group average error (pixels) as a function of Modulation (**M**) and Spatial Frequency (Ω)

		Spatial Frequency – Ω (cycles/degree)					
		1.00	**2.50**	**6.29**	**15.19**	**36.45**	**91.14**
Modulation – M	**1.00**	32.7	41.8	38.3	35.7	42.6	47.9
	0.89	33.4	38.5	38.5	41.4	36.8	44.4
	0.76	40.1	40.4	36.9	37.5	40.5	56.5
	0.58	45.9	37.4	37.3	36.9	37.8	75.7
	0.36	38.6	37.2	41.3	39.8	37.3	104.1
	0.04	37.1	43.5	37.0	40.3	111.6	115.7

3.2.3 Correlation with 20/20 Vision

Both the PC and the RC experiments had a sharply-defined region of high error that occurred at the highest spatial frequencies. Since the error at the combinations that made up the region were considerably higher (almost 300% greater than the test minimum), the data has one strong indication on their use as visual cues. These combinations were not just "poor" visual cues (with modest error increases); they were fully "insufficient." That is, the average operator was unable to perform the compensatory tasks at all because they could not *see* the target shape.

These combinations were outside the approximate border of 20/20 vision. Reference [38] provides an approximation for 20/20 vision in MTF format as shown by Eqn. 3.1. This approximation came from testing human subjects sensitivity to grat-

ing patterns.

$$C_{threshold}(f_a) = \frac{v_e}{\exp(-c_1 f_a) - \exp(-c_2 f_a)} \tag{3.1}$$

where $v_e = 0.001033$ is the intrinsic noise value, $c_1 = 0.1138°$, $c_2 = 0.3250°$, and f_a is the angular spatial frequency in $\frac{cycles}{degrees}$

The MTF curve produced by Eqn. 3.1 is represented by a magenta line in Fig. 3.7a for the PC system, and Fig. 3.7b for the RC system.

The data show that there is a good qualitative correlation to the group's performance of the simple compensatory task and the psychological limits of human vision. In the PC case, there seems to be a small degradation in performance around spatial frequency values of 30-50 cycles/degree that occurs before the 20/20 limit is reached.

Examining the corresponding tests states on the RC system, it appears that the PC errors become more in line with the error associated with the RC system at the value of 30-50 cycles/degree. For the seven combinations that exceed the 20/20 vision threshold, the error values between both joystick control laws were within 3-11 pixels (see Tables 3.1 and 3.2 for exact values).

Overall, the values of error that occurred within the threshold of 20/20 vision were relatively low (28-45 pixels) for both control laws, and were relatively high (48-120 pixels) once the 20/20 threshold was surpassed. There was only minor performance degradation before the limit was reached, suggesting a quick deterioration in performance corresponding to exceeding the 20/20 vision limit. It is important

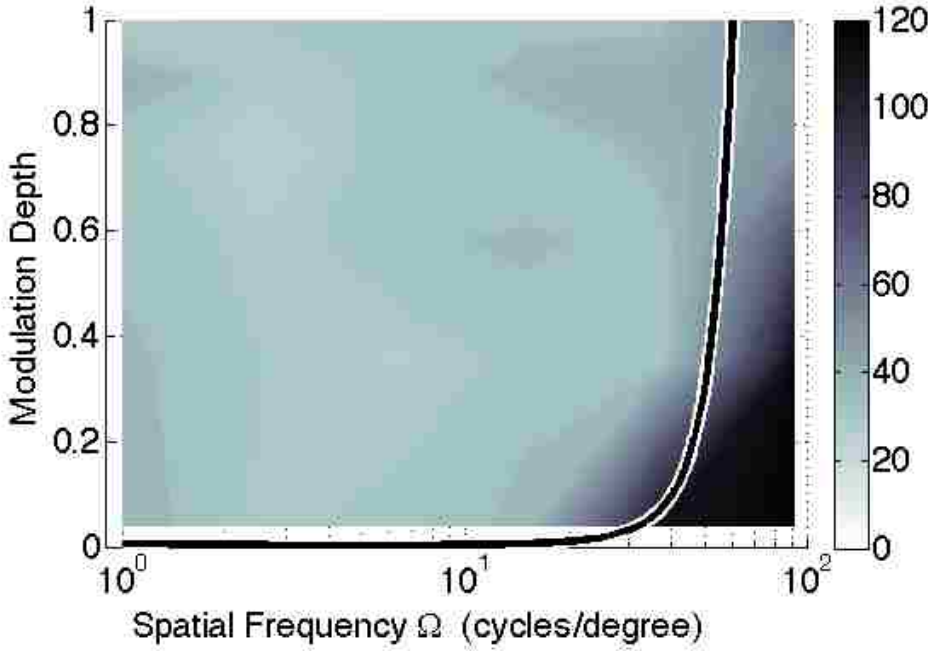

(a) Proportional control

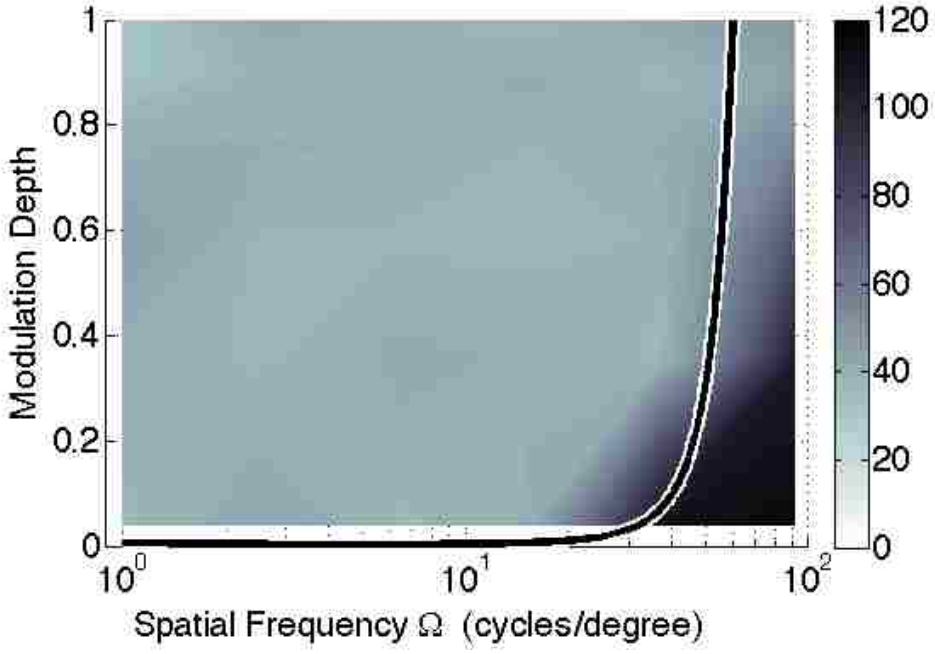

(b) Rate control

Figure 3.7: 20/20 Vision MTF super-imposed over group error (pixels). Both sub-figures have the same error color scale.

to note that a formal measure of the test subjects' vision was not performed (i.e. a clinical vision test). With 18 of the 25 total subjects having legally performed civilian and/or military flying duty in the past three years, it was assumed that the group's vision was qualitatively representative of the larger pilot population.

3.2.4 Inner Circle Controlled

For the following four variants of the circle-based tests, the operator controlled in the *inner* circle. This circle changed modulation value over the course of the test. The target circle was the outer, red circle. See Section 2.4.3.2 for more detail on the methodology used.

3.2.4.1 Joystick using Proportional Control

The group average error for this variant was very low across all combinations of modulation and spatial frequency. The resulting contour plot, shown in Fig. 3.8a, had two distinct regions similar to the previous testing variants.

There is a region of relatively low error values for 29 of the 36 combinations. The error values, listed in Table 3.3, are mostly between 20 and 30 pixels. On average, these were around 10 pixels lower than the previous circle-based tests, indicating that the methodology itself was responsible for a decrease in error.

There is a sharp degradation in relative performance at the remaining seven combinations, suggesting correlation to the 20/20 vision MTF given by Eqn. 3.1. The 20/20 approximation is overlaid on the contour in Fig. 3.9a. The degradation

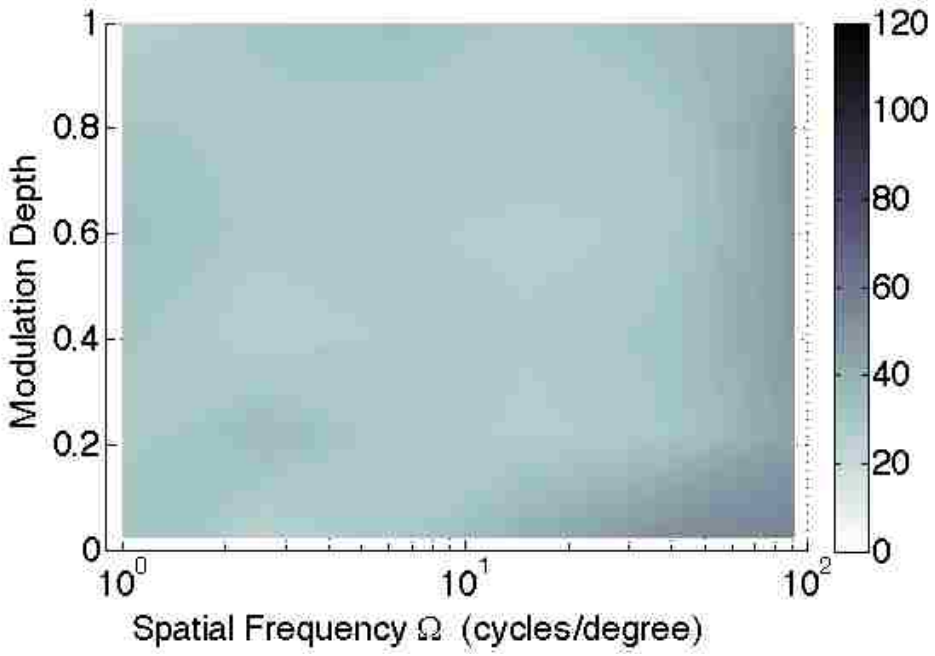

(a) Proportional control

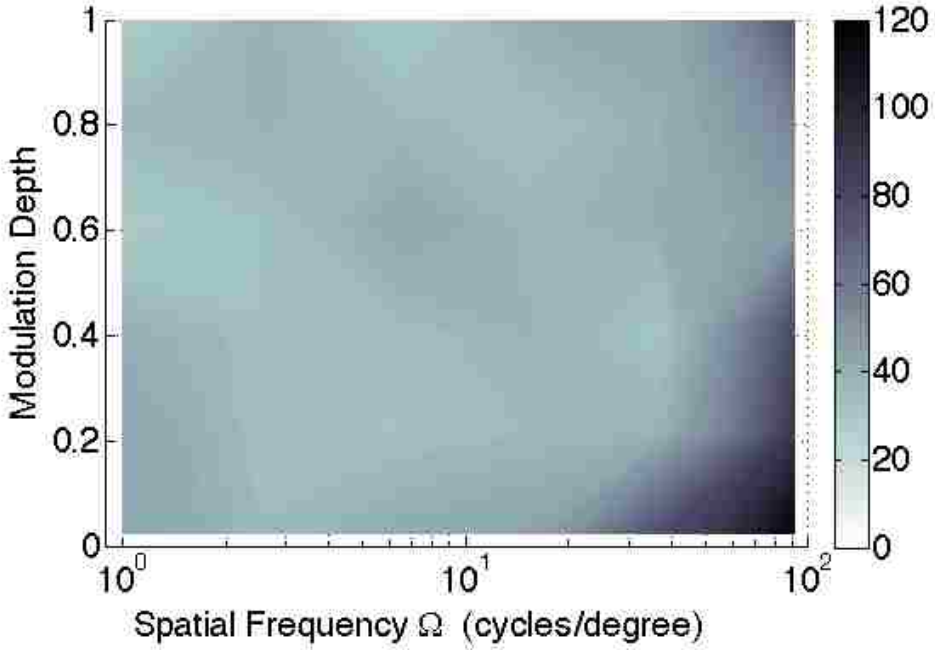

(b) Velocity control

Figure 3.8: Inner circle - joystick input group average error (pixels)

associated with crossing the 20/20 threshold was not quite as strong as it was in the previous testing, The lowest error for this test was approximately 26 pixels and the highest was only 57 pixels, representing a 120% increase in average error once the 20/20 threshold was exceeded.

The small degradation in performance when crossing the 20/20 vision threshold is believed to be the result of the experimental procedures. Since the operator's shape was the one that faded, the target shape was always visible. Even in absence of their own shape as a visual cue (when beyond their personal vision threshold), the operator was able to mimic the target shape's movement. This would produce some additional error (compared to a case with sufficient visual cues), but lower error values as compared to the previous circle testing.

3.2.4.2 Joystick using Rate Control

The RC Joystick showed slightly different trends than the PC experiment. As seen in Fig. 3.8b, the region of relatively low error was considerably smaller. The data itself was much more varied in this region as well, which can be seen by the number values listed in Table 3.4. This indicates that some of the operators tested may have had difficulty with the RC dynamics of the controlled shape.

The region of poor performance also has a correlation with the 20/20 vision approximation, as seen in Fig. 3.9b. The degradation encompasses a few additional combinations when compared to the PC system.

At the lowest value of modulation ($\mathbf{M} = 0.02$) the spatial frequencies of $\Omega =$

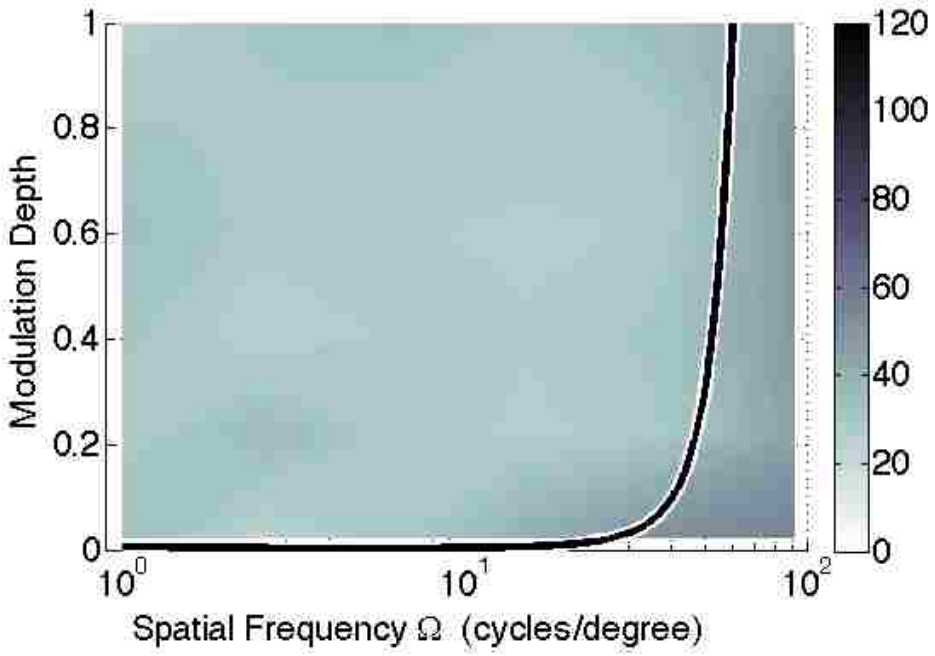

(a) Proportional control

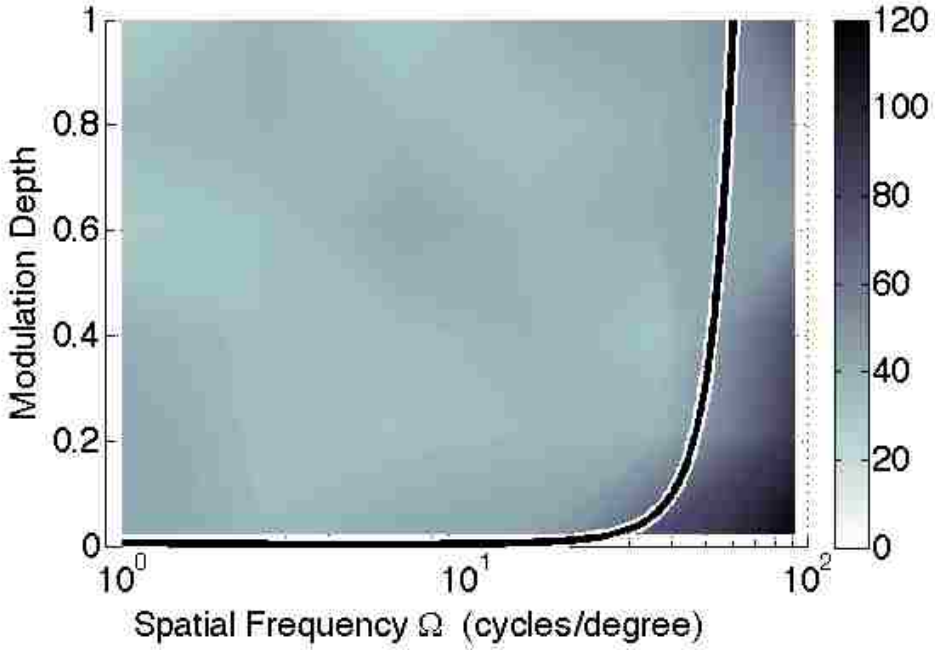

(b) Velocity control

Figure 3.9: 20/20 Vision MTF & inner circle group error (pixels) - joystick input

15.19 and $\Omega = 6.29$ have an increase in error over their respective errors at the the greater modulation value of $\mathbf{M} = 0.22$. There is a degradation when modulation drops below 61% for the largest object size ($\Omega = 1.00$), as seen in the lower left hand of Fig. 3.8b. This suggests that the middle-values of spatial frequency result in the highest performance of the compensatory task. However, the general variability in the group average error from combination to combination does not mathematically support a strong correlation.

Table 3.3: Inner circle PC group average error (pixels) as a function of Modulation (**M**) and Spatial Frequency (Ω)

		Spatial Frequency − Ω (cycles/degree)					
		1.00	**2.50**	**6.29**	**15.19**	**36.45**	**91.14**
Modulation − M	**1.00**	25.8	32.0	34.2	29.8	35.4	40.7
	0.80	31.5	29.1	28.5	29.7	28.9	51.5
	0.61	34.5	29.3	28.4	27.6	28.7	50.6
	0.41	31.3	25.5	28.7	28.5	31.7	49.2
	0.22	29.4	25.8	29.3	27.5	30.1	46.2
	0.02	33.7	24.2	30.6	40.7	52.5	57.2

3.2.4.3 Mouse using Proportional Control

Like the PC testing performed with the joystick, the mouse-based PC variant had a large region of very low error values. This region of darker contours in Fig 3.10a

Table 3.4: Inner circle RC joystick group average error (pixels) as a function of Modulation (**M**) and Spatial Frequency (Ω)

		Spatial Frequency – Ω (cycles/degree)					
		1.00	**2.50**	**6.29**	**15.19**	**36.45**	**91.14**
Modulation – M	**1.00**	28.3	38.8	30.1	40.0	40.5	75.3
	0.80	36.7	38.3	37.0	34.4	39.7	57.2
	0.61	28.7	33.9	42.9	37.3	40.1	47.8
	0.41	39.4	34.6	35.4	38.5	32.5	81.6
	0.22	42.9	34.7	34.3	36.3	38.8	89.2
	0.02	43.5	36.6	41.3	44.4	78.3	118.6

spans almost all of the 36 combinations. A closer inspection of the value, listed in Table 3.5, shows two notable trends.

First, the 20/20 vision threshold causes for a relative increase in error at the higher spatial frequencies. Similar to the Joystick PC case, there is a low amount of error (25.8 pixels) at the highest spatial frequency and highest modulation combination ($\mathbf{M} = 1.00, \Omega = 91.14$). Overall, the data correlates well with the 20/20 vision threshold, which is overlaid on the contour plot in Fig. 3.11a.

Second, there is a region of very low error that covers the middle four spatial frequencies ($\Omega = [2.50, 6.29, 15.19, 36.45]$) at almost every modulation value. This suggests that these middle spatial frequency values may provide the necessary visual cues for minimizing error in a compensatory task.

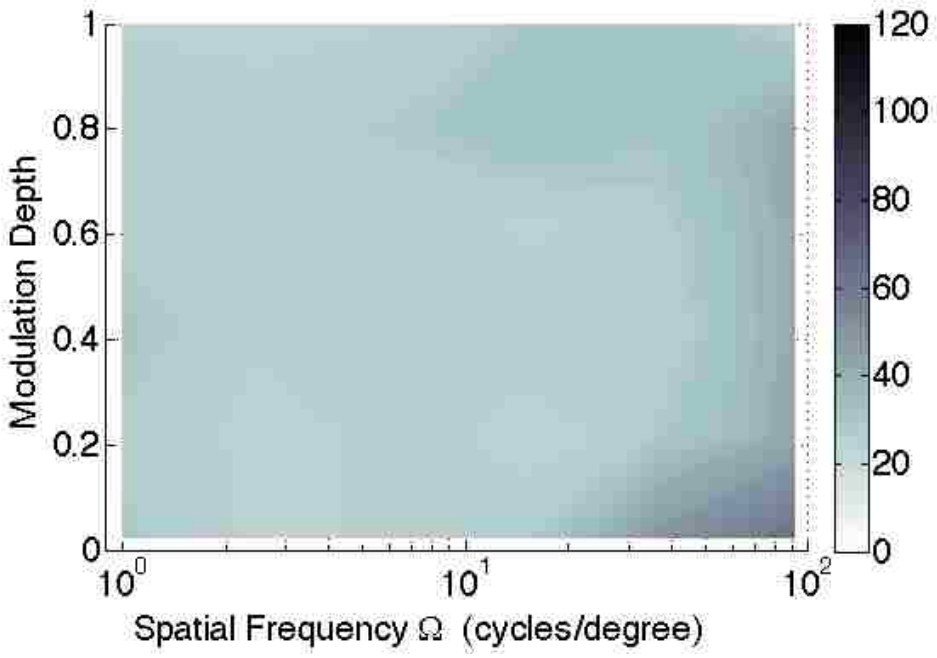

(a) Proportional control

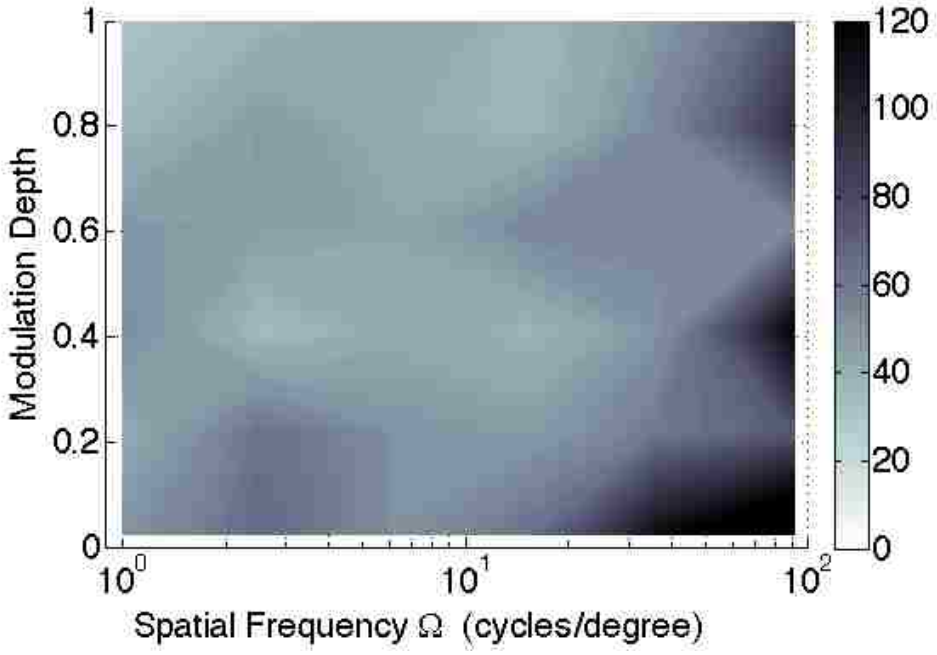

(b) Rate control

Figure 3.10: Inner circle- mouse input group average error (pixels)

3.2.4.4 Mouse using Rate Control

The RC case had higher average error than the PC case at every single combination as seen in Fig. 3.10 and listed in Table 3.6. The 20/20 vision trend was more noticeable in the RC case (Fig. 3.11b) with pixel errors near or above 100 pixels for four combinations outside the 20/20 vision threshold.

The increase in error relative to the PC case is assumed to be due to the difficulty inherent for the operators controlling a RC system for this compensatory task. For the PC case, the operator could simply "mimic" the motion of the target shape even when they could not see their own shape. Performing this type of open-loop control of a RC system does not appear to be as intuitive for the operators (compared to the PC system) This will be analyzed in more depth in the following section.

Table 3.5: Inner circle PC mouse average error (Pixels) as a function of Modulation (**M**) and Spatial Frequency (Ω)

		Spatial Frequency − Ω (cycles/degree)					
		1.00	**2.50**	**6.29**	**15.19**	**36.45**	**91.14**
Modulation − M	**1.00**	24.7	23.4	25.2	30.0	31.8	25.8
	0.80	28.1	28.2	29.4	33.9	30.7	43.8
	0.61	28.4	25.4	27.2	24.4	27.8	41.7
	0.41	30.7	25.6	25.8	28.1	26.1	42.2
	0.22	28.0	23.4	26.8	22.9	29.6	42.1
	0.02	29.7	24.1	25.9	29.1	50.7	65.3

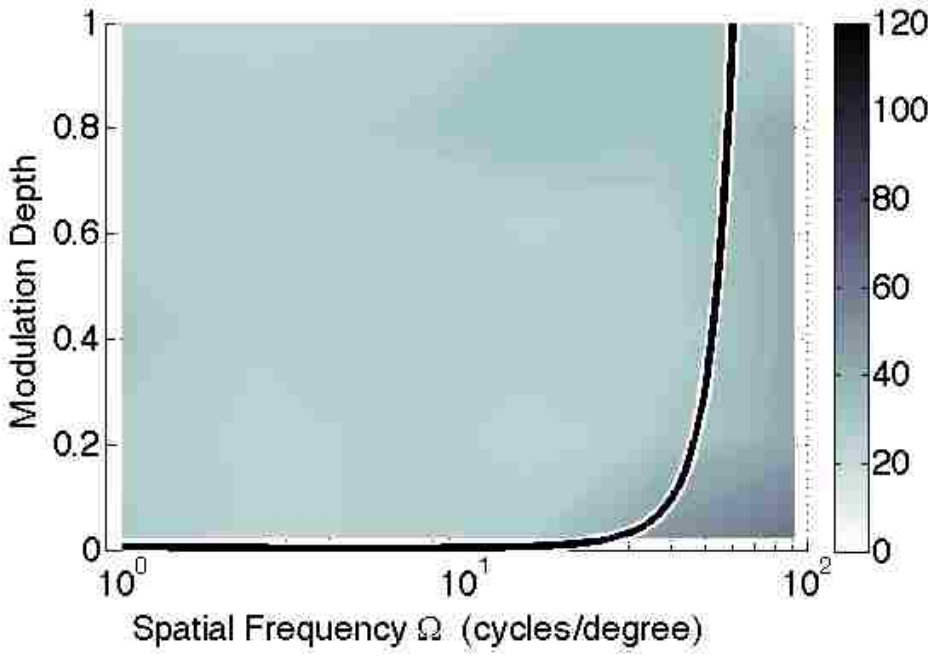

(a) Proportional control

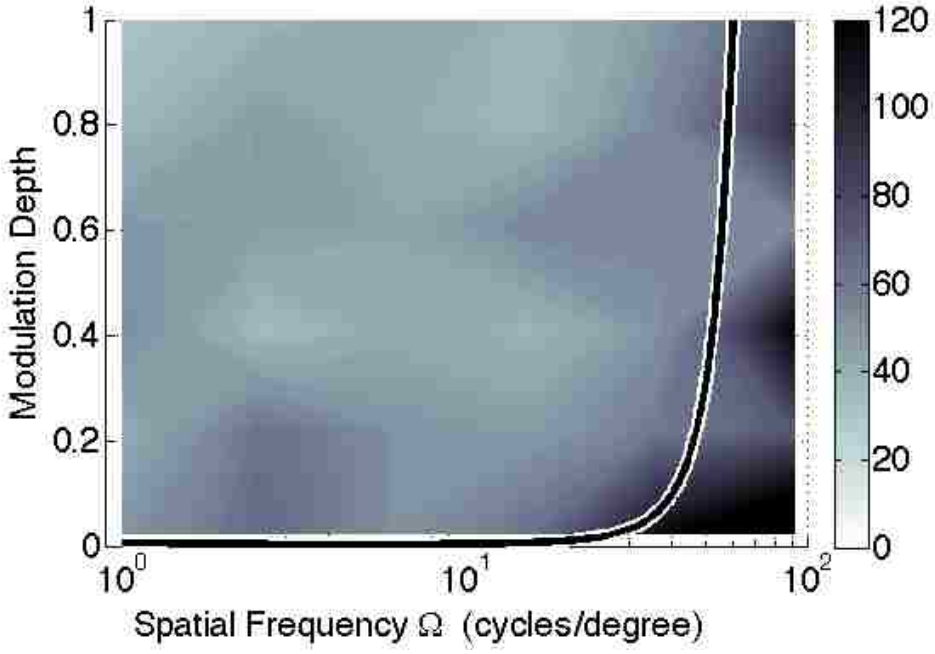

(b) Rate control

Figure 3.11: 20/20 Vision MTF & inner circle group error (pixels) - mouse input

Table 3.6: Inner circle RC mouse group average error (pixels) as a function of Modulation (**M**) and Spatial Frequency (Ω)

		Spatial Frequency – Ω (cycles/degree)					
		1.00	**2.50**	**6.29**	**15.19**	**36.45**	**91.14**
Modulation – M	**1.00**	33.5	37.8	43.4	36.4	48.7	79.2
	0.80	36.3	49.0	39.9	37.0	55.4	96.2
	0.61	49.4	47.2	44.6	55.0	53.6	54.2
	0.41	52.5	34.7	42.5	37.5	51.3	120.4
	0.22	42.0	63.4	50.6	47.6	61.3	74.6
	0.02	51.1	67.1	51.4	64.5	115.4	153.5

3.2.4.5 Comparison of Control Dynamics

The average group errors for the four different combination of control laws and input devices are shown together on the same scale in Fig. 3.12. There are two trends to note.

First, when the compensatory task was governed by the PC control law, the group average error had a lower amount of error at every single one of the 36 combinations. This trend held for both input devices. It is assumed that this is due to the similarity of the compensatory task under PC conditions to a common, compensatory task that the operators each had a great deal of experience with. When error between the target and the controlled shape was observed, the operator would move the input device to achieve a corresponding scaled movement of the controlled shape on the screen. This is fundamentally no different than the compensatory movement required for an average computer user to move their pointer around a

computer screen. Each individual in the tested population had years of experience using computers, so they had a great deal of "practice" moving a shape with PC dynamics to a desired location on a computer screen.

The RC system is not as intuitive to the average operator. For the individuals tested without piloting experience, they would presumably not have much experience controlling a system with RC dynamics. McRuer and Krendel note in Ref. [26] that an idealized representation of an every-day RC system would be heading control at low to moderate speeds in an automobile. While all individuals tested had driving experience (and thus experience controlling a RC system), the compensatory task in the present testing was not as closely related to the PC computer tasks.

The second trend is the performance of the operator at the limit of 20/20 vision as seen in Fig. 3.13. The general contours of the increase in error associated with crossing the 20/20 vision threshold all have similar patterns. However, both RC systems experienced a large relative increase in error once the MTF for 20/20 vision was surpassed.

When shown the marginal (or completely insufficient) visual cue in the PC cases, the group performed the compensatory task with larger errors. Error values typically doubled (from approximately 25 up to 50 pixels) as the contrast and the size of the visual cues crossed below the 20/20 threshold. For the RC case, some of the error values were 3 to 4 times as great once the vision threshold was passed. This suggests there the group had an inherent difficulty judging the movement of a RC system when presented with marginal (or completely insufficient) visual cues for determining their shape's position on the screen.

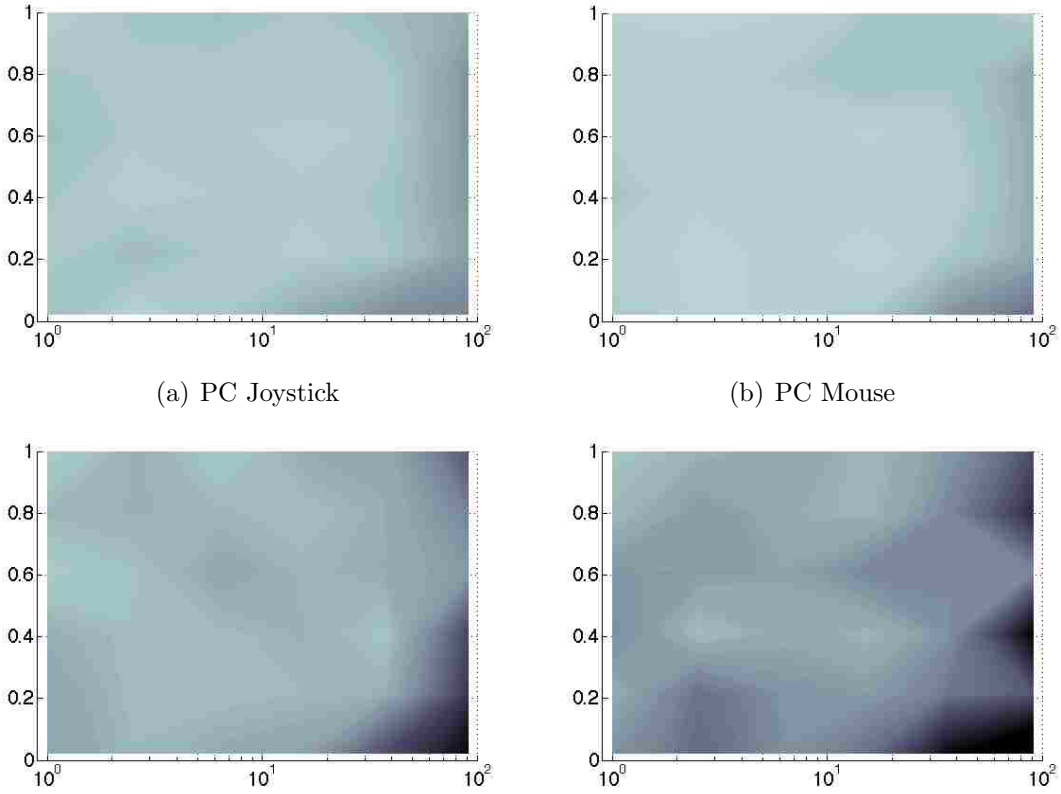

(a) PC Joystick

(b) PC Mouse

(c) RC Joystick

(d) RC Mouse

Figure 3.12: Comparison of control law and input devices - group average error (pixels)

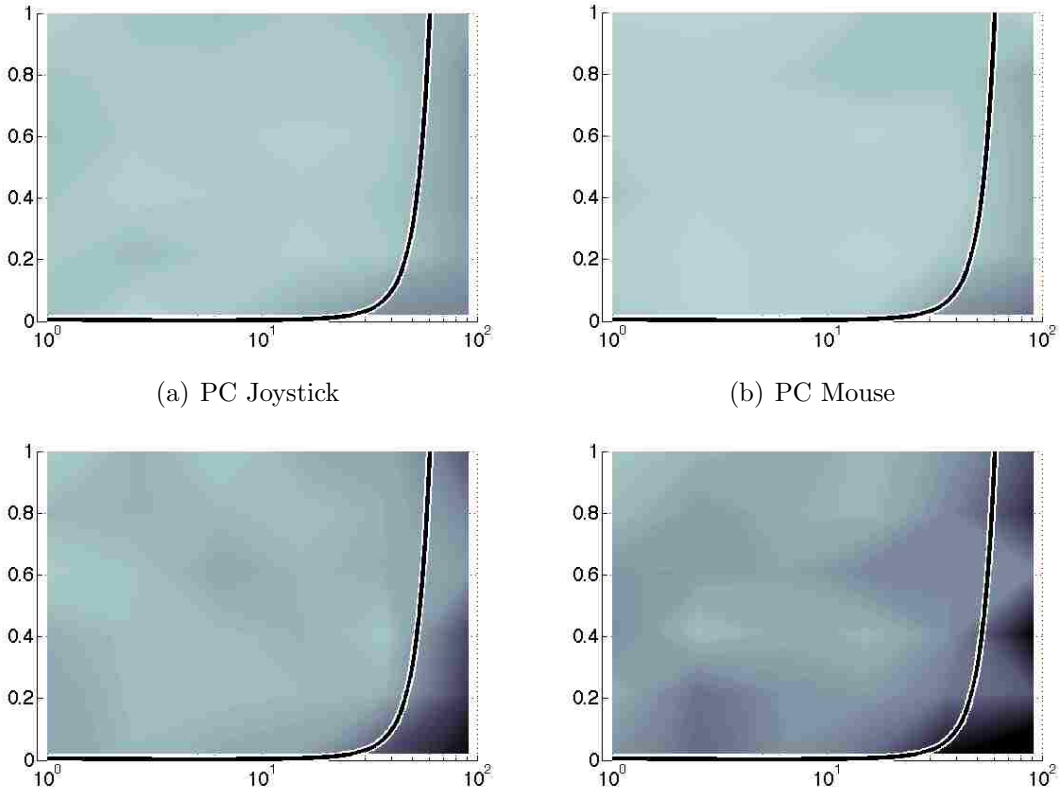

(a) PC Joystick

(b) PC Mouse

(c) RC Joystick

(d) RC Mouse

Figure 3.13: Comparison of control law and input devices with 20/20 vision threshold - group average error (pixels)

3.2.4.6 Comparison on Input Devices

When a pair of time histories (one mouse-input, one joystick-input) are examined for a particular individual, the reasons for the error patterns mentioned in the previous section become apparent. For the time histories shown in Fig. 3.14, the control law was RC in both cases. The same two combinations are shown on each graph. Mouse-input is shown on the top graph; joystick-input on the bottom. The target shape's position is the thin line and the user target shape position is the thick line.

For the mouse case, the operator tracks the target shape with an error that increases rapidly from the beginning of the test. This is assumed to be the result of the operator imparting a small rate on the controlled shape near the beginning of the test. This velocity, coupled with the poor level of visual cues, results in the operator no longer tracking the location of their own shape. Since the compensatory task requires the operator to minimize the error between the target shape *and* their own shape, the visual cues available are no longer sufficient to close the visual feedback loop necessary for the task.

However, the red target shape is always visible to the operator. When the visual cues are not sufficient to compensate for the error directly, the operator begins to "mimic" the target movement (similar to the results found in Ref. [36]). An example of this behavior is labeled on Fig. 3.14a.

At Point "A" the operator attempts to mimic the downward movement of the red line (with some inherent delay). Very quickly however, the user has imparted a

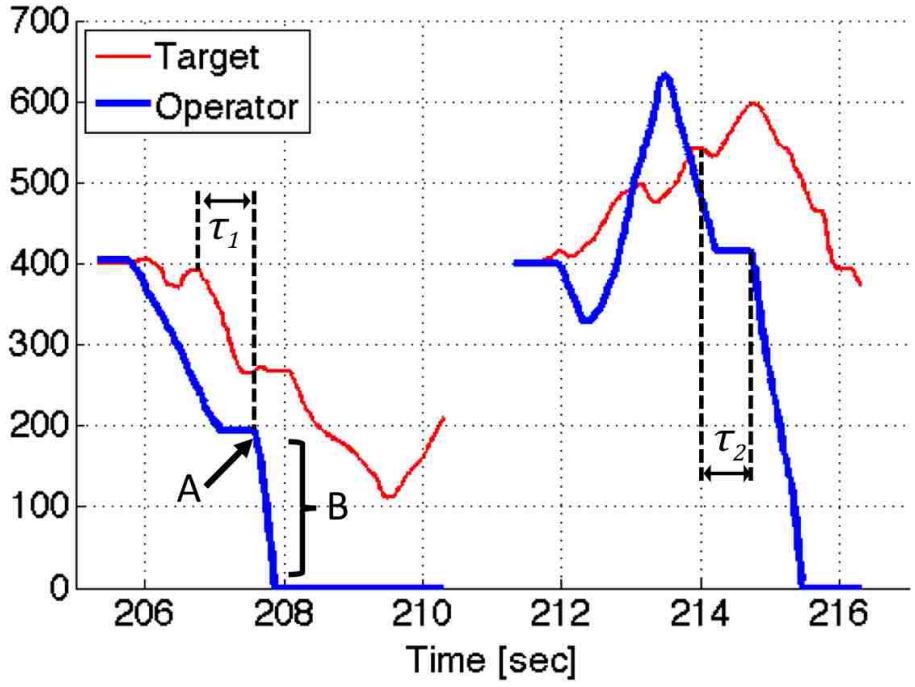

(a) Mouse input

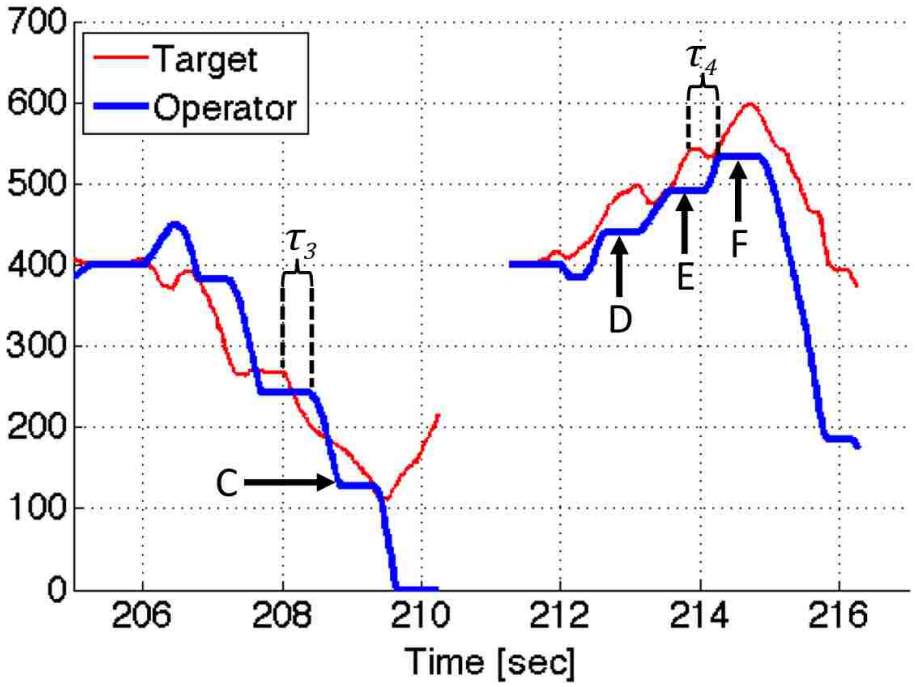

(b) Joystick input

Figure 3.14: Time histories for two test combination with different input devices. The left portion of both subfigures corresponds to ($\mathbf{M} = 0.02$, $\Omega = 36.45$); the right portion of both subfigures corresponds to combination ($\mathbf{M} = 0.02$, $\Omega = 91.14$).

large velocity onto their shape (Portion "B") due to the open visual feedback loop. This results in the operator displacing his shape so far that it reaches the boundary of the screen (the horizontal axis).

The estimated operator delay τ for the mouse input was calculated for this operator. For the combination on the left side of Fig. 3.14a, which corresponded to ($\mathbf{M} = 0.02$, $\Omega = 36.45$), the estimated delay $\tau_1 = 0.83$ seconds. For the combination on the right side of Fig. 3.14a, which corresponded to ($\mathbf{M} = 0.02$, $\Omega = 91.14$), the estimated delay $\tau_2 = 0.77$ seconds. The *decrease* in estimated delay is attributed to the fact that the sample is only this one operator. Additionally, both combinations are below the 20/20 threshold.

If the same two combinations are examined for the joystick-input case, Fig. 3.14b, the tracking is significantly better. In fact, these two cases strongly resemble "normal" time histories of combinations where the shapes are plainly visible. However, closer examination reveals two important points.

First, the individual frequently stops moving their shape (represented by flat portions of the history, e.g., Portions "C," "D," "E," and "F") before the target shape slows down or changes direction. This means the individual is intermittently allowing the joystick to return to its neutral point (where RC law imparts zero velocity) via the built-in springs.

We can assumed that this is the result of the inability to close the visual feedback loop because of insufficient visual cues- the same insufficient visual cues that caused the very large errors shown in Fig. 3.14a. In this case, the operator tends to let the joystick return to the neutral position, thanks to the built-in springs.

Secondly, the operator seldom "overshot" the target in an effort to mimic its motion when using the joystick. This is seen best in the second combination in Fig 3.14b. The individual allowed the joystick to return to the neutral position (Points "D," "E," & "F") when the target either slowed down or changed direction entirely. This resulted in zero velocity of the controlled shape, which could not strongly under- or over-shoot the target shape and thereby induce large amounts of error. The result was a low overall tracking error, seldom off by more than 100 pixels at any given time.

The estimated operator delay τ for the joystick input was also calculated. For the combination on the left side of Fig. 3.14a, which corresponded to ($\mathbf{M} = 0.02$, $\Omega = 36.45$), the estimated delay $\tau_3 = 0.44$ seconds. For the combination on the right side of Fig. 3.14a, which corresponded to ($\mathbf{M} = 0.02$, $\Omega = 91.14$), the estimated delay $\tau_4 = 0.46$ seconds. As mentioned before, both combinations are below the 20/20 threshold. However, the estimated time delay was almost half the time (0.44 and 0.46 seconds) using the joystick input device compared to the respective delays using mouse input (0.83 and 0.77 seconds).

3.3 Lateral Repositioning Experiments

3.3.1 Measurements and Example Time Histories

The average error at a given combination was calculated across the entire sample population, similar to the previous experiments. Since this experiment had two different shapes to track (the first shape, which started on the left side of

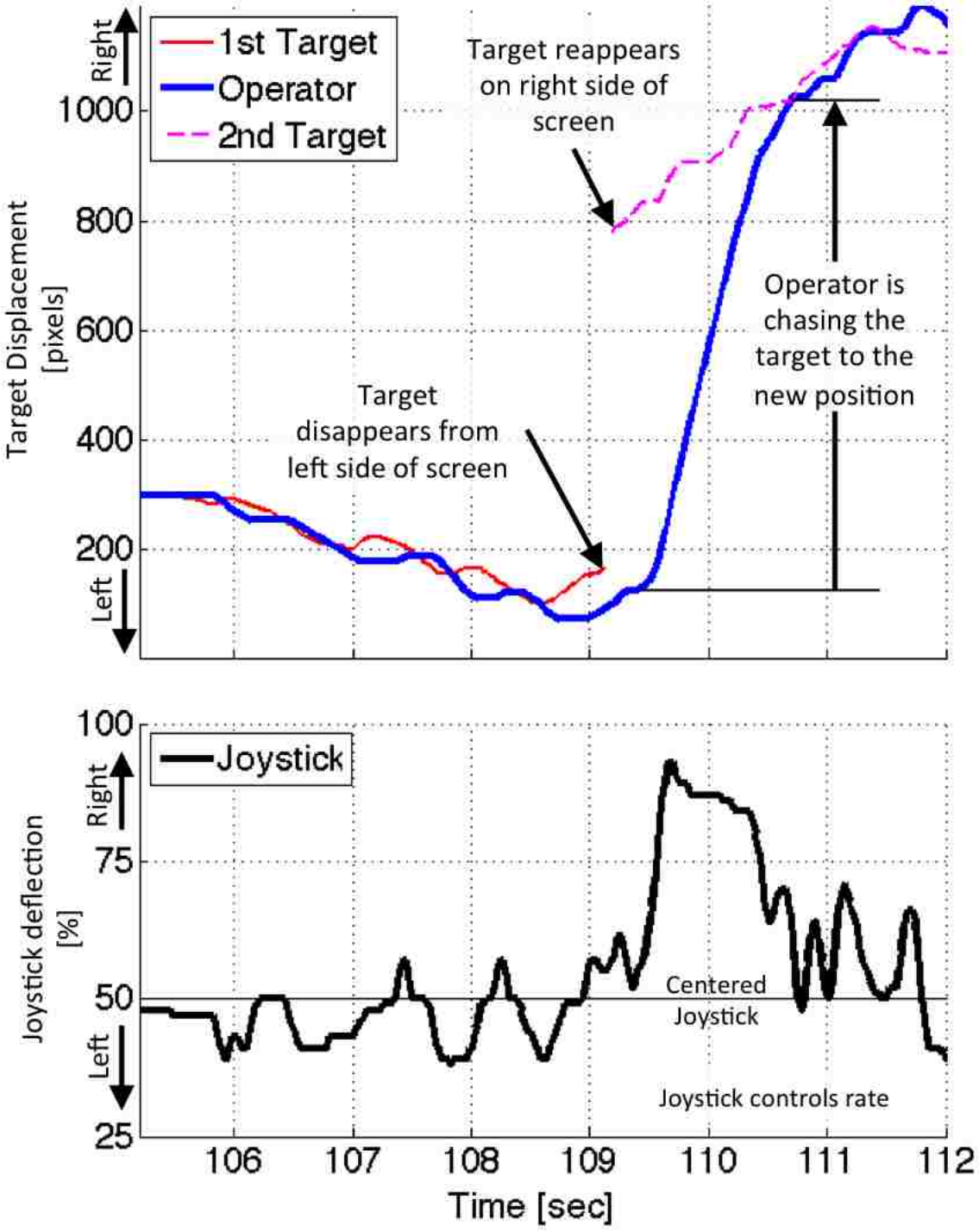

Figure 3.15: Key features of the lateral repositioning time histories for a good visibility case. These time histories are for one operator, at one specific combination ($\mathbf{M} = 0.61$ and $\Omega = 2.50$ cycles/degree).

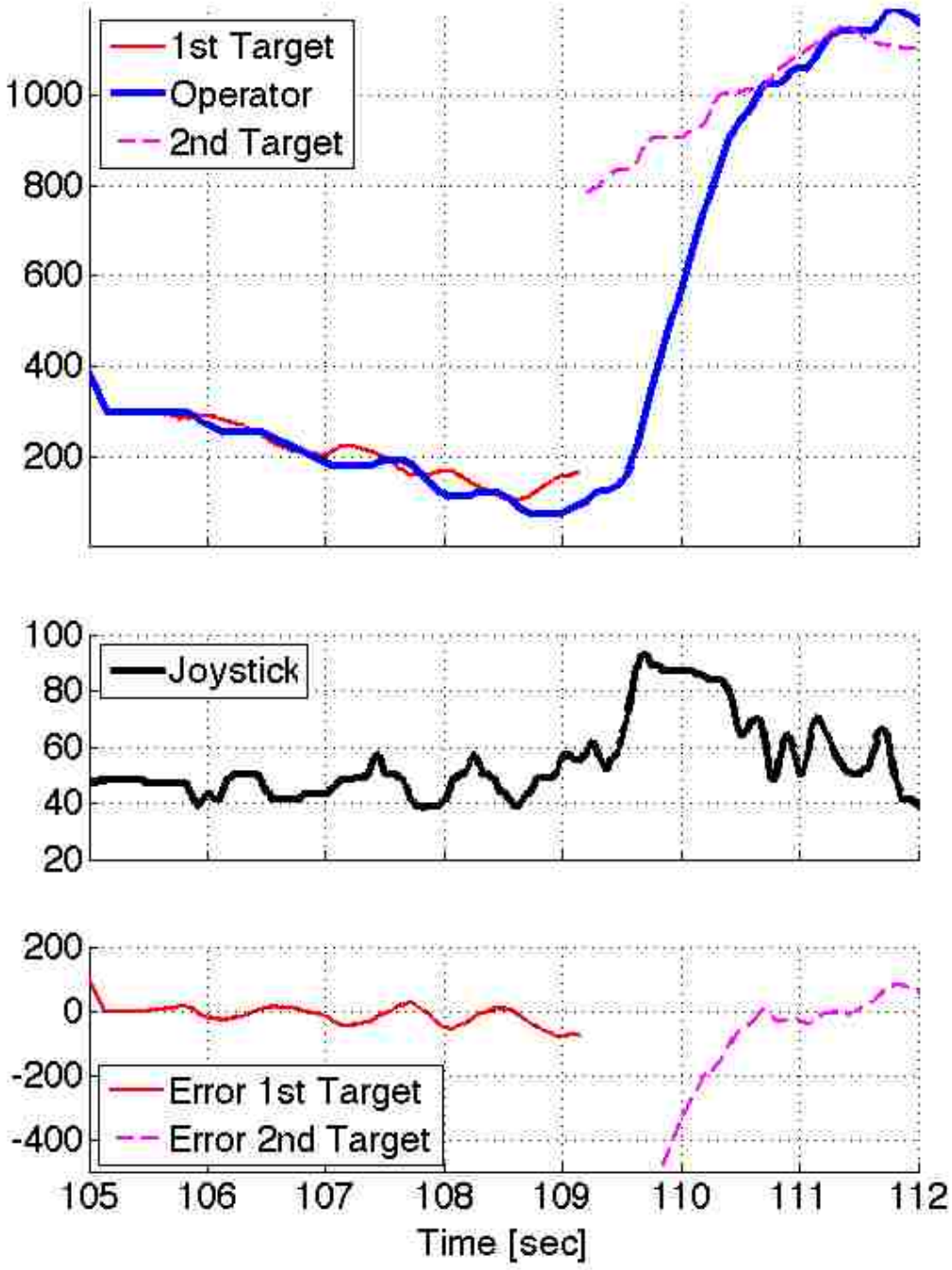

Figure 3.16: Lateral repositioning time history. This time history is for one operator, at one combination of modulation and spatial frequency ($\mathbf{M} = 0.61$ and $\Omega = 2.50$ cycles/degree).

the screen and the second shape, which would appear on the right side), the error analysis was performed for both targets independently.

For the second target, the acquisition portion of the compensatory task is much more difficult. While the second target would always initially appear 600 pixels to the right of the first target (as the first disappeared), the second target's motion was immediately pseudo-random. This required the individual to shift their eyes, acquire the second target, and then resume the compensatory tracking task of an already-moving target. An example time history, with these events labeled, is shown in Fig. 3.15

For the joystick used in this test, 0% was full-left physical deflection, 50% was the neutral position, and 100% was the full-right deflection. Since the repositioning was always from the left side of the screen to the right, the joystick deflections of interest were always above 50% regardless of whether the joystick controlled displacement or rate. The higher the joystick deflection, the more "aggressive" the operator was being with the repositioning.

An example time history of both targets, the operator shape, and the joystick deflection over the course of one combination is shown in Fig. 3.16.

The average error at a given combination was calculated across the entire sample population, similar to the method described in Section 3.2.1. The lateral repositioning experiment had two different shapes to track (the first target, which started on the left side of the screen and the second target, which would appear on the right side). The error analysis was performed for both targets independently. An example time history of the data collected at one combination, including the

calculated error for both targets, is shown in Fig. 3.16. This is the same combination shown in Fig. 3.15.

A time history for each of the 21 operators was analyzed to find specific values for each individual operator at the 36 tested combination of modulation and spatial frequency. The individual operator values could then be averaged across the tested populated. An example showing four of the 21 operators and their error tracking the first target is shown in Fig. 3.17.

For the case with the delay, the joystick position value reported to the software was the value that the operator put in at that particular timestep, not the delayed value that was numerically used to update the shape velocity and position during that iteration.

The numeric characteristics of the lateral repositioning inputs can further categorized into additional metrics, which will be shown later this chapter.

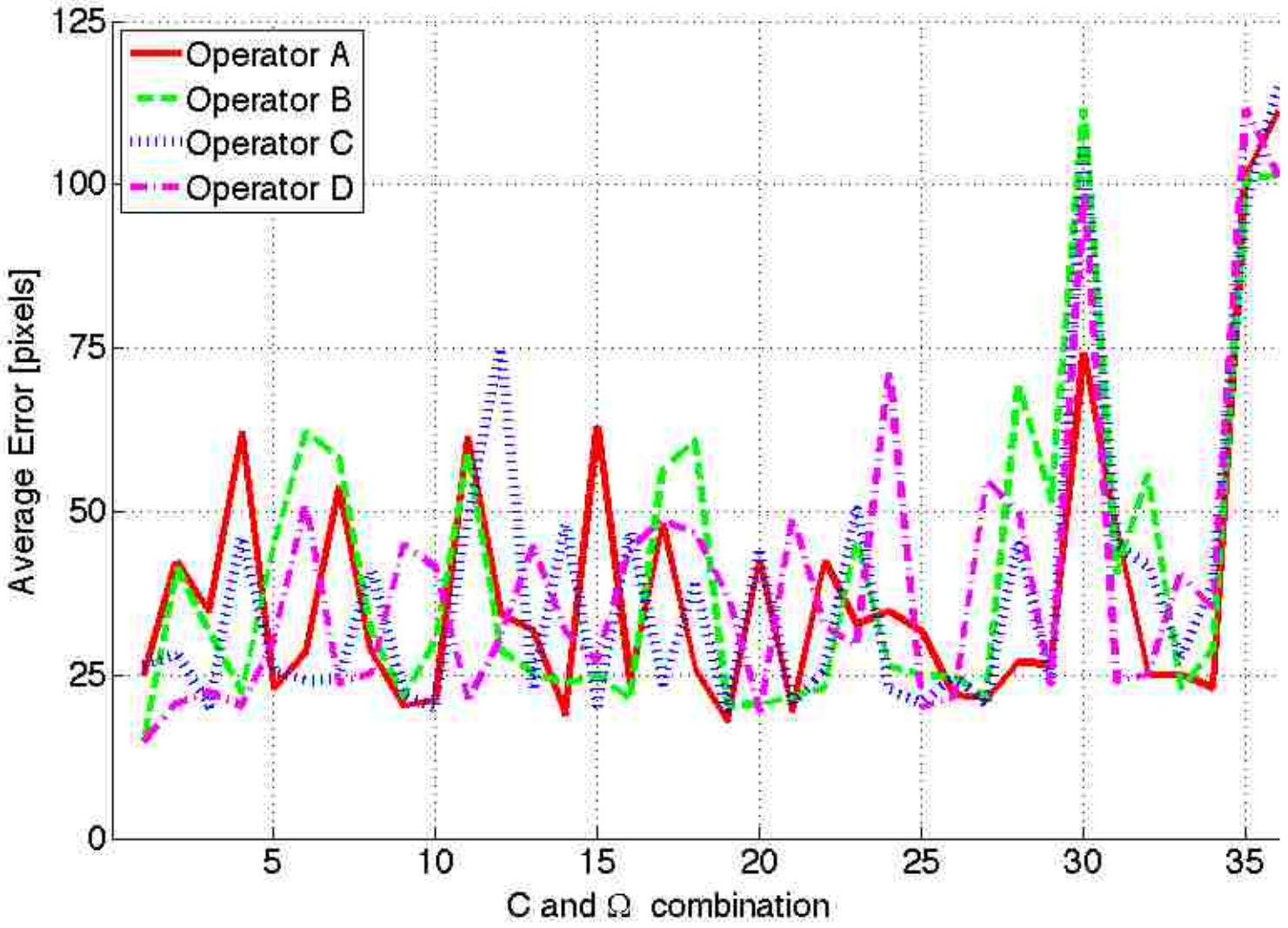

Figure 3.17: Operator variability performing lateral repositioning at all combinations of modulation and spatial frequency. These are the average error values associated with tracking the 1st target for each operator at a given combination.

3.3.2 Idealized Case

The error for the first shape is shown in Fig. 3.18a, with the error for the second shape shown in Fig. 3.18b. It is important to note that these graphs have different contour scales.

Both figures show trends similar to those outlined for previous experiments. The degradation of tracking performance on the first target is still clearly visible as the combinations that approach the 20/20 vision limit. For the second target, the relative error was consistently low for combinations that fell within 20/20 vision limits. Once this limit was reached on either target, relative performance degraded quite rapidly.

Note that the tracking task performed in this experiment was slightly different when comparing the left target and the right target. For the first target, the individuals shape and the randomly-moving shape start out concentric. Therefore the individual knows where to look to visually acquire their shape and begin the compensatory tracking task.

3.3.3 Proposed Objective Performance Metrics

The VCR criteria from ADS-33 requires the pilot to qualitatively evaluate if they could "make *aggressive* and *precise* corrections *with confidence*..." (Ref. [8], italics added.) The words "aggressive," "precise," and "confidence" are inherently subjective in this context.

The present analysis uses the average combination error (specifically in regards

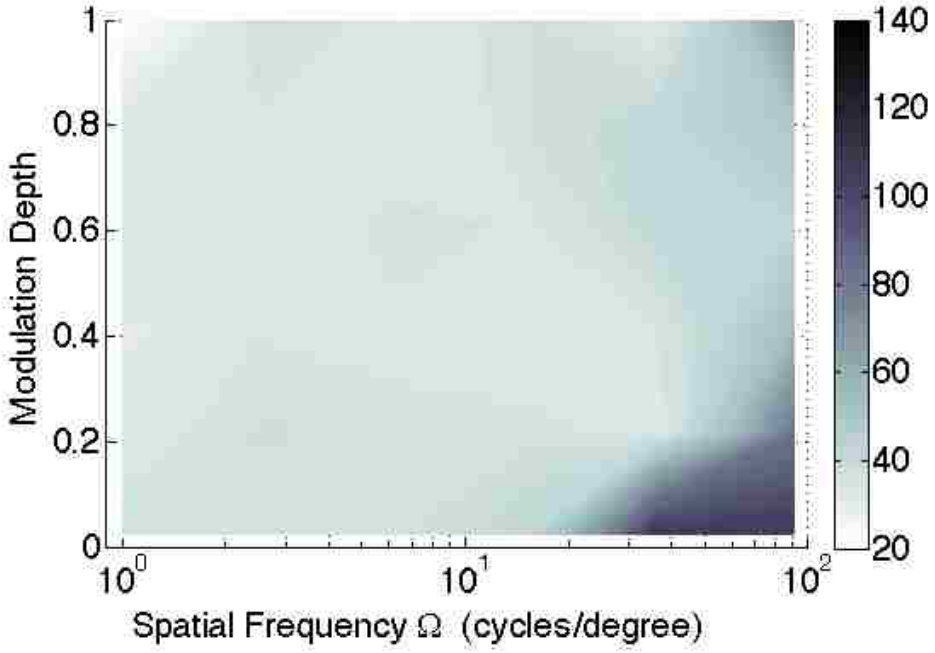

(a) Group average error - 1st Target

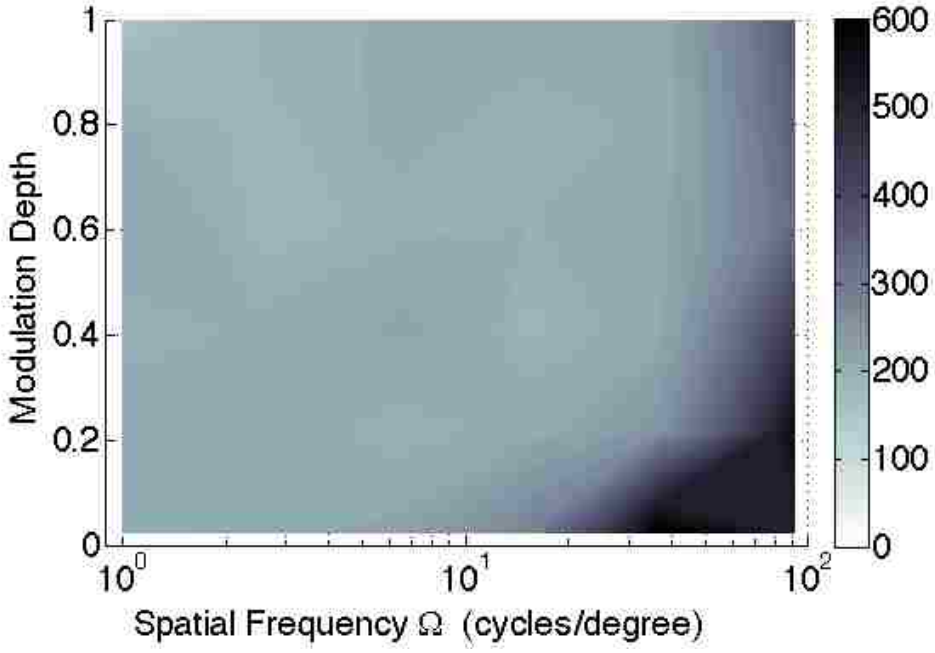

(b) Group average error - 2nd Target

Figure 3.18: Group error during idealized lateral repositioning.

to tracking the second target) as the objective metric for the operators' ability to be "precise." To objectively rate operator ability to be "aggressive" and to be "confident" in performing the compensatory task, three additional metrics were defined.

The first proposed metric is "Time to React" T_r defined as the amount of time after the second target becomes visible that it takes the operator to impart a velocity to their controlled shape greater than 500 pixels/second. The definition of T_r is shown in Fig. 3.15.

The second proposed metric is the "Aggressiveness" A defined as the maximum joystick deflection (in percentage) the individual used to laterally reposition their shape to track the second target. This peak value had to take place *after* the "Time to React" T_r has passed. This ensures that the joystick value is indeed related to the lateral repositioning portion of the task. If A was the peak value after the second target was visible but *before* T_r had passed, then the input may not necessarily be correlated to the lateral repositioning itself. For example, Point A' in Fig. 3.19 shows the first local maximum value of joystick displacement, but it clearly does not characterize the repositioning that is the result of the deflections shown in Portion "B."

The third proposed metric is the "Confidence" C, defined as how quickly, in seconds, it took operator to put in their maximum joystick deflection at a given combination. In this metric, lower objective values of time correspond to higher levels of "confidence" that the individual has in their control inputs. This metric is coupled to the "Aggressiveness" metric, as shown in Fig. 3.19.

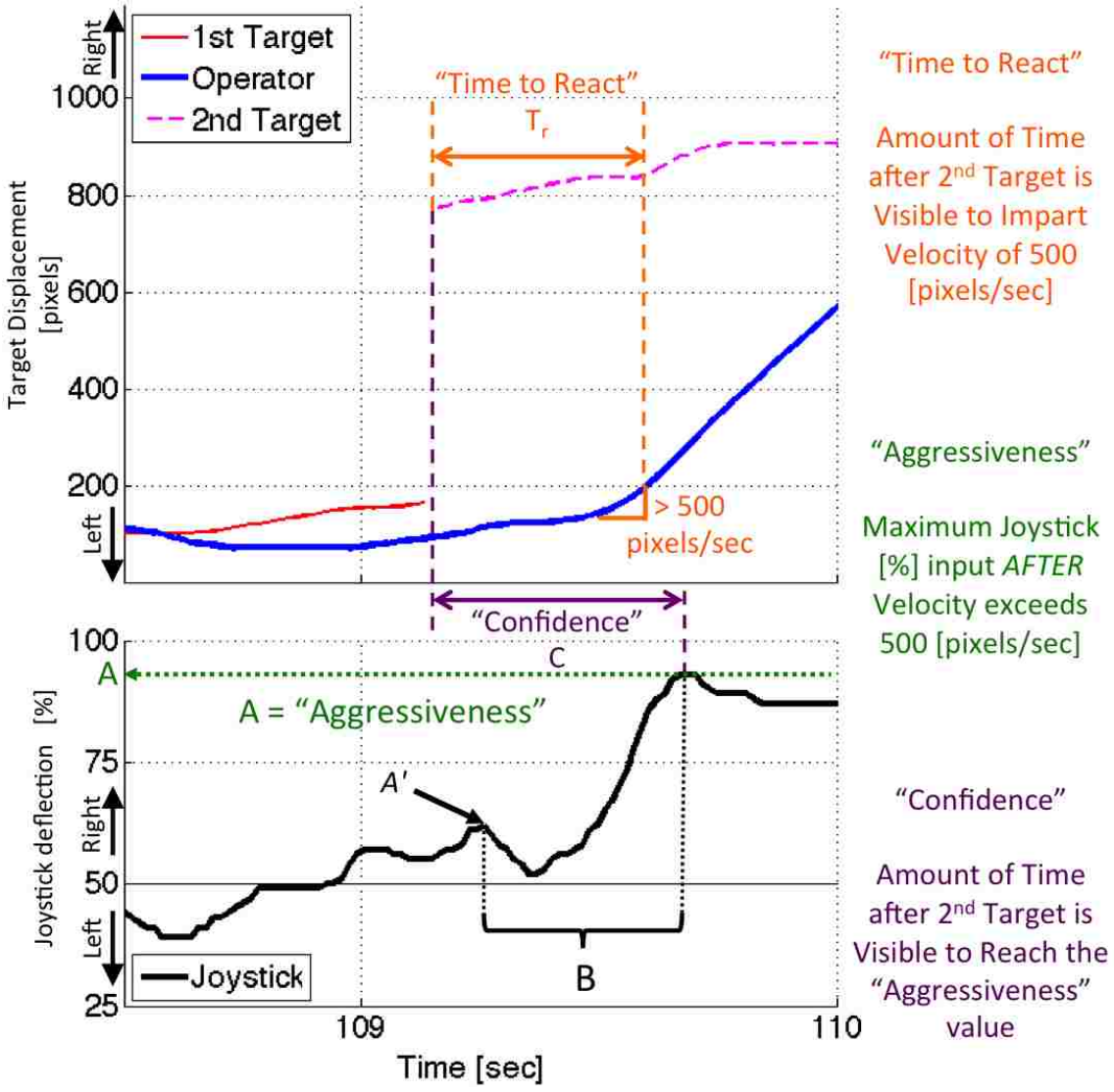

Figure 3.19: Proposed metrics for time to react, confidence, and aggressiveness.

This numeric characterization helps determine whether the individual's response is a more of a step input (a short time to maximum deflection, exhibiting high "confidence") or was a slower, ramped input (longer time to maximum deflection, exhibiting low "Confidence"). "Confidence" does not indicate how "Aggressive" the inputs were; it merely quantifies how long it took to reach the maximum joystick deflection value.

Figure 3.20 shows two hypothetical pilot responses for "Operator A" and "Operator B." Both operators have the same aggressiveness A at this particular visual combination. However, they have different confidence values, which are labeled C_A and C_B.

In this example, Operator A is more "confident" because it took him a *shorter* amount of time to displace the joystick to the "aggressiveness" value, compared to longer time it took Operator B to displace the joystick with the same "aggressiveness" value.

3.3.3.1 Idealized Case - Objective Metric Performance

The group's performance, as characterized by the proposed aggressiveness and confidence metrics, is shown in Fig. 3.21. "Time to React" is not included and is simply used to define "Aggressiveness."

Both contour plots in Fig. 3.21 show a trend of higher "aggressiveness" and "confidence" for the middle values of spatial frequency. Aggressiveness has a region of higher values in the upper-middle ranges of modulation, and a slight decrease

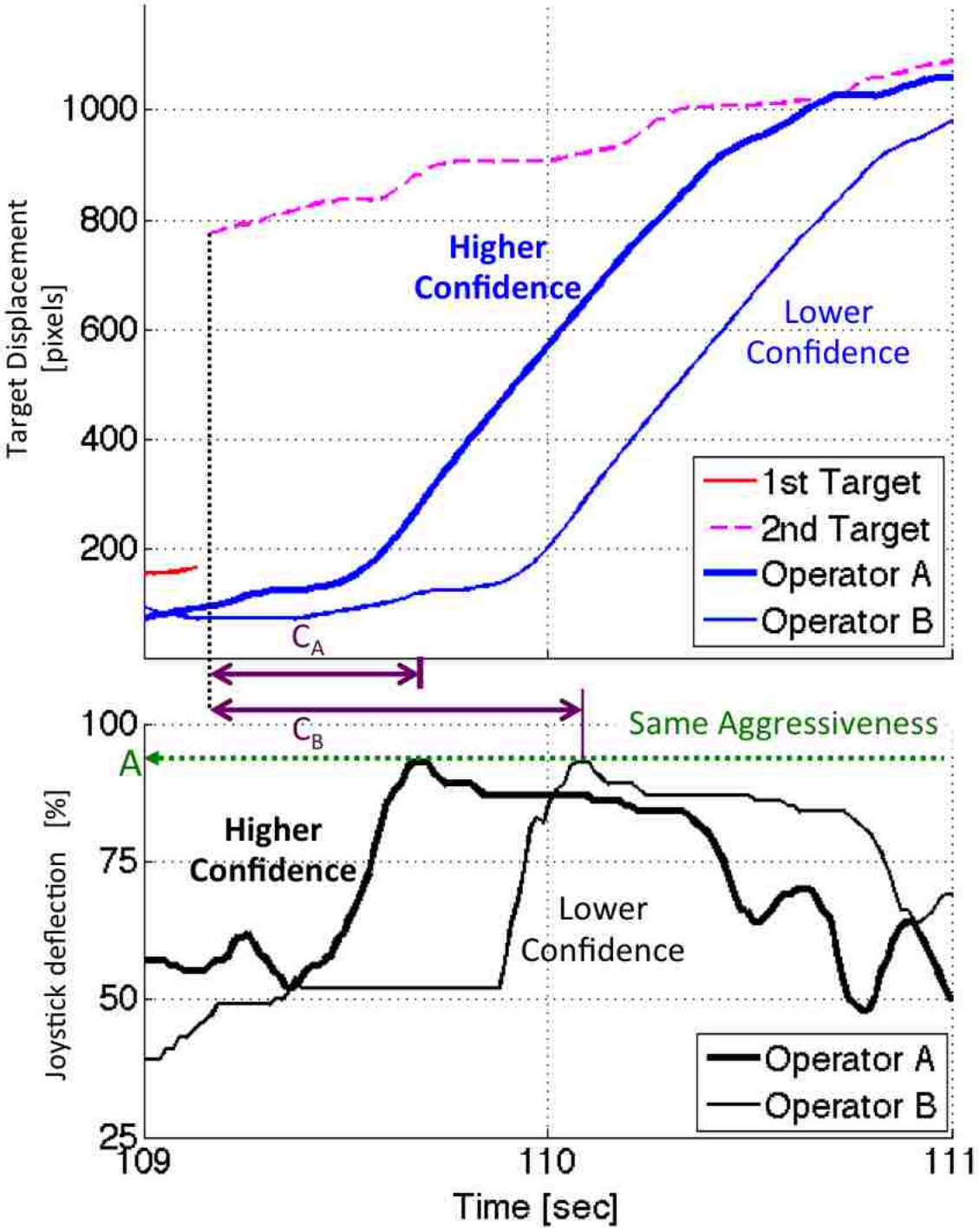

Figure 3.20: Time histories with similar aggressiveness but different confidence.

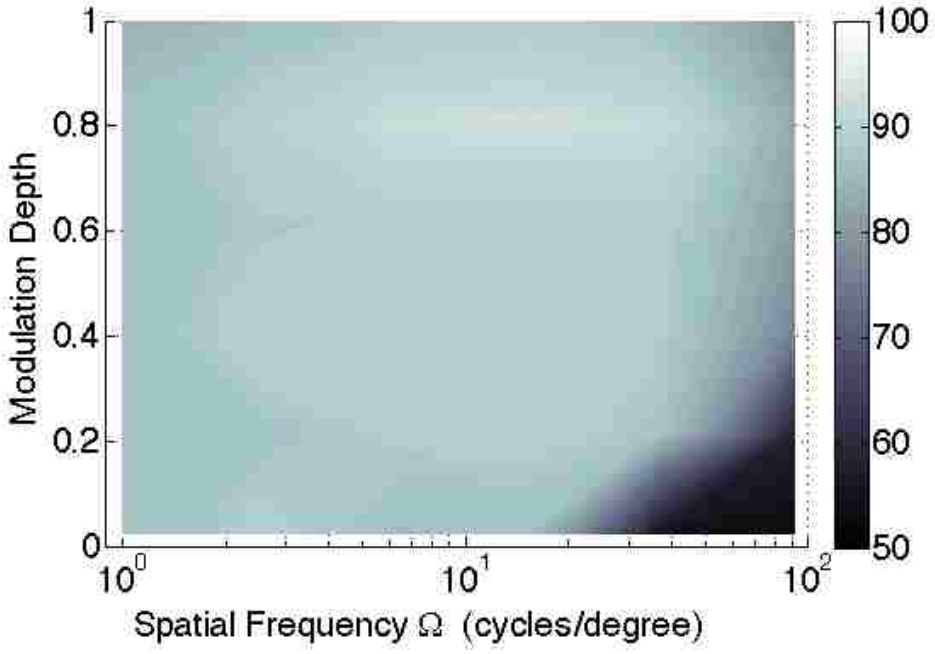

(a) Group Aggressiveness

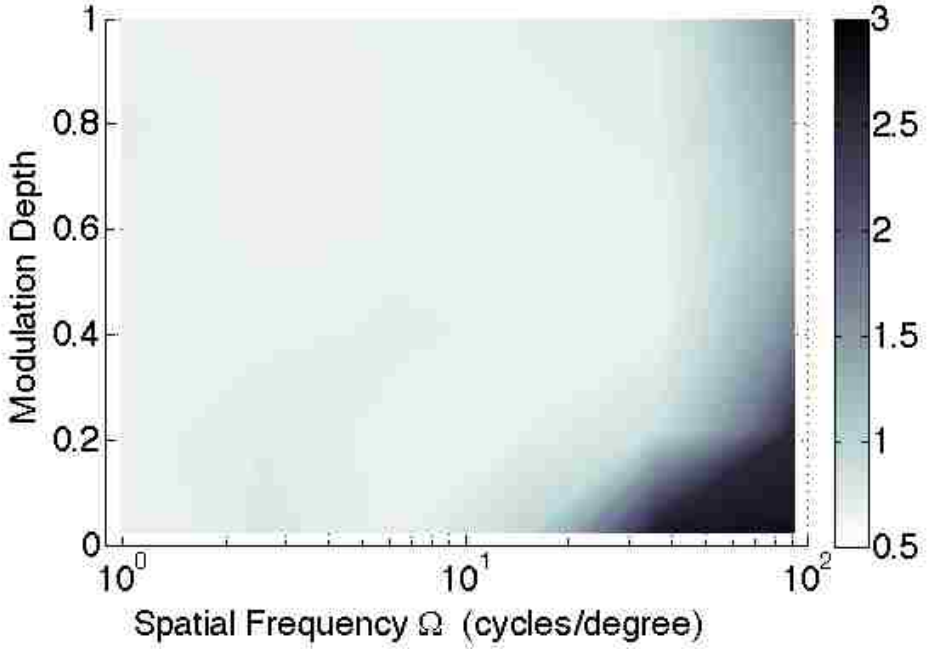

(b) Group Confidence

Figure 3.21: Group ideazlied lateral repositioning characterization.

approaching full modulation. It is not entirely clear whether this slight decrease is real, which would suggest that high contrast visual cues do not solely dictate the human operator's aggressiveness in performing this type of compensatory task, or if it is simply the consequence of some variability in he test subject or conditions. It is interesting to note the similarities between Fig. 3.21 and Fig. 1.11 (Hoh, Ref. [23]).

Additionally, the proposed necessary visual cues for pilot-in-the-loop flight simulators in Fig. 1.11 ("Need Visual Information in This Region") have a similar shape to the regions of the highest aggressiveness of Fig. 3.21a. There is a strong decrease in aggressiveness as the limit of 20/20 vision is reached on the lower right portion of the graph.

Confidence was greatest (meaning it took the operators the shortest amount of time to reach maximum joystick deflection) at the largest values of contrast above the 20/20 threshold. Confidence generally decreased as contrast decreased as expected. The confidence is also adversely affected by contrast and spatial frequency combinations below the limit of 20/20 vision. As mentioned earlier, these confidence results include some time spent performing target acquisition on the second target. The areas of greatest confidence also showed a similar shape to the region of greater aggressiveness.

3.3.3.2 160-ms Delay Case - Objective Metric Performance

The effect of the 160-ms control input delay on the idealized lateral repositioning experiment was examined for the three proposed metrics. The group per-

formance on these metrics is contrasted directly with the idealized no-delay case.

First, the effect on the group average error tracking the second target is shown in Fig. 3.22. These results quantify that adding time delay into the system introduces additional error. The case with no delay had a few combinations of relatively low error. When repeated with the delay, these same combinations had relatively higher areas, which were more in line with the other combinations within the threshold of 20/20 vision. The values of error for the combinations beyond the 20/20 vision threshold also increased slightly.

The effect of the delay on the "Aggressiveness" metric appears to contain a considerable amount of variability. The case with no delay, shown again in Fig. 3.23a, has a central region of high aggressiveness that is fairly well defined. There is similar, but smaller region associated with the delay case, shown in Fig. 3.23b. There are a few sporadic test points, specifically at full modulation, that have a very high aggressiveness value. This sporadic data shows that the delay affected the individual operator's aggressiveness quite differently.

The "Confidence" metric was largely unaffected by the inclusion of the delay. The contour plots, shown in Fig. 3.24, have many similarities. The large regions of high "confidence" (low numeric values) cover the same combinations and have similar low numeric values. The delay case saw a slightly greater degradation in confidence at a given object size as modulation decreased.

The delay case saw a small increase in confidence in comparison to the no-delay case *beyond* the 20/20 vision threshold. While this appears to be counter-intuitive, revisiting the metric's numeric definition provides some explanation.

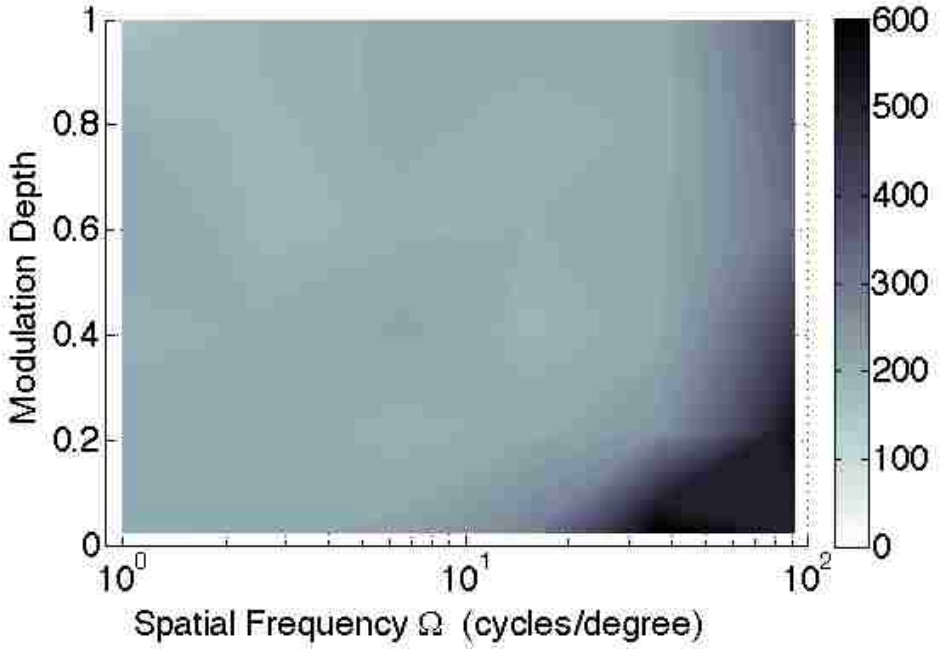

(a) 2nd Target (no delay)

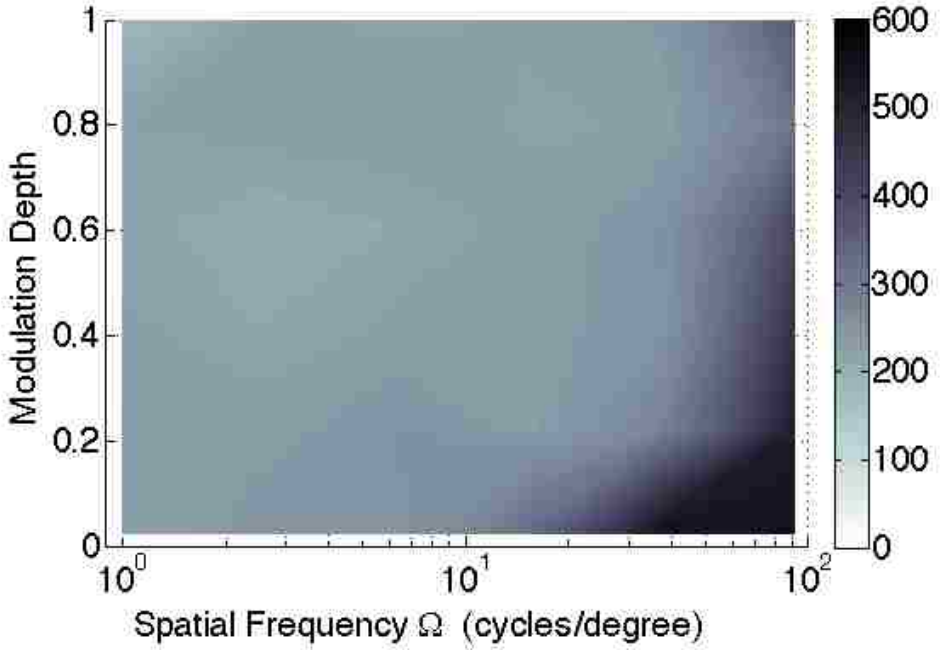

(b) 2nd Target (approx. 160-ms delay)

Figure 3.22: Effects of control input delay on error in idealized lateral repositioning task.

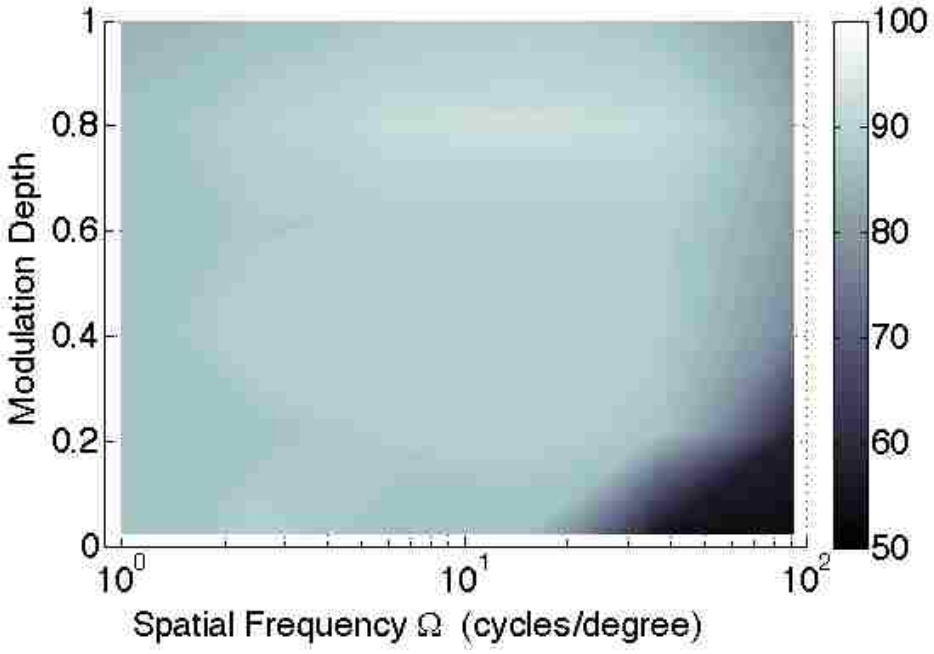

(a) Aggressiveness (no delay)

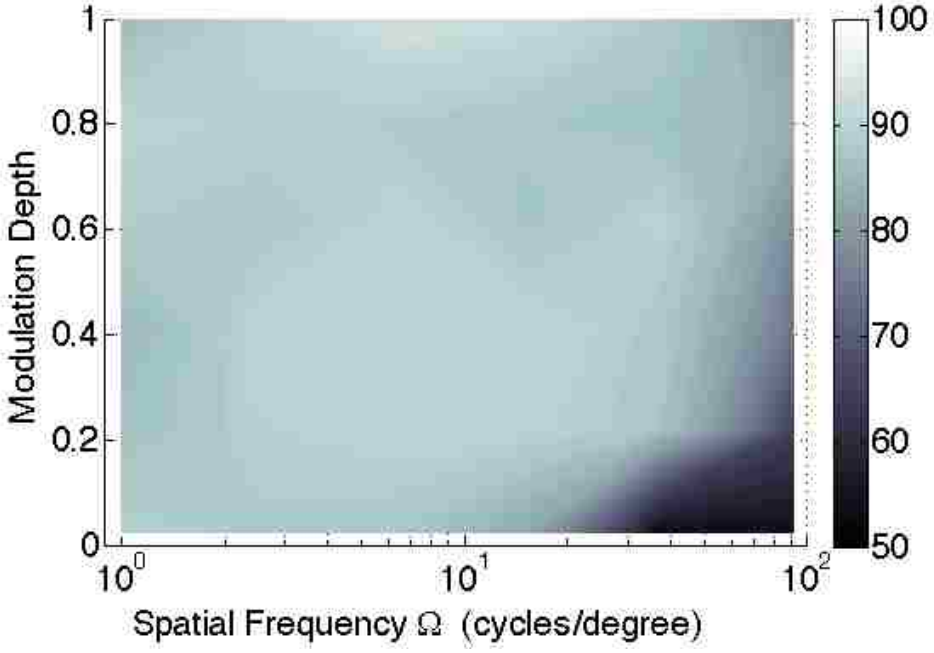

(b) Aggressiveness (approx. 160-ms delay)

Figure 3.23: Effects of control input delay on "Aggressiveness."

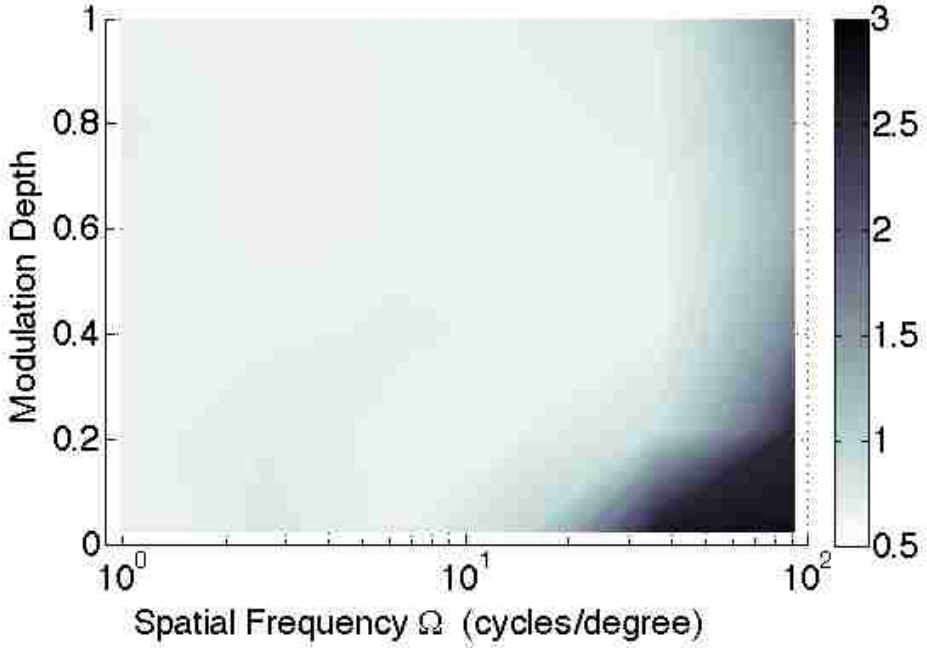

(a) Confidence (no delay)

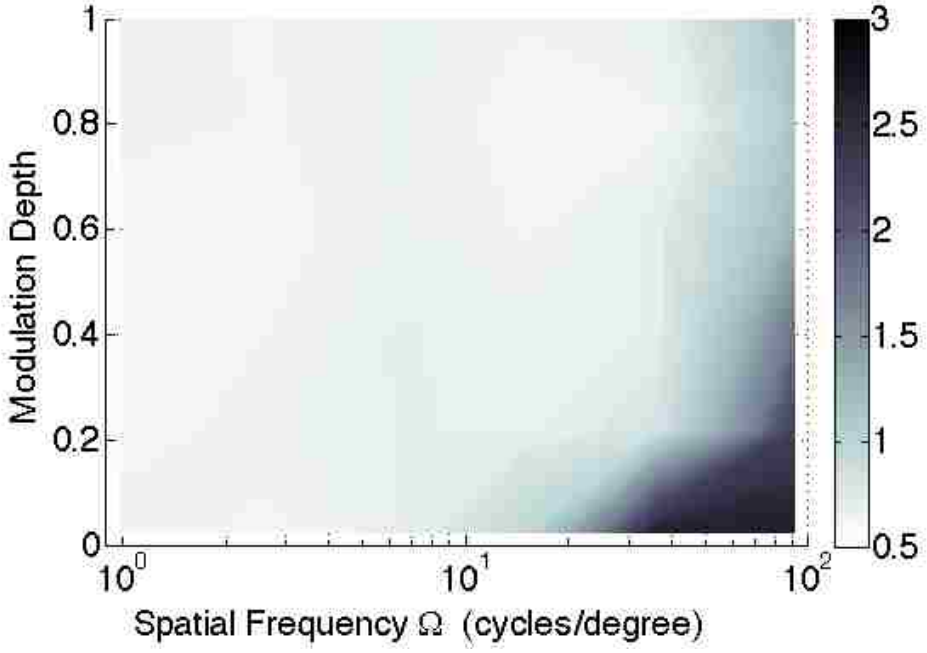

(b) Confidence (approx. 160-ms delay)

Figure 3.24: Effects of control input delay on "Confidence."

"Confidence" was defined to be inversely proportional to the amount of time it took the operator to put in the maximum joystick value (the maximum "aggressiveness" during a lateral repositioning). While it makes no direct connection to the actual joystick value, the "aggressiveness" values shown in Fig. 3.23b are slightly higher beyond the 20/20 threshold then the no delay case shown in Fig. 3.23a. This increase in both aggressiveness *and* confidence are likely attributed to the operator's becoming more familiar and skilled the lateral repositioning compensatory task as testing went on.

3.3.4 Proposed Regions

From the contour plots shown in Fig. 3.18b (2nd Target Error) and Fig. 3.21 (aggressiveness and confidence), regions of quantified performance can be defined by boundaries. The contour plot for group aggressiveness is repeated in Fig. 3.25a, with an example of proposed boundaries shown in Fig. 3.25b.

While the precise cut-off value for a given boundary in Fig. 3.25b is subjective, the values themselves are based on quantified results and their associated metrics. The boundaries, which are repeated in Fig. 3.26a, show how these boundaries can be translated into regions, as shown in Fig. 3.26b.

These regions are unique for each metric, and would also be unique for each particular compensatory task. These regions represent specific characterizations of control task performance when provided specific visual cues, but they make no claim to the role of the specific metric. That is, the ability to be "aggressive" based

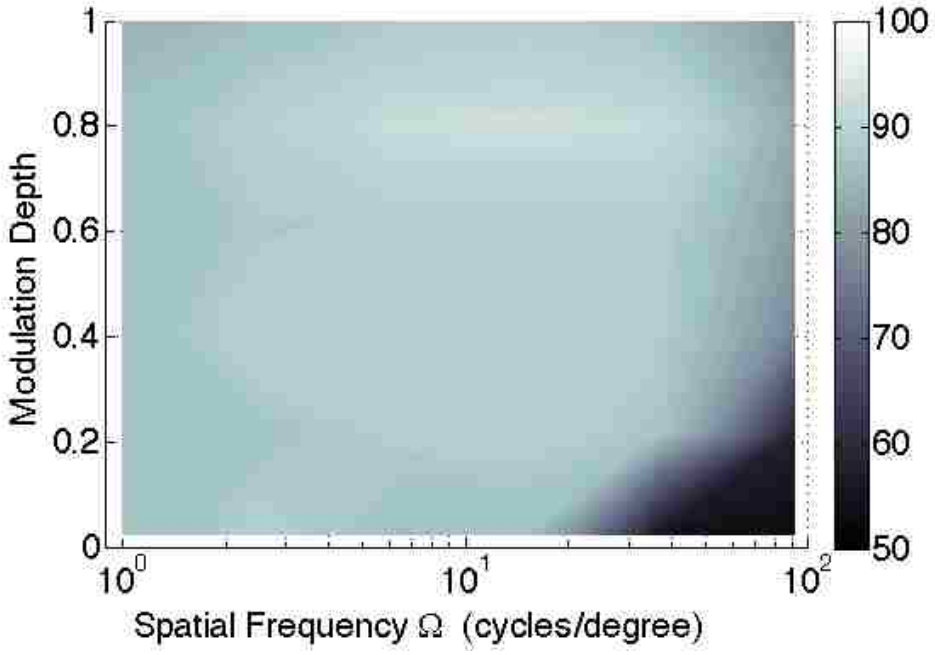

(a) Group average "Aggressiveness" (No Delay)

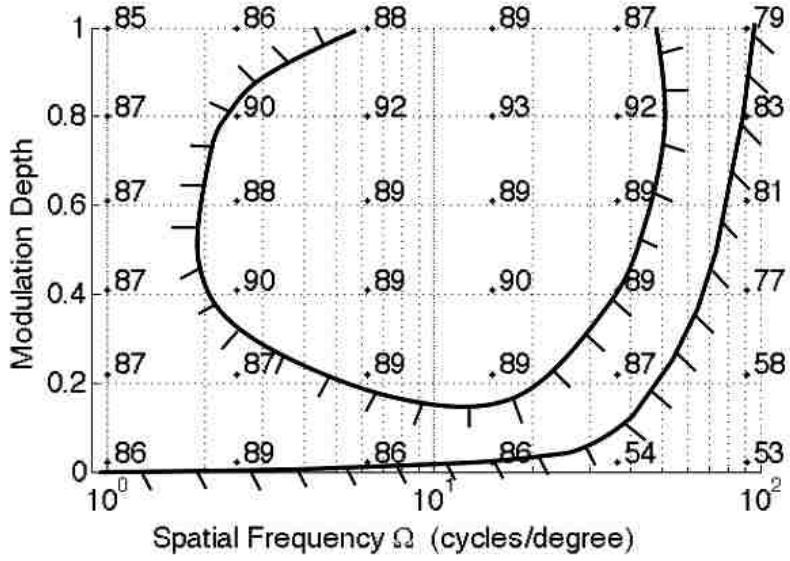

(b) Proposed "Aggressiveness" boundaries

Figure 3.25: Proposed boundaries of operator "Aggressiveness."

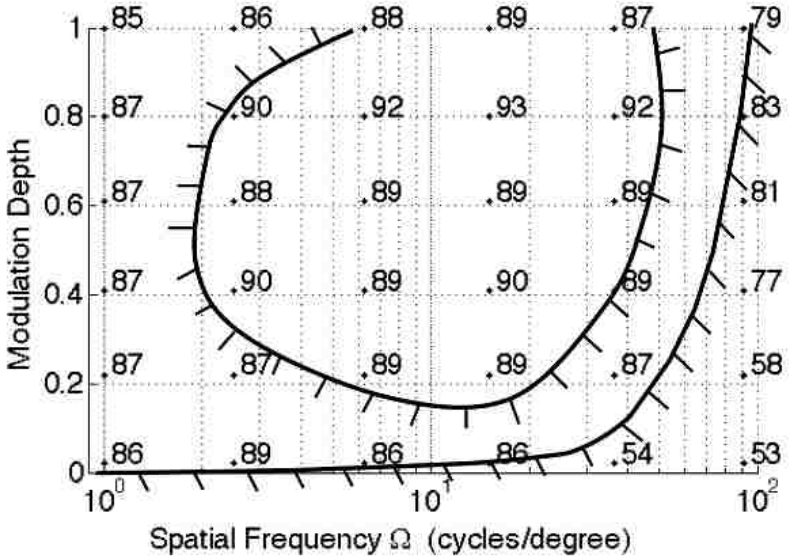

(a) Proposed "Aggressiveness" boundaries

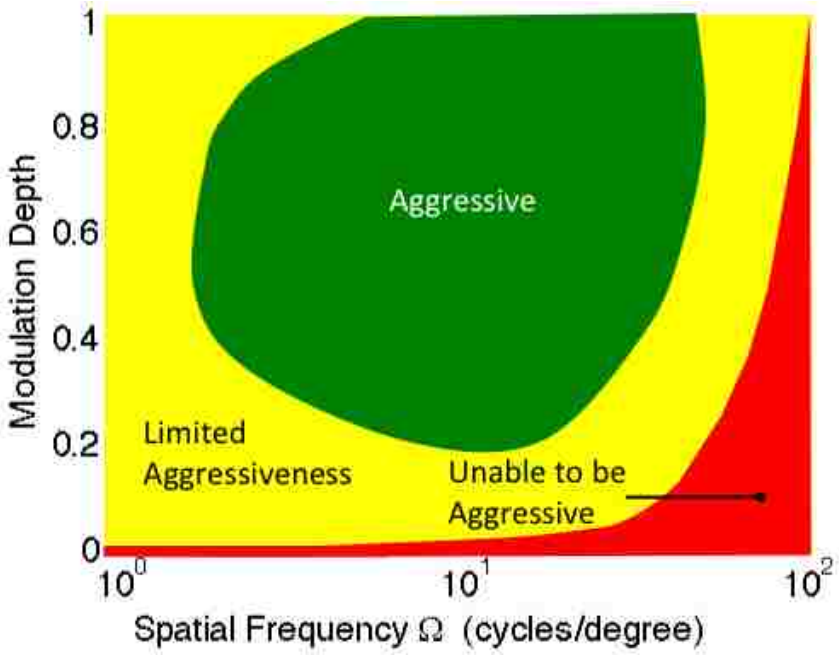

(b) Proposed "Aggressiveness" regions

Figure 3.26: Proposed objective characterization of operator "Aggressiveness."

on visual cues is objectively defined for this specific compensatory task, but the importance of aggressiveness in the task's completion is not characterized.

As previously mentioned, the aggressiveness metric had a region of high joystick displacement in the middle values of both modulation and spatial frequency. The aggressiveness was significantly reduced outside the threshold of 20/20 vision. These two notable characteristics allowed the "Aggressive" region and the "Unable to be Aggressive" region to be defined in Fig. 3.26b. The region characterized by "Limited Aggressiveness" was used to fill the remaining areas of the contour plot.

The significance of Fig. 3.26 is two-fold. First, it converts a subjective parameter, namely "aggressiveness" into a quantitative parameter that can be extracted from the analysis of control time histories. Second, it relatives the "aggressiveness" parameter to the visual quantities of contrast and spatial frequency. These two quantities can be measured even without the presence of the human operator.

Clearly, Fig. 3.26 applies only to the highly-idealized representation of the lateral repositioning maneuver previously described. Much additional research is needed to determine whether Fig. 3.26 has wider applicability and, in particular, whether it can be used as the first step toward a quantification of UCE that does not require the presence of a pilot.

For example, the scene actually observed by a pilot would include many different values of contrast and spatial frequency, and it is not currently clear which specific values best correlate with aggressiveness as defined here.

To address the pilot's ability to "make... corrections with confidence..." portion of the current VCR and UCE criteria from Ref. [8], the contour plots for the

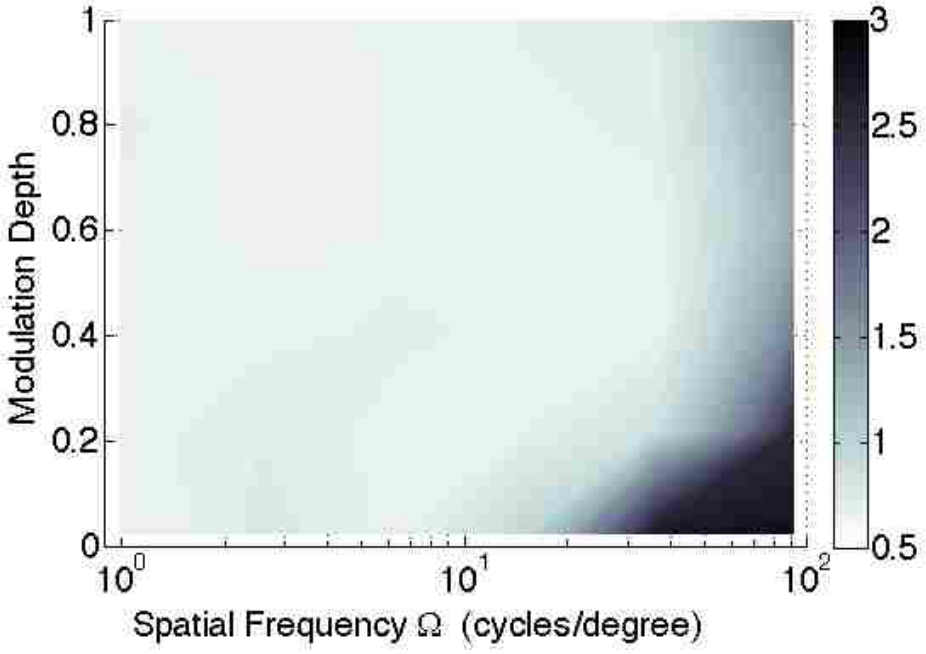

(a) "Confidence" - group contour (no delay)

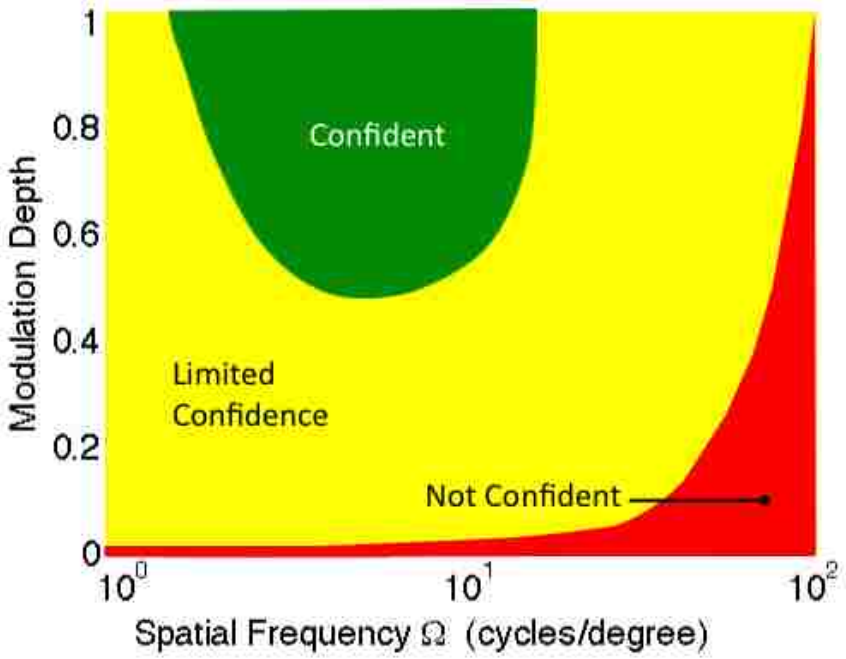

(b) Proposed "Confidence" regions

Figure 3.27: Proposed objective regions of operator Confidence

objective "Confidence" metric was also similarly classified into regions of similar performance. The increase in time it took the operators to impart their maximum joystick deflections was noted earlier to drastically increase past the 20/20 vision threshold. This region was characterized as the operators being "Not Confident" in their compensatory task control inputs, as seen in Fig. 3.27b. The region of low numeric values corresponding to higher "Confidence" was smaller than the aggressiveness metric, but still was a significant region of moderate spatial frequencies. The modulation values that made up this region were also slightly lower than the aggressiveness metric, resulting in a majority of the plot being classified as a region of "limited confidence."

To address the final portion of the VCR criteria from Ref. [8] of making "precise corrections," the operator error tracking the second target was also categorized into regions as shown in Fig. 3.28b. The region of large amounts of error (approximately 375 pixels and above) that corresponded to visual cues outside the 20/20 vision MTF was defined as a region where the operators were expected to be "Not Precise." The values of error corresponding to approximately 250 pixels and lower were categorized as the operators having the ability to be "Precise" with their compensatory task inputs.

The Confidence regions had a similar shape to a MTF region proposed by Hoh in Ref. [23]. Hoh's proposed region, shown again in Fig. 3.29a, addressed a group of modulation and spatial frequency combinations of the visual cues pilots needed to hover with an acceptable work load. While the confidence metric cannot directly address Hoh's qualitative criteria of acceptable work load, confidence in

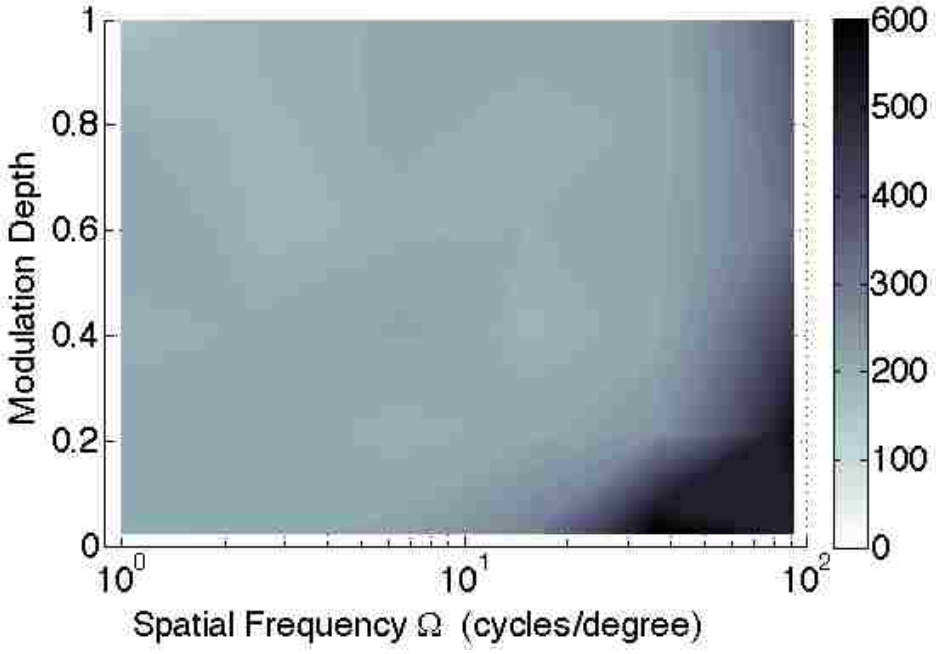

(a) Group average error (no delay)

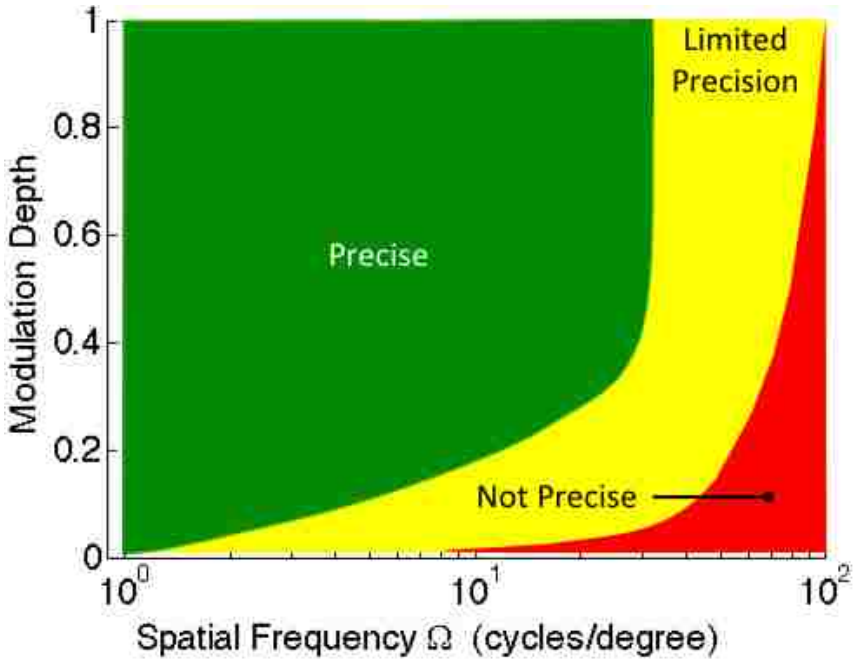

(b) Proposed "Precision" regions

Figure 3.28: Proposed objective regions of operator "Precision"

control inputs could be seen as a necessary qualitative condition for a pilot hovering an aircraft without having to exert an unnecessarily large amount of piloting ability.

These regions of "Aggressiveness," "Confidence," and "Precision" could represent one small component of a future objective metric of pilot control ability in DVE. These regions would allow for objective characterization of the ability to perform a specific task (or MTE) without having to go through the subjective, two-step process of using both a VCR and a UCE.

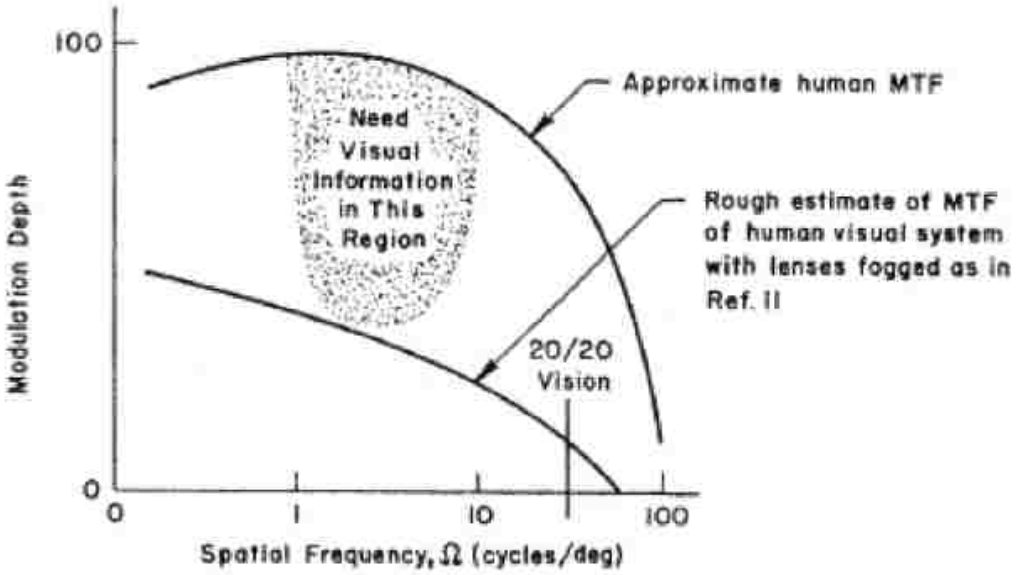

(a) Region of required visuals proposed by Hoh in Ref. [23]

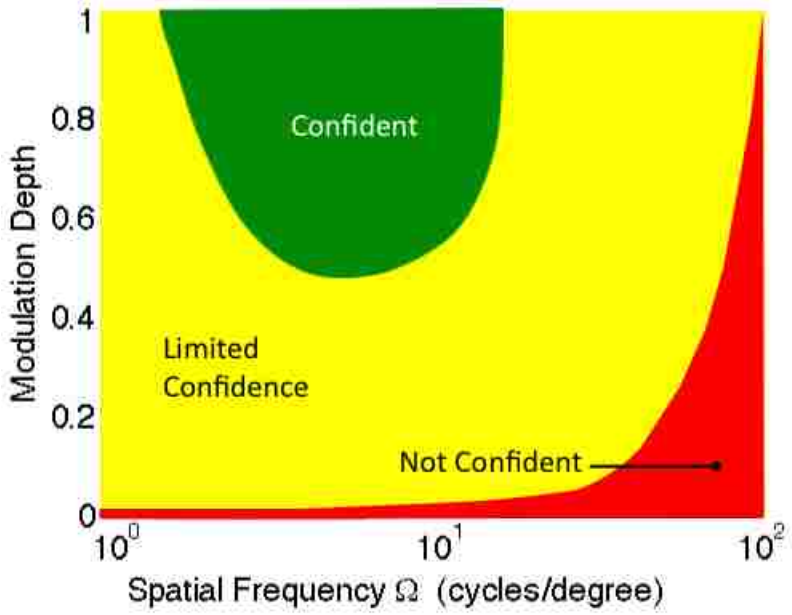

(b) Confidence region for no delay case

Figure 3.29: Possible correlation to regions of visuals proposed by Ref. [23]

Chapter 4: Conclusions and Future Work

4.1 Conclusions

On the basis of the results presented in this thesis, the following can be concluded:

1. "Seeing is Controlling" for simple compensatory tests that idealize piloting tasks. This held true for both the simple, one-dimensional experiments with vertical movement, as well as the idealized lateral repositioning MTE from ADS-33E. In these idealized cases, error contour lines follow very similar to the MTF associated with 20/20 vision. There was relatively little task performance degradation until the physiological limits of the users eyes were reached, indicating that contrast and spatial frequency are key factors for manual control. This held for both the proportional command and the rate command control laws, and was consistent across shape geometry as well (i.e. rectangles and circles).

2. For the Proportional Control cases, the computer mouse as an input device resulted in the lowest amount of group error. For the Rate Control cases, use of the joystick input device resulted in significantly lower group error. Examining

the time histories suggests that the operators used the built-in springs of the joystick to prevent significant tracking overshoots that otherwise led to large error values when the mouse was the input device. The use of a built-in spring force (as an error-reduction mechanism) has potential implication for operational procedures in DVE flight conditions. When a "Force Trim" system is installed and used in a helicopter, it provides a tactile "neutral point" to the pilot of their relative control displacement from the "trimmed" position due to a magnetic brake or similar device. If flight in DVE is anticipated (such as an approach to the ground in a sandy environment) then the helicopter flight controls, specifically the cyclic, could be set to a known trim value (either from operational experience or flight testing) for a stable approach. The pilot could then make modest control displacements relative to the set neutral point, all while receiving tactile feedback of those displacements in an effort to prevent large flight control excursions while flying with minimal visual cues.

3. It is possible to correlates subjective assessments (such as the ability to "make aggressive and precise corrections with confidence..." from Ref. [8]) with specific features that can be extracted from time histories of control inputs. In turn, these control input time histories can be correlated with the visual quantities (contrast and spatial frequency) the operator was receiving at the time the inputs were made. The extraction of various numeric features of the time histories, specifically when characterized by the MTF of the present visual cues, may have future value for determining UCE in the ADS-33 Handling

Qualities specifications.

4.2 Future Work

The experimental testing presented in the present work could be extended on many fronts. One improvement would be to develop additional experiments that idealize other MTEs from current Handling Qualities specifications in an effort to see how quantified performance in MTF format changes based on the task. This experimental testing should incorporate multiple DOFs, and it may be necessary to use more than one computer monitor.

The multiple DOF testing could use the current experimental testing procedures and be performed as an "update" to the current work. The Lateral Repositioning task presented here could be modified to include a vertical DOF (with associated vertical target movement). This would allow for a testing scenario where the pilot had to track (and thus minimize) both a horizontal error and a vertical error. This would be qualitatively-less "idealized" (i.e. a more"realistic" representation) of the piloting tasks required to perform the Lateral Reposition MTE than the present work.

Multiple monitors could be incorporated in the experimental setup as well. This would help with tasks that would specifically require a wide FOV to perform in-flight. For example, the "Hover" task could be idealized using two computer monitors. The first monitor, placed directly in front of the pilot, could contain visual cues for aircraft attitude and fore/aft translation. Meanwhile, a second monitor

placed to the side of the pilot could give additional visual cues on the horizontal translation (as well as some secondary attitude information). The Lateral Reposition task examined in the present work could also be less "idealized" by a similar experimental layout.

If future experiments elaborate on the present analysis by including multiple DOFs and a wide FOV through multiple computer screens, the characteristics and nuances of the associated piloting tasks involved with that MTE need to be rigorously analyzed. The relative location and the characterization of visual cues used for certain piloting tasks have been showing by Refs. [23, 39, 42] and others to depend on the specific flight maneuver being performed. For instance, a hovering task would need to take into account the location and the type of cues found necessary to pilots in Refs. [23, 39], while a landing MTE would need to be modeled after the piloting cues found in Ref. [42].

Future experimental procedure should allow for the operators responses to be analyzed in the frequency domain. This would help classify the pilot transfer function in regards to the MTF of visual cues, and would also allow for specific comparison to previous work performed in Refs. [26], [32] and [40]. This could be an intermediate step towards the improvement of existing pilot control models by inclusion of visual pathways.

Lastly, there is a connection to cockpit displays and symbology that needs to be thoroughly explored. MacIssac *et al.* have developed cockpit display symbology that is designed specifically for use in DVE landings [41]. The contrast values and spatial frequencies of the visual cues that make up the display symbology could be

tuned to provide the pilots cues in the MTF regions that allow for aggressive and confident maneuvering with good precision.

Bibliography

[1] Key, D. L, "Analysis of Army Helicopter Pilot Error Mishap Data and the Implications for Handling Qualities," Paper L4, 25th European Rotorcraft Forum, Rome, Italy, September 14-16, 1999.

[2] Hoh, R. H., "The Effects of Degraded Visual Cueing and Divided Attention on Obstruction Avoidance in Rotorcraft," DOT/FAA/RD-90/40, 1990.

[3] Albery, W., "Rotary-Wing Brownout Mitigation Technologies and Training," NATO RTO Technical Report, TR-HFM-162, 2012.

[4] Anonymous, "Aeromedical Training for Flight Personel," US Army FM 3-04.301, Sep. 29, 2000.

[5] Tritschler, J., *Contributions to the Characterization and Mitigation of Rotorcraft Brownout*, Ph.D. Dissertation, Department of Aerospace Engineering, University of Maryland - College Park, 2012.

[6] Cooper, G. E., Harper, R. P., "The Use of Pilot Rating in the Evaluation of Aircraft Handling Qualities," AGARD Report 567, 1969.

[7] Mitchell, D. G.,"The Evolution, Revolution, and Challenges of Handling Qualities," AFRL-VA-WP-TP-2003-328, 2003.

[8] Anonymous, "Aeronautical Design Standard, Performance Specification, Handling Qualities Requirements for Military Rotorcraft," ADS-33E-PRF, Mar. 21, 2000.

[9] Key, D. L., Blanken, C. L., and Hoh, R. H., "Some Lessons Learned in Three Years with ADS-33C," Piloting Vertical Flight Aircraft: A Conference on Flying Qualities and Human Factors, San Francisco, CA, January 20-22, 1993.

[10] Hoh, R. H., Baillie, S. W., and Morgan, J. M., "Flight Investigation on the Tradeoff Between Augmentation and Displays for NOE Flight in Low Visibility," AHS National Specialists' Meeting on Flight Controls and Avionics, Cherry Hill, NJ, Oct. 13, 1987.

[11] Milluzzo, J., and Leishman, J. G., "Assessment of Rotorcraft Brownout Severity in Terms of Rotor Design Parameters," *Journal of the American Helicopter Society*, Volume 55, (3), July 2010, pp. 032009. doi: 10.4050/JAHS.55.032009

[12] Syal, M., Rauleder, J., Tritschler, J., and Leishman, J.G., "On the Possibilities of Brownout Mitigation Using a Slotted-Tip Rotor Blade," 29th AIAA Applied Aerodynamics Conference, Honolulu, HI, Jun. 27-30, 2011.

[13] Whitehouse, G. R., Wachspress, D. A., and Quackenbush, T. R., "Aerodynamic Design of Helicopter Rotors for Reduced Brownout," International Powered Lift Conference, Philadelphia, PA, October 5-7, 2010.

[14] Alfred, J., *Rotorcraft Brownout Mitigation Through Flight Path Optimization using a High Fidelity Rotorcraft Simulation Model*, M.S. Thesis, Department of Aerospace Engineering, University of Maryland - College Park, 2012.

[15] Sykora, B,. "BAE Systems Brownout Landing Aid System Technology (BLAST) System Overview and Flight Test Results," *Proceedings SPIE*, Vol. 8360, Airborne Intelligence, Surveillance, Reconnaissance (ISR) Systems and Applications IX, May 2012, pp. 8360M. doi:10.1117/12.918506

[16] Colucci, F., "Making Sense of Sandblaster," *VertiFlite*, Vol. 55, (2), 2009, pp 24-28.

[17] Zhu, X., Church, P., and Labrie, M., "Lidar for Obstacle Detection During Helicopter Landing," *Proceedings of SPIE*, Vol. 6950, Laser Radar Technology and Applications XIII, Apr. 2008, pp. 6950T1-8. doi:10.1117/12.777160

[18] Seidel, C., Schwartz, I., Kielhorn, P., "Helicopter Collision Avoidance and Brown-out Recovery with HELLAS," *Proceedings of SPIE*, Vol. 7114, Electro-Optical Remote Sensing, Photonic Technologies, and Applications II, Oct. 2008, pp. 71140G. doi:10.1117/12.800180

[19] Wong, O. D., and Tanner, P. E., "Photogrammetric Measurements of an EH-60L Brownout Cloud," American Helicopter Society 66th Annual Forum, Phoenix, AZ, May 11-13, 2010.

[20] Tritschler, J., Celi, R., "Brownout Cloud Characterization Using the Modulation Transfer Function," *Journal of the American Helicopter Society*, Volume 58, (1), Jan. 2013, pp. 1-13. doi: 10.4050/JAHS.58.012001

[21] Kopeika, N. S., *A System Engineering Approach to Imaging*, SPIE Optical Engineering Press, Bellingham, WA, 1998, Chapter 12.

[22] Sadot, D., and Kopeika, N. S., "Effects of Absorption on Image Quality through a Particulate Medium," *Applied Optics*, Volume 33, (30), Oct. 1994, pp. 7107-7111.

[23] Hoh, R. H., "Investigation of Outside Visual Cues Required for Low Speed and Hover," AIAA 12th Atmospheric Flight Mechanics Conference, Snowmass, CO, Aug. 19-21, 1985.

[24] Dillow, J. D., "The 'Paper-Pilot' - A Digital Computer Program to Predict Pilot Rating for the Hover Task," AFFDL-TR-70-40, Feb. 19, 1971.

[25] Blakelock, J. H., *Automatic Control of Aircraft and Missiles*, John Wiley & Sons, Inc., New York, NY, 1991, Chapter 13.

[26] McRuer, D. T. and Krendel, E. S., "Mathematical Models of Human Pilot Behavior," AGARD-AG-188, 1974.

[27] Overington, I., *Vision and Acquisition: Fundamentals of Human Visual Performance, Environmental Influences, and Applications in Instrumental Optics*, Pentech Press, London, UK, 1976, Chapter 4.

[28] Howell, E. R., and Hess, R. F.,"The Functional Area for Summation to Threshold for Sinusoidal Gratings," *Vision Research*, Vol. 18, (4), 1978, pp. 369-374.

[29] Banks, M. S., Geisler, W. S., and Bennett, P. J., "The Physical Limits of Grating Visibility," *Vision Research*, Vol. 2, (11), 1987, pp. 1915-1924.

[30] Cornsweet, T. N., *Visual Perception*, Academic Press, Inc., New York, NY, 1970, Chapter 12.

[31] Van Nes, F. L., and Bouman, M. A., "Spatial Modulation Transfer in the Human Eye," *Journal of the Optical Society of America*, Vol. 57, (3), Mar. 1967, pp. 401-406.

[32] Li, L., Sweet, B. T., and Stone, L. S., "Effect of Contrast on the Active Control of a Moving Line," *Journal of Neurophysiology*, Vol. 93, (5), 2005, pp. 2873-2886.

[33] Stone, L. S., and Thompson, P., "Human Speed Perception is Contrast Dependent," *Vision Research*, Vol. 32, (8), 1992, pp. 1535-1549.

[34] Snowden, R. J., Stimpson, N, and Ruddle, R. A., "Speed Perception Fogs Up as Visibility Drops," *Nature*, Vol 392, Apr. 1998, pp. 450.

[35] Blakemore, M. R., and Snowden, R. J., "The Effect of Contrast upon Perceived Speed: A General Phenomenon?," *Perception*, Vol. 28, (1), 1999, pp. 33-48.

[36] Miall, R. C., Weir, D. J., Stein, J. F., "Visuomotor Tracking with Delayed Visual Feedback," *Neuroscience*, Vol. 16, (3), 1985, pp. 511-520.

[37] Reed, D. W., Xuguang, L., Miall, R. C., "On-line Feedback Control of Human Visually Guided Slow Ramp Tracking: Effects of Spatial Separation of Visual Cues," *Neuroscience Letters*, Vol. 33, (8), 2003, pp. 209-212.

[38] Schulze, T. J., "A procedure for calculating the resolution of electro-optical system," *Proceedings SPIE*, Vol. 1342, Airborne Reconnsaissance XIV, Nov. 1990, pp. 317-327. doi:10.1117/12.23130

[39] Johnson, W.W., and Phatak, A. V., "Optical Variables and Control Strategy used in a Visual Hover Task," IEEE International Conference on Systems, Man and Cybernetics, Cambridge, MA, Nov. 14-17, 1989.

[40] Hess, R. A., "Simplified Approach for Modelling Pilot Pursuit Control Behaviour in Multi-loop Flight Control Tasks," *Proceedings of the Institution of Mechanical Engineers, Part G: Journal of Aerospace Engineering*, Vol. 220, (2), Feb. 2006, pp. 85-102. DOI: 10.1243/09544100JAERO33

[41] MacIssac, M. A., Stiles, L., and Judge, J. H., "Flight Symbology to Aid in Approach and Landing in Degraded Visual Environments," American Helicopter Society 61st Annual Forum, Grapevine, TX, Jun. 1-3, 2005.

[42] Dearing, M., Schroeder, J., Sweet, B., Kaiser, M., "Effects of Visual Texture, Grids, and Platform Motion on Unpowered Helicopter Landings," Paper AIAA 2001-4251, AIAA Modelling and Simulation Technologies Conference, Montreal, Canada, Aug. 6-9, 2001.